MAXIMIZING THE PERFORMANCE OF SEMI-CLOSED O_2/CO_2 GAS TURBINE COMBINED CYCLES FOR POWER GENERATION

by

Lorne G. Allaby

A thesis submitted to the Faculty of Graduate Studies and Research in partial fulfillment of the requirements for the degree of

Master of Applied Science

in Mechanical Engineering

Ottawa-Carleton Institute for Mechanical and Aerospace Engineering

Department of Mechanical and Aerospace Engineering

Carleton University

Ottawa, Ontario, Canada

Lorne Allaby

April 2006

Your file Votre référence
ISBN: 978-0-494-16450-1
Our file Notre référence
ISBN: 978-0-494-16450-1

The undersigned recommend to

The Faculty of Graduate Studies and Research

Acceptance of the thesis

Maximizing the Performance of Semi-Closed O_2/CO_2 Gas Turbine Combined Cycles for Power Generation

submitted by

Lorne G. Allaby, B.Eng.

in partial fulfillment of the requirements for the degree of

Master of Applied Science in Mechanical Engineering

Thesis Supervisor:

Professor Steen A. Sjolander

Department of Mechanical and Aerospace Engineering

Department Chair:

Professor Johnathan C. Beddoes

Department of Mechanical and Aerospace Engineering

Carleton University

April 2006

Abstract

The performance of oxy-fuel semi-closed gas turbine power generation cycles has been under investigation in recent years. These cycles have the advantage of capturing and sequestering the carbon dioxide and other pollutants generated by combustion, thus making them zero-emission cycles.

This thesis investigates and compares the performance potential of simple combined cycles and recuperative combined cycles employing state of the art technology. A review of previous literature is also included. The cycles are modeled using a chemically rigorous heat and mass balance simulation tool, ASPEN PLUS 12.1. Investigations include: the effects of fuel gas purity and oxygen purity on working fluid composition; the effects of excess oxygen specification on overall thermal efficiency; the effects of working fluid properties on performance; and the effects of steam injection on performance. Peak performance values are presented for both types of cycle at two levels of oxygen purity. Observations are made on the efficiency and specific work trends.

The developed numerical models were used in combination with general turbomachinery theory to predict the performance of a semi-closed plant based on the Solar Turbines Mercury 50 gas turbine. A single operating point is investigated. The results suggest some modifications to the engine may be required due to improper matching of the turbine to the compressor.

For my grandmother

Cora Allaby

(March 16, 1923 - November 18, 2004)

who showed me how one person can make a positive difference in the lives of many.

Acknowledgements

The author gratefully acknowledges the financial support from the CANMET Energy Technology Centre, Natural Resources Canada, and the Natural Sciences and Engineering Research Council of Canada.

The author also would like to express gratitude to his thesis supervisor, Professor Sjolander; for his patience and his well-anchored guidance throughout the project.

The author also thanks Dr. L. Zheng and Dr. Y. Tan of the CANMET Energy Technology Centre specifically for their guidance with the Aspen product.

The author thanks those who were around during this project. This includes: Gregory Davis, who showed me that everything looks better after a good lunch. Trevor Wallace, who showed me how things are always created first in one's mind. Ian Turgoose, who helped me realize that I can actualize my ideas. My mother and father, who gave me the tools and mindset to succeed.

Finally, the author thanks Lara for her love and continuous support.

Table of Contents

List of Tables

List of Figures

List of Symbols

ASU	Air Separation Unit
a	Sound speed
BC	British Columbia
c_p	Gas heat capacity at constant pressure (kJ/kg.K)
c_v	Gas heat capacity heat at constant volume (kJ/kg.K)
CO_2	Carbon dioxide
D	Diameter
H	Enthalpy (kJ/kg mol.K)
H_2O	Water
HRSG	Heat-Recovery Steam Generator
ISO	International Standards Organization
kg	kilogram
kJ	kilo-joules
K	Kelvin
LHV	Lower Heating Value (MJ/kg)
MJ	Mega-Joule
MW	Mega-watt
Mmscfd	Million standard cubic feet per day
$\dot{m}$	Mass flow (kg/s)

N	Speed, shaft speed, revolutions-per-minute (RPM)
n	Empirical correlation correction value; correlation dependent
N/A	Not Applicable
O_2	Oxygen
OTSG	Once-Through Steam Generator
P	Total pressure (Pa)
PR	Pressure Ratio
R	Gas constant (kJ/kg.K)
r	Compressor pressure ratio
Re_D	Reynolds number based on diameter
RPM	Revolutions per minute
T	Total temperature (K)
TIT	Turbine Inlet Temperature (K)
V	Volume (m)
Ws	The specific work output of the engine (kJ/kg)
γ	Gamma, heat capacity ratio (C_p/C_v)
δ	$\delta/\delta x$ = derivative
η	Cycle overall thermal efficiency, or component isentropic efficiency
η_c	Isentropic efficiency of compressor
η_t	Isentropic efficiency of turbine

η_m	Mechanical transmission efficiency
η_∞	Polytropic efficiency
$\eta_{\infty c}$	Polytropic efficiency of compressor
μ	Viscosity (N-s/m^2)
Π	Capital Pi; non-dimensional similarity parameter as specified by subscript
ρ	Density (kg/m^3)
χ	Steam quality ratio

Subscripts

a	Air	f	Fuel
A	Known operating point	N	Speed, shaft speed,
B	Unknown/forecast operating point		revolutions-per-minute (RPM)
C	Compressor	T	Turbine
Cr	Critical	01	Stagnation condition location 1
D	Diameter		
cr	critical	∞	Polytropic

Chapter 1 – Introduction

1.1 Motivation

The study of zero-emission gas turbine power generation cycles has been increasing since the early 1990s. Zero-emission power cycles do not release any emissions into the environment. A zero-emission cycle can burn fossil fuels as long as all the resulting carbon dioxide and other pollutants are captured. The captured carbon dioxide can be reused in industrial processes, used in enhanced oil and gas recovery, or permanently stored in geological formations.

Canada has agreed to limit greenhouse gas production to 6% below 1990s level in its ratification of the Kyoto Protocol, which dictates making every effort to reduce the planet's collective greenhouse gas emissions by 5.2% below its 1990 output level by the year 2012. Given current trends, the required reduction is

anticipated to grow to 30% by the year 2010 (Government of Canada, 2002). It is forecasted that by 2010, if significant gains toward Kyoto targets are not made, power generation by fossil fuels will produce 16% of Canada's greenhouse gas emissions (NRCan, 1999). As of 1997, 84% of power generation emissions were the result of coal fired plants, while 9% were from natural gas and only 7% from oil fired plants (NRCan, 1999). These values suggest that significant reductions in greenhouse gas emissions are possible by retiring coal fired plants in favour of high-efficiency natural gas-fired combined cycle plants. An even greater greenhouse gas reduction can be achieved if zero-emission semi-closed combined-cycle plants are installed instead of high-efficiency natural gas-fired combined cycle plants. Unfortunately, the cost of natural gas has risen to the point that retiring coal plants in favour of natural gas fuelled plants is not feasible. Many other countries also desire to reduce their greenhouse gas production. This has led to interest in the study of zero-emission power generation cycles.

The demand for electricity continues to grow around the world. In 2001, 60% of Canadian electricity was generated from hydro, 19% from coal, and 12% from nuclear sources (World Nuclear Association, 2005). Considering the generally negative public opinion of nuclear power, and even with full exploitation of renewable energy resources, fossil fuels will continue to be required to meet Canada's energy needs. Greenhouse gas emissions from the combustion of fossil

fuels need to be reduced until alternative energy sources become available.

The concentration of carbon dioxide in the Earth's atmosphere has increased from 277 parts per million by volume (ppmv) in 1740 (Friedli et al., 1986) to 373 ppmv in 2003 (Keeling et al., 2003). This change is believed to be responsible for 60% of the atmospheric greenhouse effect (Government of Canada, 2002), which refers to the Earth's atmosphere retaining energy which would otherwise radiate into space. As a result, the Earth's surface temperature is increasing. Other gases which contribute to the greenhouse effect are nitrous oxide, methane, halocarbons, perfluorocarbons, and sulphur hexafluoride (Government of Canada, 2002). Global warming is feared to have consequences including rising sea levels, climate change, and increases in the strength and frequency of extreme weather systems.

In the design of power generation cycles, it is important to select specifications which give the highest efficiency at a marketable cost. If the list of variables in the specifications is short, the optimum combination can be chosen based on parametric studies; however, if the list is long it is best to use optimization algorithms which investigate many combinations of specifications and identify the highest efficiency over the ranges of all the combinations of individual parameters, known as the global optimum.

Zero-emission power generation cycles typically require more equipment than a comparable open cycle using air. More equipment leads to more variables to

consider in finding an optimum cycle. As a result, global optimization studies may yield increases in performance, which can improve a project's viability by decreasing fuel costs.

Since the combustion of fossil fuels is the primary source of carbon dioxide emissions and a significant portion of those emissions come from power generation, converting the fossil fuel power generation to zero-emission systems would go far toward meeting the Kyoto driven emissions targets.

1.2 Thesis Objectives

The following list is a summary of the primary objectives of this thesis:

1. Complete a literature review
2. Compare and contrast performance details between two zero-emission combined cycles, one using a simple cycle gas turbine, and the other using a recuperative gas turbine.
3. Determine the thermodynamic potential of the Solar Turbines Mercury 50 gas turbine to be operated in a zero-emissions semi-closed O_2/CO_2 cycle, giving a glimpse into potential required alterations

Below is a list of secondary objectives which follow under the second primary objective:

- Determine the maximum performance of the proposed cycles
- Determine the working fluid composition at steady state
- Determine the effect of oxygen purity on working fluid composition
- Determine the effect of fuel purity on working fluid composition
- Determine the effect of excess oxygen on overall thermal efficiency
- Determine the effect of working fluid properties on cycle performance
- Determine the effect of steam injection on cycle performance
- Determine the suitability of ASPEN PLUS OPTIMIZER as a tool for optimizing gas turbine-driven power generation combined cycles

1.3 Approach

In this thesis, the term *gas turbine* (GT) is used to refer to a compressor mated to a turbine with a combustor between the two. A simplified schematic of a gas turbine is shown in Figure 1-1. The working fluid enters the gas turbine through the compressor, which raises the pressure of the fluid and discharges it into a combustor. In the combustor, fuel is added and burned to raise the working fluid temperature at a temperature called the *turbine inlet temperature* (TIT). The

working fluid then expands through the turbine section, providing kinetic energy to the compressor and to the electrical generator. Gas turbines produce a net

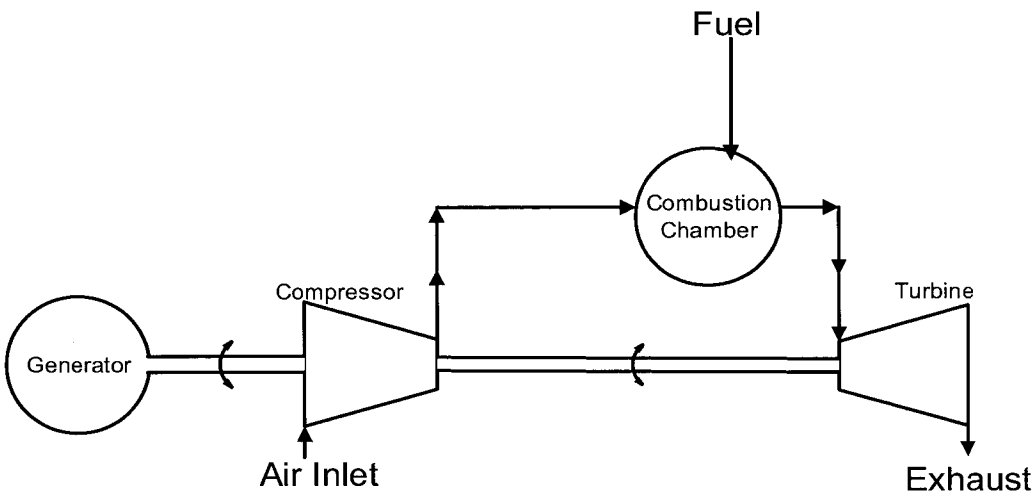

Figure 1-1: Simplified gas turbine schematic

mechanical power, as the power required to compress the working fluid through the compressor is much less than the power available from the expansion of the hot working fluid though the turbine.

Many methods can be employed to predict the performance of a gas turbine cycle. Provided suitable specifications are known, one can reasonably estimate this performance with hand calculations. This estimation involves determining the pressures and temperatures at each location with the help of assumed efficiencies of the compressor and turbine. Reasonably accurate results can be achieved with this method, even though assumptions of ideal gas, constant specific heats with temperature and pressure are used. To increase the level of accuracy, a spreadsheet

or other software such as MATHCAD can be used. Software tools enable the use of variable specific heats with temperature, and an average ratio of specific heats. The average ratio of specific heats method will average the values from upstream and downstream of the compressor or turbine. This method works well when the working fluid is closer to an ideal gas; however, this is not the case in zero-emission semi-closed combined cycles, as the fluid composition is a mixture of carbon dioxide, water, oxygen, argon and other substances. Since the zero-emission semi-closed gas turbine combined cycle has a working fluid of variable composition, it was opted to use a tool which does not make the ideal gas assumption, and can handle variable specific heats with temperature and pressure for chemical mixtures.

Component efficiency assumptions and cycle configuration selection has been guided by the review of previous research. Cycles have been modeled in ASPEN PLUS 12.1, a commercially available code, and the modeling strategy has been validated against actual cogeneration plant data. Two zero-emission cycles have been optimized using the ASPEN code. Optimization validation and performance studies were also completed.

1.4 Overview

This thesis continues with a literature review of relevant past work in Chapter 2. Literature reviews on the subject of zero-emission semi-closed combined cycles

have been conducted in the past by other authors. An example of such a review is Zhou and Gauthier (1998). The goal of Chapter 2 is to serve as an up-to-date rendition of such reviews, focused solely on low- and zero-emission gas turbine cycles, mainly of the oxy-fuel combustion variety. Chapter 3 introduces the software, ASPEN PLUS 12.1 (ASPEN), which was used to conduct the cycle analyses. Also in Chapter 3 is a section giving the results of a validation exercise where an open-cycle cogeneration plant was modeled. Chapter 4 presents details about the cycle configurations for the two zero-emission semi-closed cycles which are the main models under study in this thesis. Chapter 4 also covers model details, such as specifications, component efficiencies, loss assumptions, and fuel composition. Specific details are presented for how each component was simulated in the ASPEN software. Details about the optimization of the cycles are presented in Chapter 5. The cycles were studied by parametric analysis before optimization was attempted, and the resulting charts are presented before the final optimized performance figures. Chapter 6 looks further into the cycles, reviewing the effects of oxygen and fuel purity, excess oxygen, working fluid composition, and steam power augmentation on the cycle. Chapter 7 presents the findings of the investigation into using the Solar Turbines Mercury 50 as the basis for a zero-emission semi-closed O_2/CO_2 cycle. Chapter 8 summarizes the conclusions from the present research and summarizes the recommendations for future work.

Chapter 2 – Review of Previous Work

2.1 Zero-Emission Cycles - Background

This thesis is an investigation of the performance of zero-emission O_2/CO_2 semi-closed gas turbine combined cycles. The cycles under investigation use fossil fuels. Fossil fuels will continue to be the energy source of choice for power generation cycles in the near future. The attraction of zero-emission cycles is that no atmospheric emissions are produced from the combustion process.

When fossil fuels are burned, the products of combustion are typically emitted to the atmosphere. These products are mainly carbon dioxide and water, but also typically include carbon monoxide, sulphur oxides, and oxides of nitrogen. Carbon dioxide emissions from the burning of fossil fuels are causing an abnormal rise in the carbon dioxide concentration in the atmosphere. The change in

concentration of atmospheric carbon dioxide affects the flow of energy between the earth and space. The earth emits energy in two forms: solar radiation and thermal black body radiation (Wikipedia, 2006). Solar radiation accounts for 30% of the Earth's total radiation (Wikipedia, 2006). The remaining 70% is thermal black body radiation (Wikipedia, 2006). The wavelength at the peak output of the Earth's thermal black body radiation is 10 microns (Wikipedia, 2006). This peak output at wavelengths of 10 microns lies within the range of 8 microns to 15 microns, over which the Earth's atmosphere is largely transparent to radiation (Wikipedia, 2006). Carbon dioxide absorbs radiation in certain bands of wavelengths in the important range between 8 microns and 15 microns. With the increase in carbon dioxide concentration, the Earth's atmosphere retains more energy. Thus, the atmospheric temperatures rise. This is what is known as the greenhouse effect. Zero-emission cycles do not emit their carbon dioxide to the atmosphere. In zero-emission cycles, the water is separated from the exhaust gases, which then allows the carbon dioxide to be completely captured. Thus, the ideal zero-emission cycle emits none of the products of combustion. This results in the collection of carbon dioxide which can be used for other purposes, or disposed of in a manner which keeps the carbon dioxide from entering the atmosphere, referred to as sequestering.

The focus of this thesis is one type of zero-emission cycle; the zero-emission semi-closed O_2/CO_2 gas turbine combined cycle. It must be shown where this cycle

fits on the spectrum of low- or zero-emission fossil fuel cycles. Low- and zero-emission cycles can be divided into three approaches: (A) post-combustion decarbonisation, (B) pre-combustion de-carbonization, and (C) oxy-fuel combustion. Oxy-fuel combustion cycles include semi-closed loop cycles, chemical looping cycles, and fuel cell cycles. All of methods (A), (B), and (C) can be applied to plants which burn natural gas or coal. All of methods (A), (B), and (C) have the potential to capture 100% of the carbon dioxide generated during combustion, thus earning the name *zero-emission cycles*. However, some cycles will only become zero-emission at a large cost. The present study focuses on the optimization of type (C) oxy-fuel combustion semi-closed loop cycles, in which the primary working fluid is carbon dioxide, thus facilitating direct sequestration. A high-level review of other popular concepts will be presented. Each division of cycle type is described below:

(A) Post-Combustion Decarbonisation Cycles

Post-Combustion Decarbonisation involves post processing the cycle's working fluid in order to reduce the undesirable emissions. In this case, the emission targeted for reduction is carbon dioxide. There are four methods for the reduction of carbon dioxide: chemical absorption, physical absorption, cryogenic fractionation, and membrane separation (Bolland and Sæther, 1992). Fulkerson et al. (1990) reported that chemical absorption, specifically amine scrubbing, is the most energy efficient method. Amine scrubbing is most effective when the targeted emission is

low in concentration. In open-cycle gas turbines, the carbon dioxide concentration in the exhaust stream is low. Gas turbines operate with a fuel-to-air ratio which leaves much of the oxygen from the air in the exhaust flow. An open-cycle gas turbine entrains about 0.05% (mass) of carbon dioxide from the atmosphere (Keeling et al., 2003). As such, in a typical open-cycle gas turbine, the level of carbon dioxide in the exhaust stream increases from about 0.05% (mass) to about 5% (mass) (TransCanada Log, 2000). Most scrubbing systems remove at least 85% of the carbon dioxide. A scrubber system can be employed using a direct contact circulating amine. Scrubber systems require a heat source, a cooling flow, and mechanical power for circulation. The fluid to be scrubbed is brought into direct contact with the amine. The amine binds the carbon dioxide and the rich amine is sent to a stripper column where it is heated and the carbon dioxide is released (Yeh et al., 2000). It has been estimated that the efficiency penalty to a combined cycle plant by an amine cleanup unit removing carbon dioxide is 8% points relative to a particular open cycle with no emissions reduction systems (Möller et al., 2003). Amine scrubbing is a mature technology for chemical plants; however, in power plants, the economics are such that plants allow up to 15% of the carbon dioxide to remain in the plant's exhaust stream. Thus, alternative cycles are under investigation.

(B) Pre-Combustion Decarbonisation Cycles

In Pre-Combustion Decarbonisation, the carbon dioxide is captured before burning the fuel (Eide and Bailey, 2005). The decarbonised fuel has a high concentration of hydrogen and can be burned in the presence of air. The process of generating decarbonised fuel from natural gas requires heat and steam. Natural gas enters the system and two reactions take place with the result being the formation of decarbonised fuel and carbon dioxide. The reforming process uses the following reactions (Corradetti et al., 2004):

$$CH_4 + H_2O \Leftrightarrow CO + 3H_2 \quad (1) \qquad \Delta H = 206.11\,kJ/mol$$

$$CO + H_2O \Leftrightarrow CO_2 + H_2 \quad (2) \qquad \Delta H = -41.17\,kJ/mol$$

The carbon dioxide is separated from the hydrogen by means of pressure swing absorption. The decarbonised fuel is then sent to the combustor and burned. The combustion occurs in a cycle which is open to atmosphere and thus creates undesirable emissions, for example, oxides of nitrogen. It is not classified as a zero-emission cycle; however, it can be made zero-emission at a large cost. For a specific theoretical case using a turbine inlet temperature of 1523 K (1250°C), it was found that the overall efficiency penalty in comparison to a natural gas fuelled combined cycle would be near 11% points, resulting in a 47% overall thermal efficiency when reducing carbon dioxide emissions by 90% (Kvamsdal et al., 2002). Similarly, using a turbine inlet temperature of 1623 K (1350°C), Corradetti et al. (2004) found that

one can expect plant overall thermal efficiencies as high as 48% when reducing carbon dioxide emissions by 90%. Changing the cycle from open cycle to semi-closed cycle increases the emissions reduction from 90% to towards 100%. Using the same pre-combustion decarbonisation technology as Kvamsdal et al. (2002), and Corradetti et al. (2004) in a semi-closed loop and with the turbine inlet temperature is lower at 1523 K (1250°C), Cau and Cocco (2000) estimated a cycle overall thermal efficiency of 42% while producing zero-emissions.

(C) Oxy-Fuel Combustion Cycles

Oxy-fuel combustion cycles involve the combustion of fuel and oxygen in a nitrogen free environment. Oxy-fuel combustion cycles can be created around a gas turbine or fossil fuel fired boiler. Oxy-fuel combustion cycles generate the working fluid, carbon dioxide, as a result of combustion. The cycles require a fuel source and an oxygen source to do this. As the working fluid is generated it is captured, thus allowing the cycle to release no emissions. Research in gas turbine powered oxy-fuel cycles has been significant and increasing for the past 15 years, but began in the 1940s and 1950s (Boza et al., 2003) with research performed by Sulzer Brothers, Westinghouse, and U.S. Navy with the aim of increasing the stealthiness of submarines (Gasparovic, 1965). In the 1990s, efforts were made to update performance predictions of oxy-fuel cycles using state-of-the-art turbomachinery performance values, and new cycles were proposed. Recent investigations have

focused on performance improvements due to process modifications, such as an integrated liquefied natural gas fuel source (Zhang et al., 2003). Other work is focusing on quantifying the accuracy of various methods of turbine cooling (Jordal et al., 2003), modeling transients (Ulfsnes et al., 2003), and control (Imslad et al., 2004). This thesis is focused on gas turbine based oxy-fuel cycles, also referred to as zero-emission semi-closed O_2/CO_2 gas turbine combined cycles. These terms can be defined separately. *Zero-emission* means all emissions are captured by the cycle. Zero-emission cycles are theoretically feasible, and practical systems are near-zero emission. *Semi-closed* cycles differ from closed cycles in that mass is continuously added to and removed from the closed loop that is followed by the working fluid. Mass is added in the form of fuel and oxidizer that is injected into the combustion chamber. To maintain steady state, mass must then be removed at an equal rate elsewhere in the loop. In the case of the cycles under consideration, the mass is removed mainly in the form of CO_2 at the discharge of the compressor and water at the condenser. The term *O_2/CO_2* refers to the flue gas recycling process; where O_2 is and fuel are supplied to the combustor and the exhaust gas is recycled. The result is that at steady state conditions the working fluid is primarily CO_2. The term *gas turbine*, refers to *gas turbine engines*, which are the heart of the cycle. Finally, a *combined cycle* is a cycle made up of two or more cycles, for example, a gas turbine combined with a steam cycle.

A schematic of a zero-emission, semi-closed, O_2/CO_2 gas turbine combined cycle is shown for reference in Figure 2-1. The semi-closed cycle re-circulates the primarily carbon dioxide working fluid in a loop. The working fluid in the loop moves through the following components, starting from the compressor: compressor, combustion chamber, turbine, steam generator, condenser. Fuel and oxygen are injected into the combustion chamber in nominally stoichiometric proportions. As noted, high-purity oxygen is generated by an air separation unit. Figure 2-1 shows

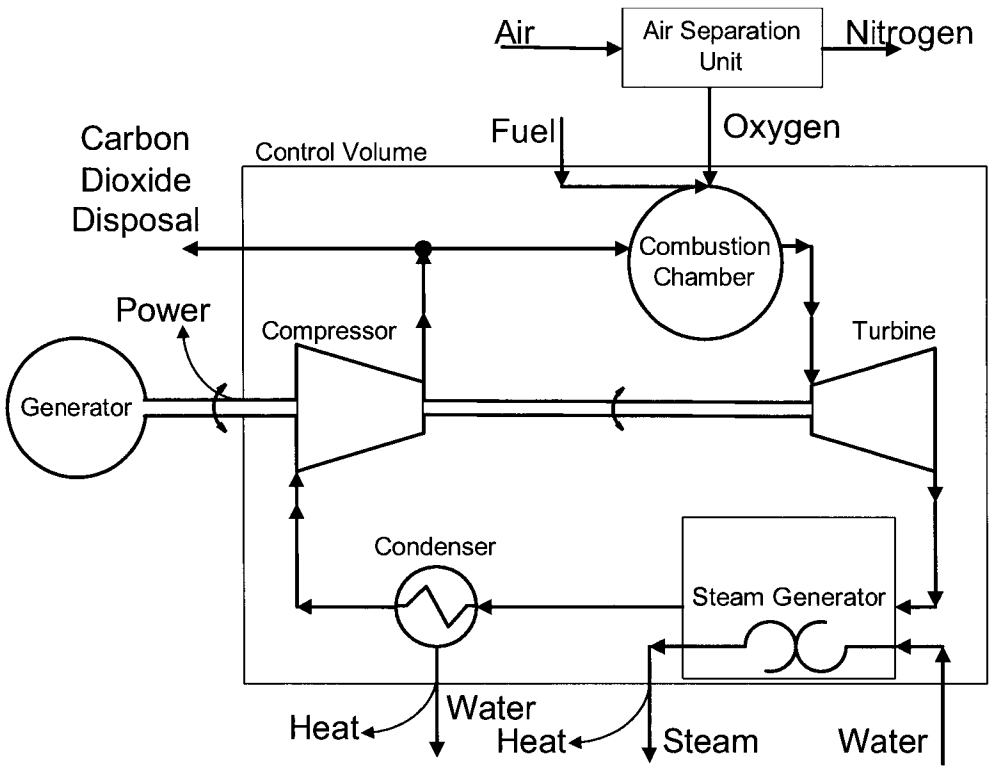

Figure 2-1: Cycle 1: Simplified schematic of semi-closed carbon dioxide/oxy-fuel natural gas combined cycle

the air separation unit supplying oxygen to the combustion chamber. After the combustion chamber, the high-temperature, high-pressure mixture of carbon dioxide and steam is expanded through the turbine. A shaft connects the turbine to the compressor and electrical generator. It is through that shaft that the mechanical work is transferred to those components. After the turbine, the pressure in the working fluid is slightly above the compressor inlet pressure, but the temperature is still high. The steam generator removes some of the energy from the hot working fluid and uses it to make steam. That steam can then be used to drive steam turbines and produce more electricity. The working fluid leaves the steam generator at a temperature that is still much higher than ambient temperature. To maximize the cycle efficiency, the temperature at the inlet to the compressor must be as low as possible. The condenser, which is located between the steam generator and the compressor, works to cool the working fluid to as close to ambient temperature as is practical. In the process of cooling the working fluid, the water generated by the combustion process is condensed and drained off. The working fluid leaving the condenser moves then to the compressor inlet. The compressor raises the pressure of the working fluid. As mass is added in the combustion chamber, some mass must be removed from the cycle. Water was removed in the condenser, but the additional carbon dioxide generated by combustion must also be removed. This can be done at various locations, but in Figure 2-1 the carbon dioxide is bled between the

compressor and the combustion chamber. It is done at this location to take advantage of the high efficiency of the main compressor. The optimum location for bleeding the carbon dioxide is different depending on whether or not further cleanup of the carbon dioxide is required, and if so, which method is used. Bleeding after the compressor is ideal if pressure swing absorption is to be used to increase the purity of the carbon dioxide. If the bled carbon dioxide is required to be at a higher pressure than the main compressor delivers, then an additional smaller compressor will be used. If amine scrubbing is to be used to increase the purity of the bled carbon dioxide, it is best to extract the carbon dioxide before the main compressor. Figure 2-1 also shows the main locations where power and heat leaves the cycle. Power is transmitted through the shaft to the generator. Heat is removed from the cycle in Figure 2-1 mainly by the steam generator and the condenser.

2.2 Zero-Emission O_2/CO_2 Semi-Closed Cycle - Previous Investigations

There have been a number of investigations which analyzed the performance of zero-emission oxy-fuel cycles over the past 15 years. Table 2-2, consisting of parts A and B, summarizes the most important contributions to the study of zero-emission semi-closed O_2/CO_2 gas turbine combined cycles. Many investigations

quantify the performance of semi- closed cycles by comparison with open-cycles. Thus, Table 2-2 also shows the types of open-cycles which were investigated. The table includes the reference, the type of investigation, the types of cycles investigated, some of the cycle specifications which were included in the paper, and the cycle performance in terms of overall thermal efficiency. A few abbreviations are used in Table 2-2. These are defined in Table 2-1.

Very little experimentation has been done due to the high cost associated with building and operating models of zero-emission gas turbines. Successful tests have been conducted on oxy-fuel combustors by Clean Energy Systems of the United States (Anderson et al., 2004) and one of the designs is being integrated into a 5 MW test plant near Bakersfield California (Hustad et al., 2005). Other future testing is planned in Norway (Hustad et al., 2005). All work presented in Table 2-2 is numerical with the exception of some of the material covered by Hustad et al. (2005).

The text following Table 2-2 will discuss the trends observed in Table 2-2. Discussion will be guided by the Table 2-2's headings, beginning with *Cycle Types*. *Cycle Specifications* follows, first for the gas turbine and then for the steam system. Lastly, *Performance* is discussed.

Table 2-1: Definition of abbreviations in Table 2-2

Abbreviation	Definition		Abbreviation	Definition
LNG	Liquified natural gas		NC	Natural circulation
N/A	Not applicable		OT	Once-through

Table 2-2A: Review of previous zero-emission O_2/CO_2 semi-closed cycle work

Reference	Cycle Types																								
	Open Cycles											Zero-Emission Semi-Closed Cycles													
	Simple Cycle	Simple Combined Cycle	Recuperative Combined Cycle	Reheat Combined Cycle	Scrubber	85+% reduction	Partial Recirculation	Absorption Refrigeration	Liquified Natural Gas Integration	Natural Gas Reforming Cooling	Simple Cycle	Recuperative Cycle	Intercooled Reheat Cycle	Simple Combined Cycle	Recuperative Combined Cycle	Intercooled-Recuperative Combined Cycle	Reheat Combined Cycle	Fired Rankine	Absorption Refrigeration	Fuel Decarbonization	Chemical Recuperation	Liquified Natural Gas Integration	Special Configuration
Bolland and Mathieu (1998)	-	√	-	-	√	√	√	-	-	-	-	-	-	√	-	-	-	-	-	-	-	-	-
Bolland and Sæther (1992)	-	√	-	-	√	√	√	-	-	-	-	-	-	√	-	-	-	√	-	-	-	-	-
Bolland and Undrum (1998)	-	√	-	-	√	√	√	-	-	-	-	-	-	√	-	-	-	-	-	√	-	-	-
Boza et al. (2003)	-	-	√	-	-	-	√	√	-	-	-	-	-	-	-	-	-	-	-	-	-	-	-
Cau and Cocco (2000)	-	√	-	-	-	-	-	-	-	-	-	-	-	√	-	-	-	-	-	√	√	-	-
Dillion et al. (2003)	-	-	-	-	-	-	-	-	-	-	-	-	-	√	-	-	-	-	-	-	-	-	-
Foley (2003)	-	-	-	-	-	-	-	-	-	-	-	-	-	√	-	-	-	-	√	-	-	-	-
Groom and Foley (2002)	-	-	-	-	-	-	-	-	-	-	-	-	-	√	-	-	-	-	√	-	-	-	-
Hustad et al. (2005)	-	-	-	-	-	-	-	-	-	-	-	-	-	-	-	-	√	√	-	-	-	-	-
Imslad et al. (2004)	-	-	-	-	-	-	-	-	-	-	-	-	-	√	-	-	-	-	-	-	-	-	-
Jackson et al. (2000)	√	-	-	-	-	-	-	-	-	-	√	-	-	-	-	-	-	-	-	-	-	-	-
Jordal et al. (2003)	-	-	-	-	-	-	-	-	-	-	√	-	-	-	-	-	-	-	-	-	-	-	-
Jerica et al. (2003)	-	-	-	-	-	-	-	-	-	-	-	-	-	√	-	-	-	-	-	-	-	-	√
Martinas-Frias et al. (2004)	-	-	-	-	-	-	-	-	-	-	-	-	-	-	-	-	√	√	-	-	-	-	√
Mathieu et al. (1994)	-	-	-	-	-	-	-	-	-	-	√	-	-	-	-	-	-	-	-	-	-	-	-
Mathieu et al. (2000)	-	-	-	-	-	-	-	-	-	-	-	√	√	-	-	-	-	-	-	-	-	-	-
Moller et al. (2003)	-	√	-	-	√	√	-	-	-	-	-	-	-	-	-	-	-	-	-	-	-	-	-
Moritsuka (2004)	-	-	-	√	-	-	-	-	√	√	-	-	-	-	-	-	-	-	-	-	-	-	-
Navaratnam (1994)	-	-	-	-	-	-	-	-	-	-	√	-	-	-	-	-	-	-	-	-	-	-	-
Sanz et al. (2004)	-	-	-	-	-	-	-	-	-	-	-	-	-	√	-	-	-	-	-	-	-	-	√
Sanz et al. (2005)	-	-	-	-	-	-	-	-	-	-	-	-	-	√	-	-	-	-	-	-	-	-	√
Ulizar et al. (1997)	-	-	-	-	-	-	-	-	-	-	-	-	-	√	√	√	-	-	-	-	-	-	-
Ulizar et al. (2000)	-	-	-	-	-	-	-	-	-	-	-	-	-	√	-	-	-	-	-	-	-	-	-
Zhang et al. (2003)	-	-	-	-	-	-	-	-	-	-	-	-	-	-	-	√	-	√	-	-	-	√	-

Table 2-2B: Review of previous zero-emission O_2/CO_2 semi-closed cycle work

Reference	Cycle Specifications: Gas Turbine: Turbine Inlet Temperature (K)	Gas Turbine: Compressor Pressure ratio	Gas Turbine: Turbine Cooling Flow (% of Compressor Inlet)	Gas Turbine: Carbon Dioxide Storage Pressure (bar)	Gas Turbine: Air Separation Unit Power (MJ/kg O_2)	Steam System: Type: Once-Through (OT) vs. Natural Circulation (NC)	Steam System: Maximum Steam Temperature (°C) HP,IP,LP	Steam System: Maximum Steam Pressure (bar)	Steam System: Condenser Pressure (bar)	Performance: Open Cycle Overall Thermal Efficiency	Performance: Semi-Closed Cycle Overall Thermal Efficiency	Comments
Bolland and Mathieu (1998)	1592	25-30	16.3	150	0.89	NC	562	106	0.04	47.5	44.9	Exhaust gas recirculation with amine scrubbing versus zero-emission semi-closed combined cycle
Bolland and Sæther (1992)	-	30	-	150	-	NC	-	-	0.15	44.6	41.4	Results for 5 operating modes of 3 cycles, Exhaust gas recirculation with amine scrubbing, fired Rankine cycle, and zero-emission semi-closed combined cycle
Bolland and Undrum (1998)	-	35	-	100	0.9	NC	-	-	-	51.1	48.1	3 Cycle concepts: Exhaust gas recirculation with amine scrubbing, zero-emission semi-closed combined cycle, and a pre-combustion partial decarbonization
Boza et al. (2003)	1623	-	-	N/A	N/A	N/A	N/A	N/A	N/A	62	N/A	Inlet refrigeration
Cau and Cocco (2000)	1523	30-35	-	-	-	-	-	-	-	46.5	42.4	Comparative analysis of zero-emission combined cycle with and without thermochemical recuperation
Dillion et al. (2003)	1662	-	-	110	-	-	600	-	-	-	44.7	Two cycles, one is applicable; with heat integration
Foley (2003)	1523	35	-	80	1.08	NC	566	138	0.06	-	44	Economic analysis
Groom and Foley (2002)	1523	35	-	80	1.08	NC	566	138	0.06	-	23,41, 44	Absorption chiller and steam system gives efficiency in the 41-44% range
Hustad et al. (2005)	-	-	-	7.5	-	NC	600, 945	150	0.15	-	44-46	Project nearing test phase
Imslad et al. (2004)	1597	19	-	-	-	-	-	-	-	-	-	Main focus is modeling and control
Jackson et al. (2000)	1550	17	6	-	-	N/A	N/A	N/A	N/A	38.7	33.9	Not a combined cycle
Jordal et al. (2003)	1580	19	-	-	-	N/A	N/A	N/A	N/A	-	37	Method of implimentation of turbine cooling to models; 3 methods compared
Jerica et al. (2003)	1673	40	-	-	0.89	-	-	180	0.25	-	55	GRAZ
Martinas-Frias et al. (2004)	-	-	-	145	0.79	-	1205	122	0.06	-	46.5	Fired Rankine
Mathieu et al. (1994)	1473	50	6	60	0.89	N/A	N/A	N/A	N/A	34.4	24.7	Simple cycles only
Mathieu et al. (2000)	1573	-	-	60	-	-	-	-	-	60	47	Not combined cycle
Moller et al. (2003)	1573	22	15-19	-	-	-	-	150	0.04	53.6	45.7	
Moritsuka (2004)	1973	55	-	-	-	-	-	-	-	66.7	N/A	High performance open cycle using air only
Navaratnam (1994)	1400	8.8	-	-	-	N/A	N/A	N/A	N/A	36.7	22-28	
Sanz et al. (2004)	1673	40	11.7	100	0.9	-	567	180	0.06	-	57.7	S-GRAZ
Sanz et al. (2005)	1673	40	13.7	100	0.9	-	549	180	0.041	-	52.6	S-GRAZ as above with mainly more conservative assumptions
Ulizar et al. (1997)	1473	-	-	60	-	-	-	-	-	-	43-46	Turbine inlet temperature = 1100 K for regenerative cycles. Regenerator effectiveness specified at 80%
Ulizar et al. (2000)	1650	56	-	60	-	-	-	-	-	-	36.7	Transient analysis work
Zhang et al (2003)	1523	25-100	-	-	0.9	-	-	-	-	-	60-65	Liquified natural gas synergy exploitation; a Brayton cycle and a supercritical Rankine cycle

Cycle Types

There are many cycle types which have been investigated in the primary references present in Table 2-2. Typically, the new cycles are compared with a known reference cycle, for example, the simple combined cycle. A number of papers compare open cycles using amine scrubbing for the reduction of carbon dioxide emissions to zero-emission semi-closed combined cycles using direct carbon dioxide capture, for example, the work of Bolland and Mathieu (1998), Bolland and Saether (1992), Bolland and Undrum (1998), and Cau and Cocco (2000). Each work showed the open-cycle method would achieve superior thermal efficiency to the semi-closed cycle method. However, the assumption was that the emission reduction target was 85%. The thermal efficiency of the open-cycles using amine scrubbing will further decrease as the emission reduction target is raised.

It is noted that a large number of zero-emission cycles use the simple-combined cycle configuration. The papers in Table 2-2 are those which this author found to most closely fit with the topic of the thesis. The simple combined cycle in semi-closed configuration has been modeled many times, and is often used as a reference cycle. Although there are 13 check marks (√) in the simple combined semi-closed cycle model, six were using the cycle as a reference cycle. These are Bolland and Saether (1992), Bolland and Undrum (1998), Cau and Cocco (2000), Jerica et al. (2003), Sanz et al. (2004), and Ulizar et al. (1997). The simple combined

cycle served as a reference cycle to a fired Rankine cycle (Bolland and Saether, 1992), a pre-combustion decarbonisation cycle (Bolland and Undrum, 1998), a pre-combustion decarbonisation by chemical recuperation (Cau and Cocco, 2000), a special configuration call GRAZ (Jerica et al., 2003 and Sanz et al., 2004), and a recuperative combined cycle as well as an intercooled-recuperative combined cycle (Ulizar et al. 1997). A similar grouping can be made under the simple semi-closed cycle title. These are cycles without bottoming cycles. Four groups of authors reviewed semi-closed cycles using simple cycle gas turbines: Jackson et al. (2000), Jordal et al. (2003), Mathieu et al. (1994), and Navaratnam (1994).

Some papers are included because they have potential applications to zero-emission semi-closed combined cycles. These include Boza et al. (2003), who investigated inlet refrigeration on a recuperative-combined open cycle. Compressor inlet refrigeration can be used to enhance the performance of zero-emission semi-closed combined cycles by lowering the compressor inlet temperature. Lowering the compressor inlet temperature reduces the power required by the compressor. The paper by Boza et al. (2003) was also included to demonstrate that recuperation has been considered in gas turbine cycles. Moritsuka (2004) was included to demonstrate the highest potential performance of open-cycle gas turbines operating in a combined cycle without emissions abatement. Moritsuka achieved 66.7% overall thermal efficiency using a reheat gas turbine, combined with liquefied natural

gas integration, natural gas reforming cooling, a compressor pressure ratio of 55 and turbine inlet temperature of 1973 K. The compressor pressure ratio of 55 is higher than any engines currently in production. Zhang et al. (2003) investigated liquefied natural gas synergy potential in zero-emission semi-closed intercooled-recuperative combined cycles. Using a turbine inlet temperature of 1523 K and pressure ratios up to 100, it was estimated that efficiencies in the 60 to 65% range were possible. Another paper showing great innovation was Martinas-Frias et al. (2004). This paper investigated a zero-emission fired Rankine type cycle. Fired Rankine cycles use steam as the main thermal ballast to limit the turbine inlet temperature. This paper used multiple turbines with turbine inlet temperatures as high as 1478 K. This turbine inlet temperature is 400 K higher than what many consider to be high for a steam system, which is 1073 K (800°C), and 600 K higher than average, which this author sees as 873 K (600°C). The cycle has the potential of achieving an overall thermal efficiency of 46.5%. Three papers discuss the GRAZ-type cycles: Jerica et al. (2003), Sanz et al. (2004), and Sanz et al. (2005). In the GRAZ cycle, carbon dioxide is mixed with steam in the combustion chamber. The flow leaving the combustion chamber is expanded through a gas turbine and is then used to make steam in a heat recovery steam generator. The steam leaving the steam generator is partially expanded through one steam turbine before being sent to the combustion chamber. The flow leaving the steam generator is then expanded through a low

pressure turbine and enters a condenser. In the condenser, the carbon dioxide is bled off and sent to compressors. Some of the carbon dioxide is removed from the cycle after the first compressor. The remaining carbon dioxide is sent to the combustor. The water leaves the condenser and is routed into the feed-water system for the steam generator. The Jerica et al. (2003) indicated that this configuration would perform at an overall thermal efficiency of 52.5% (Jerica et al., 2003). Sanz et al. (2004) detailed the S-GRAZ cycle, which is similar to the GRAZ cycle with the exception of increased steam content of the working fluid. In the GRAZ cycle, the working fluid is about 25% steam and 75% carbon dioxide. In the S-GRAZ cycle, steam content increases to about 62%, and carbon dioxide content falls to about 38%. Sanz et al. (2004) predict the S-GRAZ cycle would perform at an overall thermal efficiency of 57.7%. Subsequently, Sanz et al. (2005) indicated that a number of assumptions used in the earlier cycles were too optimistic. With revised component efficiencies, the overall thermal efficiency estimate for the S-GRAZ cycle dropped to 52.7%.

Cycle Specifications – Gas Turbine

When modeling gas turbine cycles, one key parameter which must be selected is the *turbine inlet temperature.* The turbine inlet temperature is a dominant factor in a cycle's performance potential. Table 2-2 shows a range of turbine inlet

temperatures from 1400 K (1127°C) to 1973 K (1700°C). The spread in turbine inlet temperatures causes significant spread in the performance results, making it difficult to compare results. Further discussion of turbine inlet temperature is presented in Chapter 5.

The compressor pressure ratio must also be selected for gas turbine modeling. Most of the compressor pressure ratio values in Table 2-2 are the optimum which was determined during the respective research. Some are fixed values as the authors chose to model a fixed set of parameters. This includes Imslad et al. (2004), Jordal et al. (2003), and Navaratnam (1994). The majority of compressor pressure ratios of Table 2-2 are in the range of 8.8 to 56. The exception is Zhang et al. (2003), who used pressure ratios up to 100 for the supercritical fired Rankine cycle. In the supercritical fired Rankine cycle by Zhang et al. (2003), carbon dioxide is circulated in the gas turbine semi-closed loop. The cycle differs from a Brayton cycle in the carbon dioxide compression process. In the supercritical fired Rankine cycle, the liquefied natural gas fuel passes through two heat exchangers before entering the combustion chamber. The heat exchangers serve to decrease the temperature of the carbon dioxide upstream and downstream of the compressor. The heat exchangers also vapourize the natural gas. The benefit is that the carbon dioxide is in liquid form after the second heat exchanger. Thus, the carbon dioxide can be raised to high pressures using a pump. After the pump, the carbon dioxide passes through a

recuperator. In the recuperator, heat transferred from the turbine exhaust vapourizes the carbon dioxide before it enters the combustion chamber. The carbon dioxide for sequestration is bled in liquid phase at the pump outlet, and thus requires no further compression as the pressure at that location is 100 bar. The integration of the vapourization of the liquefied natural gas fuel in the cycle reduces the amount of power required to compress the carbon dioxide. Reducing the compression power results in improved overall thermal efficiency at the site. The use of liquefied natural gas has the downfall that emissions are generated in its production. Benefits from liquefied natural gas are at the detriment of increasing emissions at another location. Further discussion of compressor pressure ratio is presented in Chapter 5.

Turbine cooling mass flow is another key parameter in gas turbine modeling. High turbine inlet temperatures are achievable due to a combination of coatings and component cooling. The turbine section components are typically cooled by pressurized mass flows bled from the gas turbines compressor. Various compressor bleed locations allow various cooling flow pressures. Cooling mass flows are parasitic to gas turbine performance, but the permitted increase in turbine inlet temperature is advantageous. Most authors indicated they have included cooling, but did not explain in detail how it was accounted for in the analysis. There are no simple accurate methods in which to include turbine cooling in a heat and mass balance simulation; therefore, methods of approximation are used. The challenges

lie with the mass injection location and imperfect mixing. Jordal et al. (2003) compared three methods for modeling turbine cooling. Two methods are appropriate for heat and mass balance software, while the third is more involved. Jordal et al. (2003) suggest that the effort required for the detailed method is best reserved for detailed gas turbine models. In Table 2-2, only four groups of authors specified the turbine cooling flow, typically as a percentage of compressor inlet mass flow used for cooling. Two groups of authors used 6% of the compressor inlet flow, while the two other groups used about of 16%. The turbine inlet temperatures used in the four studies ranged from 1473 K to 1592 K. Further discussion of turbine cooling is presented in Chapter 5.

The power required for generating the oxygen flow to the combustor, or air separation unit power, is a significant load on the plant cycle. Information on the power required for creating an oxygen flow seems to come from very few sources. The most often quoted is Smith and Klosek (2001). The air separation unit power requirement is dependent on purity specification. The air separation unit power requirements shown in Table 2-2 ranged from 0.79 MJ/kg O_2 to 0.9 MJ/kg O_2, corresponding to purity values from 95.0 % by volume to 99.5 % by volume. These values do not include the power required to compress the oxygen to combustor pressures. Further discussion of air separation unit modeling is presented in Chapter 5.

Cycle Specifications – Steam System

There are four cycle specification categories under steam systems. The first defines the steam generator configuration as either the natural circulation variety or the once-through variety. The second and third cycle specification for the steam system is the maximum steam temperature and pressure, respectively. The final steam system specification is the condenser pressure. Each of these will be discussed in turn.

All steam generators found in the references listed in Table 2-2 were natural circulation types, or they were not specified. Five of the investigations did not use any steam generator and are marked not applicable (N/A). Natural circulation steam generators are the most commonly installed steam generators in industry.

The cycle maximum steam temperatures vary from 822 K (549°C) to 1478 K (1205°C). The highest steam temperatures are employed in the fired Rankine cycles. In these cycles, the turbomachinery is representative of gas turbine technology. The working fluid is not pure steam; however, it is often more than 50% steam. The highest temperatures are not being generated by a waste heat steam generator, but in a combustor which uses water or steam to cool the products of combustion down to the turbine inlet temperature. The highest published waste heat steam generator steam temperature in Table 2-2 is 873 K (600°C).

The cycle maximum steam pressures vary from high to very high in the references in Table 2-2. The lowest maximum steam system pressure shown is 106 bar (1537 PSI), and the highest is 180 bar (2611 PSI). These pressures indicate that the cases presented in Table 2-2 are subcritical.

The cycles minimum steam pressures, which occur in the condenser, also vary considerably. The lowest minimum steam system pressure mentioned in Table 2-2 is 0.04 bar (0.58 PSI), while the highest minimum steam system pressure is 0.25 bar (3.6 PSI).

Performance

The wide array of main cycle specifications leads to a wide range of performance predictions. From review of Table 2-2, zero-emission semi-closed simple combined cycle can be expected to perform at overall thermal efficiencies around 41-48% based on lower heating values. Equivalent open cycles with scrubber technology to capture most of the carbon dioxide can be expected to perform at overall thermal efficiencies around 47-53% based on lower heating values. Zero-emission fired Rankine and GRAZ-type cycles have been predicted to perform at overall thermal efficiencies between 46% and 57% based on lower heating values.

Table 2-2 has been presented with the aim of summarizing detail on key papers in the areas of zero-emission semi-closed O_2/CO_2 gas turbine combined cycles. Some of the trends observed in the table have been pointed out.

2.3 Performance of Air Turbomachinery Operating in Carbon Dioxide

2.3.1 Differences Between Air and Carbon Dioxide

There is a significant knowledge base on the behaviour of turbomachinery operating in carbon dioxide. This includes, but is not limited to, studies by De Ruyck et al. (1993), Hunter (1994), Mathieu et al. (1994), Zhou and Gauthier (1998), Jackson et al. (2000), and Sjolander et al. (2003).

A discussion comparing the performance of a given turbomachine in air and in carbon dioxide must describe the differences between the fluids. These differences will be presented a few at a time.

Table 2-3 compares the values of specific gas constant, viscosity, and specific heat ratio for air and carbon dioxide. The viscosity and specific heat ratio are at standard conditions of temperature and pressure, 288 K (15°C) and 1.013 bar. In Table 2-3, carbon dioxide has a lower specific gas constant, lower viscosity, and lower specific heat ratio. The differences in specific gas constant, viscosity, and

specific heat ratio have implications when considering turbomachinery which was designed for one fluid but used in the other. The lower viscosity of carbon dioxide in comparison to air in Table 2-3 should help contribute to lower aerodynamic losses and an increase in component efficiency (Mathieu et al. 1994). The lower values of specific heat ratio

Table 2-3: Properties of air and carbon dioxide, with viscosity and specific heat ratio at ISO standard conditions of 288 K (15°C) and 1.013 bar (Reference: White (1994) and Turns (2000))

	Specific Gas Constant, R	Viscosity, μ	Specific Heat Ratio, γ
	J/kg-K	N-s/m^2	Unitless
air	287.1	1.78E-05	1.40
carbon dioxide	188.9	1.46E-05	1.29

and specific gas constant for carbon dioxide lead to lower sound velocities. Table 2-4 compares the speed of sound in air and carbon dioxide for various temperatures. Mathieu et al. (1994) caution that if a turbomachine is operated at a given rotational speed in air and carbon dioxide, the Mach numbers in the turbomachine will increase significantly when operated in carbon dioxide. At standard conditions, the sound speed in carbon dioxide is about 78% of the sound speed in air. Mathieu et al. (1994) suggest that the magnitude of change in Mach numbers will be indicative of a significant change in the flow characteristics in the turbomachine. Thus, it may be best to change the absolute speed such that the turbomachine is operating at the same non-dimensional speed parameter. The non-dimensional speed parameter is as follows:

Speed parameter, Π_N:

$$\Pi_N = \frac{ND}{a_{01}} = \frac{ND}{\sqrt{\gamma R T_{01}}} = \frac{N}{\sqrt{T_{01}}} \frac{D}{\sqrt{\gamma R}} \tag{2-1}$$

where N is the shaft rotational speed, D is the diameter of the machine, a_{01} is the sound speed based on the inlet total temperature, γ is the ratio of specific heats, R is the gas constant, and T_{01} is the total temperature at the inlet.

Table 2-4: Speed of sound in air and carbon dioxide for various temperatures (Reference: White, 1994)

Fluid:	Air	CO_2
Temperature	Sound Speed (m/s)	Sound Speed (m/s)
288 K (15°C)	340	266
573 K (300°C)	476	364
1273 K (1000°C)	695	531

At standard conditions, the density of carbon dioxide is more than that of air. The difference can be seen in Table 2-5. The density of carbon dioxide is shown in the Table as about 1.5 times the density of air. Mathieu et al. (1994) suggests that for identical turbomachine inlet conditions and speed, the result of the density is

Table 2-5: Comparison of fluid density for air and carbon dioxide at standard conditions of 288 K (15°C) and 1.013 bar

Fluid:	Air	CO_2
Temperature and Pressure	Density (kg/m^3)	Density (kg/m^3)
288 K (15°C) and 1.013 bar	1.225	1.862

increased mass flow rate, increased aerodynamic loads, and thus increased mechanical loads on the blades.

The specific heat ratio (γ) varies considerably with temperature. Figure 2-2 shows the variation of specific heat ratio with temperature at the absolute pressures of 1 bar and 15 bar for air, carbon dioxide, and water. Roberts and Sjolander (2005) have shown that the specific heat ratio is a criterion of similarity and that the

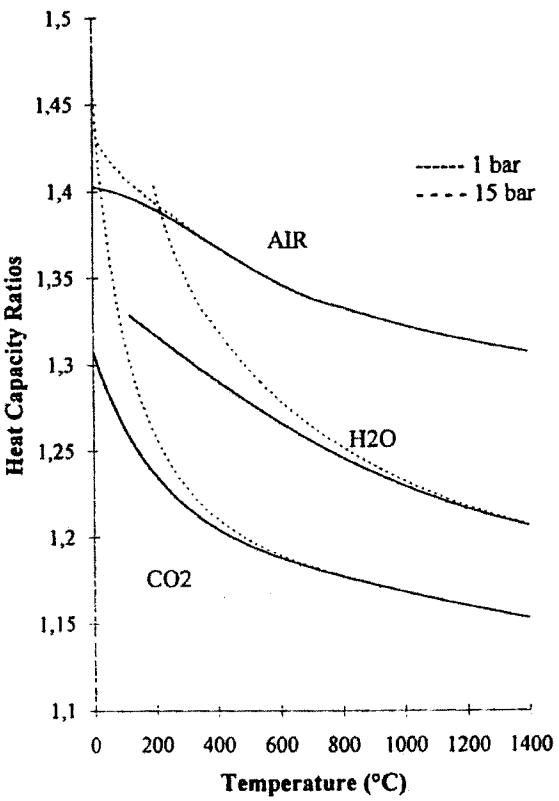

Figure 2-2: Specific heat ratio versus temperature for air, CO_2, and H_2O at 1 bar and 15 bar (Reference: Mathieu et al., 1994)

turbomachinery characteristic will vary as the γ of the working fluid varies even when the characteristic is appropriately non-dimensionalized. It is thus important to account for the changes in specific heat ratio with temperature in numerical simulation of turbomachinery. Mathieu et al. (1994) points out that in the lower temperature range, typically the compression range, that the specific heat ratio for carbon dioxide is more sensitive to changes in pressure than that of air. Another observation of Figure 2-2 by Mathieu el al. (1994) is that the 15 bar lines for carbon dioxide and air cross when the temperature approaches zero Celsius. Mathieu et al. (1994) summarizes the result of the commonly lower value of specific heat ratio for carbon dioxide than air as lower temperatures at the compressor outlets and higher temperatures at the turbine outlets for a given pressure ratio.

The specific heat capacity (C_p) for carbon dioxide also differs significantly from that of air. In a similar manner to the specific heat capacity ratio, C_p varies with temperature. Figure 2-3 shows the variation of C_p for air, carbon dioxide, and water. Mathieu et al. (1994) observed that below 250°C (523 K), C_p of carbon dioxide is less than that of air, and above 250°C (523 K) the reverse is true. Mathieu et al. (1994) suggests that these differences will affect the mass flow rate required to be bled from the compressor section to cool the turbine section of a gas turbine.

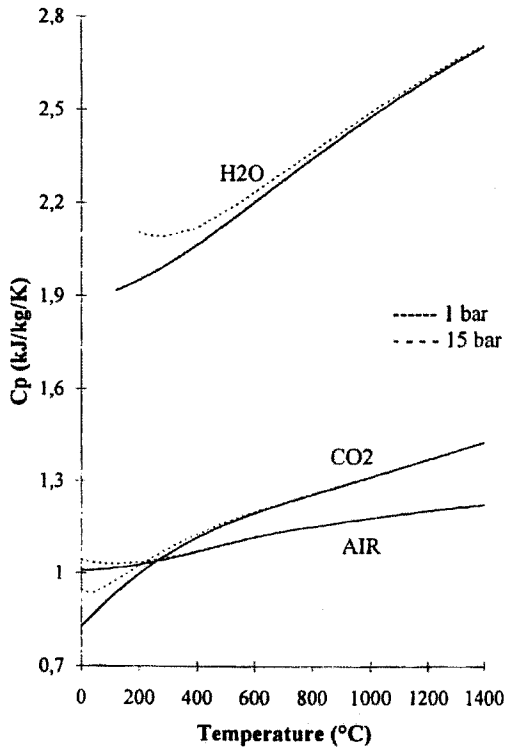

Figure 2-3: Specific heat capacity for air, CO_2, and H_2O at 1 bar and 15 bar (Reference: Mathieu et al. 1994)

2.3.2 Effects of the Differences Between Air and Carbon Dioxide on the Gas Turbine Matching

De Ruyck et al. (1993) discussed the matching of gas turbine turbomachinery components to be operated on carbon dioxide which were originally designed for use in air. A number of ideas are presented. De Ruyck et al. (1993) present that even if a compressor can operate using both carbon dioxide and air; it is possible that the gas turbine engine will not be able to operate on both fluids. De Ruyck et al. (1993) also

suggest that the differences in specific heat capacity ratio between carbon dioxide and air could yield Mach numbers at the turbine inlet which require a greater reduction in rotational speed greater than the Mach numbers at the compressor inlet. Thus, to keep the Mach numbers similar to the case of using air, the compressor and turbine may have to rotate at different speeds. This would require the two components to be on different shafts. De Ruyck et al. (1993) continue by suggesting that the matching of compressor and turbine has to be reconsidered for a given geometry and that the Mach numbers fulfill aerodynamic criteria limiting the losses. Also, the pressure ratio changes with the decrease of rotational speed and the associated impact on the compressor surge margin should be checked. The question of component matching in a specific zero-emission gas turbine is considered in Chapter 7 of this thesis.

2.4 Performance Effects of Water Injection and Steam Injection on Zero-Emission Semi-Closed Combined Cycles

Shan (2003) reviewed and compared zero-emission simple cycle and recuperative cycles in open and closed configurations using water injection. In water injection, water is injected into the combustion chamber. It was found that water-

injection favourably affected the thermal efficiency and specific work of the cycles. Shan (2003) suggests the favourable performance is due to the increase in turbine mass flow and the favourable expansion properties of the higher ratio of specific heats in the working fluid due to the addition of water. The turbine mass flow increases for two reasons. First, water injected into the combustor passes through the turbine. Secondly, water injected into the combustion chamber must be vapourized. Energy for vapourization of the water comes from the burning of the fuel, and thus the fuel flow must increase to produce identical turbine inlet temperatures. The increase in fuel flow increases the mass flow through the turbine.

All results of water injection are not positive. Shan (2003) suggests the performance improvements due to the above mentioned favourable changes in fluid properties and increases in turbine mass flow are offset by the use of heat from combustion to vapourize the injected water. The use of heat from combustion for vapourization and raising the temperature of the water sets a limit on the amount of water which can be injected. Injecting too much water into the combustor can extinguish the flame.

Shan (2003) also points out that the zero-emission semi-closed cycles using a carbon dioxide working fluid experience almost twice the performance increase due to water-injection than equivalent air cycles.

Shan (2003) concluded that steam-injection will yield performance increases in the gas turbine cycle even larger than water injection. Shan (2003) suggests two main reasons for this. Firstly, as mentioned above, water injected into the combustor must be vapourized and then heated to the turbine inlet temperature. When steam is injected instead of water, the requirement to evaporate the water inside the combustion chamber is no longer present. Thus, more energy from the burning of the fuel is available to generate power output. Secondly, the energy absorbed by the steam in the combustion chamber is partially captured as waste heat energy and used to generate more steam.

Shan (2003) investigated water injection in simple cycles of the open and semi-closed types, as well as recuperative versions of each. This thesis investigates steam injection in zero-emission semi-closed combined cycles and zero-emission semi-closed recuperative combined cycles in Section 6.6. The main differences between the investigations by Shan (2003) and Section 6.6 in this thesis is the addition of waste heat recovery and the limiting of the focus to semi-closed cycles using steam injection only.

2.5 Performance of an Advanced Open Cycle Using Air

A useful value when analyzing zero-emission cycles is the overall thermal efficiency of an air cycle of comparable technology. That is, it can be useful to

compare zero-emission cycles with those where no attempt is made at curtailing emissions. This value is useful because it can put into context the performance difference between cycles which generate emissions and those which do not. The zero-emission cycles studied in this thesis were selected to perform at a high overall efficiency. An appropriate basis for comparison is an air cycle of equivalent technology. These cycles generate the standard amount of carbon dioxide emissions. The performance values of several gas turbine combined cycles are presented in Moritsuka (2004). General Electric's 9H gas turbine is presented as a 1500°C (1773 K) Class machine, or machine with a turbine inlet temperature of about 1500°C (1773 K), which in combined cycle is anticipated to achieve 60% in overall thermal efficiency. Alstom's GT26, a 1300°C (1573 K) class machine, but with gas turbine reheat, is quoted as performing at 58% in overall thermal efficiency in combined cycle. Moritsuka (2004) estimates that with a new machine employing various high-performance technologies, including reheat, in-blade methane reforming, and inlet cooling for liquefied natural gas preheating, could achieve about 67% in overall thermal efficiency. In summary, an equivalent high-performance combined cycle using air will perform at around 60% in overall thermal efficiency with a 1500°C (1773 K) turbine inlet temperature, and additional refinements can further increase this value up to 6% points. The zero-emission cycles presented later in this thesis will be compared with the open cycle performance values presented above.

2.6 Bottoming Cycle Alternatives

2.6.1 Introduction

A bottoming cycle is a cycle which obtains energy from another. For the present thesis, a bottoming cycle is a steam cycle which recovers waste heat from the gas turbine cycle and converts it to additional output. A particular component of the steam cycle is the steam generator. There are different steam generators which can be employed in zero-emission gas turbine combined cycles. The alternatives fall into two main categories: (1) naturally circulating drum heat recovery steam generators, and (2) forced-flow once-through steam generators. Options for these two categories will be considered separately.

Steam generator options can also be categorized by the maximum pressure they use. These divisions are subcritical, supercritical, an ultra-supercritical. Subcritical units operate under 165 bar and 811 K (538°C). Supercritical units operate under 248 bar and 866 K (593°C) (Booras and Holt, 2004).

2.6.2 Heat Recovery Steam Generator (HRSG)

Drum type steam generators have been the industry standard for many years. Common options for the cycle include using two pressures, a high pressure (HP) and a low pressure (LP), or three pressures, an HP, intermediate pressure, and an LP; with or without reheat, and with or without recuperation. Yadav (2003) presented a

performance comparison of six configurations mated with an air breathing gas turbine. It was found that, in their optimized forms, a design using three pressures with reheat loops offered the highest efficiency. The other cycles followed closely.

2.6.3 Once-Through Steam Generator (OTSG)

Once-through steam generators are described by Andan and Tangney (2004) as steam generators using forced flow. The water is pumped directly through the exchangers and all water leaves as steam. This differs from a common heat-recovery steam generator in which temperature and hence density differences circulate the flow through the exchangers. In an OTSG, the location of evaporation moves backward or forward in the module depending on the conditions and the requested steam flow rate. Increasing the feed-water flow rate in the OTSG will result in an increase in steam production at lower steam temperatures. Typical OTSGs use high-temperature alloys which are resistant to damage in the cold section due to sulphur compounds in the turbine exhaust. As a result of using high-temperature alloys, it is suggested that the feed-water temperature can be lower than alternatives. The lower feed-water temperatures also result in lower OTSG gas outlet temperatures, greater waste heat recovery, and thus improved efficiency. On the other hand, lower feed-water temperatures can only be achieved using vacuum deaeration, or deaeration at condenser pressures. The use of high temperature materials also allows for increased steam temperatures, which also increases thermal efficiency.

2.7 Conclusions

It has been shown that zero-emission semi-closed O_2/CO_2 gas turbine combined cycles are grouped in the oxy-fuel cycle category. Oxy-fuel cycles achieve zero-emissions by burning fuel with injected oxygen in a semi-closed loop. At steady state, the additional carbon dioxide generated by the combustion is bled from the loop, captured, and is then not emitted to the atmosphere.

A table has been used to show the highlights of key papers. Some of the trends observed in the table have been discussed. All papers in the table present the results of numerical investigations. Review of the previous literature suggest zero-emission semi-closed simple combined cycles, similar to one of the two cycles investigated in this thesis, can be expected to perform at overall thermal efficiencies around 41-48%.

The primary differences between air and carbon dioxide have been presented. For the same temperature and pressure, carbon dioxide has a higher density, lower viscosity, and lower sound speed than air. The specific heat capacity for carbon dioxide is higher than that of air when the temperature is above 250°C (523 K). The specific heat capacity ratio for carbon dioxide is lower than that of air except when the temperature approaches 0°C (273 K) and the pressure is higher than atmospheric. These differences lead to challenges when attempting to design a gas turbine for use in carbon dioxide that reuses components which have been designed for air.

Different steam generator options have been presented for the zero-emission semi-closed gas turbine cycle. Once-through steam generators may offer performance advantages over naturally circulating types.

The maximum performance of air combined cycles has been briefly summarized. Generally, a high-performance gas turbine combined cycle using air should be able to achieve an overall thermal efficiency of near 60%. Use of additional technologies can increase this performance by up to another 6% points. The performance of combined cycles using air will be compared with the performance of the zero-emission semi-closed combined cycles presented later in this thesis.

Chapter 3 – Overview of ASPEN Plus 12.1 Modeling

3.1 Introduction

ASPEN PLUS 12.1 (ASPEN) is a code for modeling chemical plants developed by Aspen Technology, Inc. of Cambridge Massachusetts. The code was used in the present work to model the zero-emission power plant cycles.

This chapter introduces ASPEN and its modeling strategy. Model convergence strategies and optimization strategies are presented in sections 3.3 and 3.4. Property method selection is presented in section 3.5. Section 3.6 reviews effective trouble shooting strategies for gas turbine combined cycles. The results of a brief modeling validation study are presented in section 3.7. Section 3.8 discusses the appropriateness of ASPEN as software for modeling gas turbine combined cycles.

3.2 Introduction to ASPEN

ASPEN requires the user to be well versed in the system being modeled. ASPEN supplies the building blocks in the form of the components which need to be organized into the systems being modeled. One ASPEN component seldom performs the complete function of what is desired, but by combining a few components, the desired result can be achieved. The ASPEN modeling strategy is introduced in this section. Also presented are various ASPEN terms. The terms are written in italics at first introduction. Most terms in italics will be presented in greater detail in the sections which follow.

The introduction of ASPEN's modeling strategy is best started at the *block* level. *Component blocks* are placed on the *process flow-sheet*, and connected using *heat*, *material*, and *work streams*. A stream can be declared a *tear stream* when it is a stream which connects the ends of an open loop and completes a recycle loop. Once the flow-sheet is completed, the required information is entered using the *data browser*. The data browser allows access to the specification information which is part of each block.

When starting a new model, the interface requests the user to first specify the units and ambient conditions, then move on to specify all the chemical species which will be considered at any point in the model. Next, decisions must be made about *property methods*. Property method selection fixes the method which will be used in

determining material properties such as enthalpies, viscosities, and specific heats. Any stream which adds material to the system must be fully specified for temperature, pressure, mass flow, and composition. Work streams and heat streams are typically used as connectors between components and do not usually require specification beyond connection to the appropriate blocks.

Design specification blocks and *calculator blocks* are used to constrain the problem. Design specification blocks can be used to specify the operating parameters, such as the turbine inlet temperature in a gas turbine. A design specification block can be used to vary the fuel flow to the gas turbine to fix the turbine inlet temperature to the desired set-point. The correct fuel flow is not known, so a solver method must be used. The solver monitors one variable while manipulating another with the aim of achieving its target. Since the design specification block reviews a parameter, chooses a new parameter, and uses that parameter in the following iteration, design specifications are considered *feed-back* blocks. The solver varies one parameter and observes the results of the change, then further varies that parameter until the target value is obtained. The parameter supplied by the design specification block is for use in the future simulation iteration.

Calculator blocks differ from design specifications as calculator blocks are feed-foreward blocks. Calculator blocks can be used to specify a value directly or based upon calculations using information from anywhere in the model. The

calculator block is as useful as the design specification block even though the calculator block completes only direct calculations. An example use of a calculator block is to specify sufficient oxygen for complete combustion in semi-closed cycles; hence the calculator block will vary the oxygen flow rate proportional to the fuel flow rate, thus the calculator block is a *feed-foreword* block. The calculator block supplies information to the current simulation iteration.

Once the system has been completely defined, the simulation can be run with hopes of solution convergence. Results can be viewed in the *results* section of the data browser, which will show mass flow, compositions, temperatures and pressure of each stream. Plant performance properties can be calculated inside a calculator block and sent to the c*ontrol panel* for display. Further details on the ASPEN user interface are presented as Appendix A.

3.3 Convergence Methods

3.3.1 Sequential Modular Calculation Method

There are two primary types of calculation methods in ASPEN PLUS 12.1. They are called *Sequential Modular* (SM) and *Equation Oriented* (EO). SM is discussed in this section, while EO is discussed in Section 3.4.2. The SM method completes the calculations of each block sequentially. The solver sets up various

solving loops, depending on number tear streams, design specs, and single variable optimization blocks, and then progresses through each block one-by-one until the solution meets the convergence criteria. SM is the first mode of calculation; it must calculate each block at least once before the EO mode can be requested. There are a few convergence options for each of the tear stream, design spec, and optimization loops. For tear streams, one has the options of Weigstein, Direct, Broyden, and Newton convergence methods. When using a single design specification block, Secant, Broyden and Newton convergence methods are options. When the problem must use more than one design specification block, Broyden and Newton are options, and for tear streams and design specs in combination, one has the option of Broyden or Newton convergence methods. The optimization solver can be requested to use the Sequential Quadratic Programming Optimization Algorithm or the Complex Optimization Algorithm.

The solver method and calculation order can have a significant impact on problem convergence. For simple problems, the defaults should be satisfactory; however, once there is a combination of tear streams and design specs, one may have to select alternative methods and work with the tuning parameters in those methods. The ASPEN PLUS manuals make limited recommendations on the subject of solver tuning. If a flow-sheet will not converge at all it is probable that there is trouble with

the specification of the problem. It is easy to specify a system which will not operate properly.

3.3.2 Equation Oriented

The Equation Oriented mode is in many ways more robust than the sequential solver and capable of achieving great tolerances on the convergence criterion. For example, to achieve good performance from the Equation Oriented optimizer, convergence tolerances must be increased at all design spec locations. This may result in the SM solver reaching its default iteration count limit of 30 before convergence. The advantage of the EO mode is that it considers all system components simultaneously, solving the system of equations using analytical derivatives. The EO mode was found to converge in 10 iterations to a 10E-06 residual what the SM solver could not converge to a 10E-04 residual in 90 iterations. Both the SM and EO iteration count limits can be adjusted manually.

From time to time it may occur that the EO solution diverges after rapid convergence of the required initial SM solution. This may be due to a difference between the initial conditions for the SM and the following EO calculations. The best approach then is to first completely clear the EO Input form under the EO configuration tab in the data browser. While performing optimizations, specify in the EO input form the input values and the upper/lower limits for the optimized variables. The EO solution will fail if there is any slight difference between any

input values specified in the EO input form in comparison to those used in the SM convergence.

The Equation Oriented mode has many options for solver selection. At the highest level, there are three solvers to choose from; namely DMO, LSSQP, and NSOLVE. DMO and LSSQP are based on variants of the successive quadratic programming (SQP) algorithm. The SQP algorithm divides the problem into a series of quadratic sub-problems which can then be solved. NSOLVE solver uses a variant of the Newton-based algorithm. Only DMO and LSSQP solver can be used for optimization runs. Details and simplified explanations of each of the methods are given in Appendices B and C.

3.4 EO Optimization

Both Equation Oriented and Sequential Modular convergence modes have optimization capabilities; however, only the EO run mode can optimize multiple variables towards the maximization of a single objective function. As mentioned previously, only DMO and LSSQP solvers can be used during optimization runs, and they use variants of the SQP algorithm.

3.5 Property Methods

Property Methods refers to the methods of determining fluid properties such as enthalpy and ratio of specific heats. There are many methods to choose from. The method selected for gases in this thesis is the *Peng-Robinson* (PR) equation of state with *Boston-Mathias* (BM) modifications (PR-BM). For steam, the method called *NBS/NRC Tables* were adopted, which in ASPEN is titled STEAM-NBS. This makes use of the USA National Bureau of Standards/National Research Council (NBS/NRC) Steam Tables (Haar et al., 1984). The property method selections were based on ASPEN help-file recommendations. The property methods to be applied must be specified for each component. This is accomplished by selecting the appropriate property in the block options menu for each installed component.

Some property method selections suitable for use with semi-closed O_2/CO_2 gas turbine combined cycles were investigated by Yan et al. (2003), and Ulfsnes et al. (2003b). Ulfsnes showed that the Peng-Robinson equation of state performs with relative errors of similar magnitudes to the strong performing *Soave-Redlich-Kwong* (SRK) method when considering density prediction over a range of pressures. It was highlighted that SRK would not accurately predict dew-point temperatures. However, both models otherwise out-perform the ideal gas equation of state. Yan et al. (2003) compared two real-property models and two ideal-property models and demonstrate the shortcomings of the methods; however, the PR-BM method was not

one of their selected real methods. The Peng-Robinson method was presented in 1976 (Peng and Robinson, 1976) and the Boston-Mathias improvement was presented in 1980 (Boston and Mathias, 1980). Thus, the Peng-Robinson with Boston-Mathias improvement is one of the more recent equations of state.

3.6 Troubleshooting ASPEN Models

There are a few errors which can be mistakenly incorporated into models which will cause convergence trouble. The result is numerous error and warning messages appearing during simulation. Most error and warning messages do not help identify the true problem. Four particular problems that were encountered are discussed here:

(i) Two-Phase Flow

(ii) Insufficient Steam Generator Inlet Temperature

(iii) Feed-Water Pumps

(iv) Mixing Streams

(i) Two-Phase Flow

Consider first the gas turbine compressor which encounters two-phase flow. This occurs when there is significant humidity in the compressor inlet fluid. It is important to specify to ASPEN that it may encounter liquid phase, and should thus

perform calculations for vapour and liquid. In the instance where liquid phase exists and ASPEN is assuming vapour only, the simulation will not be stable. The same specification must be monitored in steam turbines, where specifying two phases is the best approach.

(ii) Insufficient Steam Generator Inlet Temperature

The second problem encountered is the modeling of heat-recovery steam generators and once-through steam generators. There are many ways to specify the heat exchangers which are the building blocks of the steam generator. Care must be taken to choose the best specification method for the given scenario. Considering a complete semi-closed cycle model which will not converge, the first likely culprit is the steam generator. First, verify that there is sufficient energy in the gas turbine working fluid to vapourize the boiler feed-water. This can be done by reducing the mass flow and the steam pressure until the solution converges. From that point, increase the mass flows and pressures to the levels where pinch-point errors and temperature-cross warnings arise. In the once-through steam generator configuration, temperature-cross warnings can be expected as the gas side and water side temperatures near the mid-point of the once-through steam generator module do approach one another. Pinch-point errors denote that the maximum available heat transfer has been reached. In some models, the calculation is slow to converge to the

correct exhaust gas temperature to the steam generator inlet. This is often the case when modeling recuperative gas turbines. The result is that the heat exchanger does not vapourize all the boiler feed-water. The mass flow control design specification block does not perform well in the situation where the feed-water is not vapourized. In order to ensure immediate vapourization of the feed-water, initialize the solution with as little as ten percent of the expected design mass flow of the feed-water, and allow the design specification control block to increase the mass flow appropriately.

(iii) Feed-Water Pumps

The third challenge is yet another steam system problem, this time involving the feed-water pumps. It was found that the feed-water pumps must have inlet temperatures which are below approximately 310 K (37°C) when pumping to high pressure. The feed-water must be suitably sub-cooled in order to remain in the liquid phase through the pump.

(iv) Mixing Streams

The final notable warning is to be wary when mixing streams. Mixing streams is done using mixing blocks. ASPEN chooses the outlet stream pressure of the mixing block as the lowest of the two or more inlet pressures. Situations may arise where ASPEN selects the stream pressure which was not the desired stream.

This can occur when the magnitudes of the pressures in the two or more streams may have been inadvertently changed. An example of this would be in a cooled turbine configuration, where the turbine inlet pressure of the downstream stage was matched to the cooling pressure instead of the previous turbine's outlet pressure. This can be fixed by increasing the turbine cooling stream pressure.

3.7 ASPEN Model Validation Using Actual Plant Data

3.7.1 Introduction

As a validation exercise, a cogeneration plant was modeled and the results compared with plant operating data. Data was provided courtesy of Duke Energy for two Siemens-Westinghouse W251B12A industrial gas turbines which are located at Duke Energy's McMahon Plant in Taylor, British Columbia, Canada. The units produce up to 58.5 MW each when at mechanical limit and generate electricity with a simple-cycle thermal-to-electrical efficiency of 34%. Each unit has its own respective two-pressure heat recovery steam generators operating at 425 psia and 70 psia. The plant supplies steam to the neighbouring 750 mmscfd natural gas processing facility, and exports electricity to the BC Hydro Grid.

3.7.2 Simplified Model of Gas Turbine

The gas turbine has a single shaft configuration with 19 compressor stages and 3 turbine stages. Cooling airflow is bled from the compressor's 9th and final rows, feeding to the disc cavities, 1st row stationary vanes, 1st row blades, and 2nd row stationary vanes. The simplified model mixes the cooling air into the main working fluid flow upstream of the stage which it cools.

3.7.3 Performance Matching Strategy

The turbine inlet temperature for the W251B12A gas turbines at this site is 1414 K (1141°C). With a complete set of operating data, the pressures and temperatures can be matched using the model. Beginning with the compressor, the efficiency must be varied to match the discharge temperature. With the pressure at the turbine outlet fixed along with the turbine inlet temperature, the turbine efficiency is then adjusted to produce the observed exhaust gas temperature. At this point, with the power output fixed, and provided the remaining assumptions are valid, the mass flow and thermal efficiency should match the supplied data. A similar approach can be taken for the heat recovery steam generator. In this case, with all the exchangers in the correct order, one simply matches the steam temperatures and attempts to match the mass flow. If the steam generator model is

reasonably accurate, it will show pinch point warnings and eventually errors with small increases in mass flow.

3.7.4 Assumptions

This model is heavily simplified, and most of the component efficiencies were estimated as part of the modeling process. As such, the assumptions list is short:

- Inlet filter pressure losses of 1.4" H_2O
- Inlet scroll losses assumed nil
- Exhaust Pressure losses of 7.0" H_2O
- Mechanical efficiency of 98%
- Total cooling flow of 7.35% of inlet flow
- Heat loss of 2% of exhaust duct temperature

The pressure losses are as measured during operation of the plant. The remaining assumptions are approximations.

3.7.5 Results

Varying the efficiencies of the compressor, turbine, and generator in order to closely match the operating data yielded the following efficiencies:

- Compressor: 88.2% Polytropic
- Turbine: 87% Isentropic

- Generator: 95.7%

These efficiencies are reasonable for the technology level of the given machine. Polytropic efficiency was used for the compressor because it was used in the research models. It was used in the research models because it is independent of pressure ratio.

The results from the ASPEN model compared with those for the actual plant are in Table 3-1. The model slightly under-predicts the required mass flow. This may be the result of not specifying a sufficiently high exhaust duct loss or inlet scroll loss, but also could easily be the result of measurement error. The model was created early in the author's experience with steam generator simulation. The actual plant steam system is much more complex than this model. It was attempted to model only the exchanger portions of the steam generator. The entire blow-down system, 20 lb steam system, deaeration system, and condensate return system were not included in this model. The blow-down system costs some energy and water in its aim of eliminating contamination from the system, but also recovers some steam in the process which potentially is measured. This could result in the exchanger flows being less than the values given. Elimination of the deaerator required a selection of inlet temperatures which are not immediately available. There is potential that these temperatures were under predicted. There are no 20 lb steam

exchangers in the HRSG's, thus that system is best neglected. The 2% temperature loss at the inlet to the steam generator to cover heat losses through the

Table 3-1: Simulation results: unit#2 operating data compared with model output data

		Unit#2	Model
Mass Flow	kg/s	166.92	164.83
Simple Cycle Efficiency		0.34278	0.34280
Compressor - Polytropic		---	0.8816
Turbine - Isentropic		---	0.8700
Generator		---	0.9572

walls of the steam generator may be too high. Also, the selecting of hot-in, cold-out temperature differences of 15 K, 20 K, or 25 K has a significant affect on the stack outlet temperature. It is possible that although the temperature difference was satisfactory in handling the steam flow, it may have been representing exchangers which are more effective than the actual units. The effort was not made to chase this discrepancy as the steam systems used in the research models are not natural convection/drum boilers, but are once-through steam generators.

3.7.6 Conclusions

This exercise was undertaken by the author for the purpose of inspiring personal confidence and familiarity in the ASPEN code. Modeling actual plants can be troublesome as the measured quantities are often imperfect due to probe location,

and mixing. Efficiency estimates from the manufacturer were not pursued as that would result in extensive discussions of degradation and component imperfections. This would add little value. The general conclusion is that ASPEN agrees with the data achieved in reality; that a simple cycle gas turbine with the given operating specifications will produce 53.7 MW at 34.2% thermal efficiency and a mass flow around 166 kg/s and that gas turbine is representative of the W251B12A. Since fuel energy, simple cycle thermal efficiency, power output, and other gas turbine temperatures and pressures are matched, it is the author's opinion that a 1.2% discrepancy in airflow shows strong performance agreement which instils confidence in the ASPEN code.

3.8 Discussion: ASPEN PLUS as a Gas Turbine Simulation Software

ASPEN PLUS is very capable of performing gas turbine combined cycle simulations; however, due to its complexity, the author recommends its use only for compelling reasons, such as determining a steady state working fluid composition, or desiring to adequately observe the effects of the working fluid composition.

Each phase of completing a project in ASPEN will be long and arduous for all but the most experienced users. This author found that coding in the design

specifications or calculator blocks, which worked well on the first day of install, would cease to function properly the following day, or at some point in the future when the model complexity had increased. The ASPEN learning curve will often have the user trying to implement an entirely elementary function and knowing that it is completely possible, but struggling to find work-a-rounds because the obvious method does not meet the intended purpose.

The model construction stage is complicated by the necessity to check every change for solution convergence. Once the model is completed, performing studies is never straight-forward. Most of the models which had a recuperator were not easily converged. Often all the calculator blocks and even the design specs must be deactivated, and reactivated one by one, while running the solver in between, in order to obtain convergence. This can significantly extend the time required to obtain results.

Two changes could be made to the ASPEN software which would make the software more appropriate for use in simulating gas turbines. The first would be the implementation of a multi-stage axial flow compressor with bleed capabilities in between any of the stages. The second change would be the means to handle a multi-stage turbine with cooling flow ports.

The author does not recommend this product for further use, and will not recommend this product in the future except for only the most specific problems. The product has an extremely steep learning curve and is not robust.

3.9 Conclusions

ASPEN PLUS 12.1 is a possible tool for performing gas turbine combined cycle plant simulations. It is best to be sure an extreme level of detail is required before selecting ASPEN PLUS 12.1 as the tool of choice. Alternative methods can produce similar results more efficiently.

Chapter 4 – Cycle Descriptions and Simulations

4.1 Introduction

This chapter presents the details which complete the background information required to build the cycle models. These details include cycle descriptions, cycle specifications, and assumptions on losses and component efficiencies. The assumed fuel-gas composition and the composition of the output stream from the air separation unit are also presented. Each block used in ASPEN to model the various components of the cycle is introduced and the method for specifying the models is explained.

Two zero-emission semi-closed cycle configurations were selected for investigation. The first, designated Cycle 1, is a simple-cycle gas turbine combined

with a heat recovery steam generator. The second, designated Cycle 2, adds recuperation, which serves to decrease the fuel requirement by transferring energy from the hot turbine outlet gases to the relatively cool combustor inlet gases.

In later chapters, portions of the systems will be referred to as *gas side* or *steam side*. The gas side is the working fluid loop which is filled by gas, or in this case mainly carbon dioxide. The gas side includes the compressor, the combustion chamber, the turbine, the gas side of the steam generator, and the cooling condenser. Steam side refers to the steam side of the steam generator, or any of the steam system components including the steam turbines, the steam condenser, and the boiler feed-pumps for the steam system. The only component with both gas and steam sides is the heat recovery steam generator.

4.2 Cycle Descriptions

4.2.1 Simple Gas Turbine in Combined Cycle with Once-Through Reheat Steam Generator

Cycle 1 is shown in Figure 4-1. Cycle 1 was based on the 2003-2004 Gas Turbine Project Advanced Design Team investigation (Bourgeois et al., 2004). Cycle 2 was created to examine the performance differences between a simple combined cycle and a recuperative combined cycle. There are other cycles which

could have been investigated. However, the focus has been on cycles which have the greatest potential to be built. Reheat gas turbines and regenerative gas turbines are operating, but they do not represent the bulk of the installed power generation gas turbines. The bulk of installed land-based gas turbines are simple cycle machines and simple cycle gas turbines combined with steam cycles. Many cycles are discussed in the literature review; however, most published zero-emission cycles are the simple combined type.

It is best to begin discussion of the gas side of the cycles by following the working fluid as it travels through the cycle starting at the compressor inlet. In Cycle 1, the working fluid exiting the condenser is a mixture composed of carbon dioxide and water vapour, with 100% humidity. This mixture enters the compressor at a pressure ranging from below to significantly above atmospheric pressure, and exits at a pressure 10 to 40 times higher, at a higher temperature. A mass flow of working fluid equivalent to the combined flows of the fuel and oxygen entering the cycle is bled from the loop at the compressor exit. This bleed flow is passed to a carbon dioxide compression train and compressed up to 80 bar. The remaining working fluid flows to the combustion chamber where some of the flow will enter the primary combustion zone and the remainder will enter further along to help anchor the flame and keep the combustor walls cool. The flame is burning natural gas which is injected through the fuel nozzle into the primary zone. The burning requires oxygen,

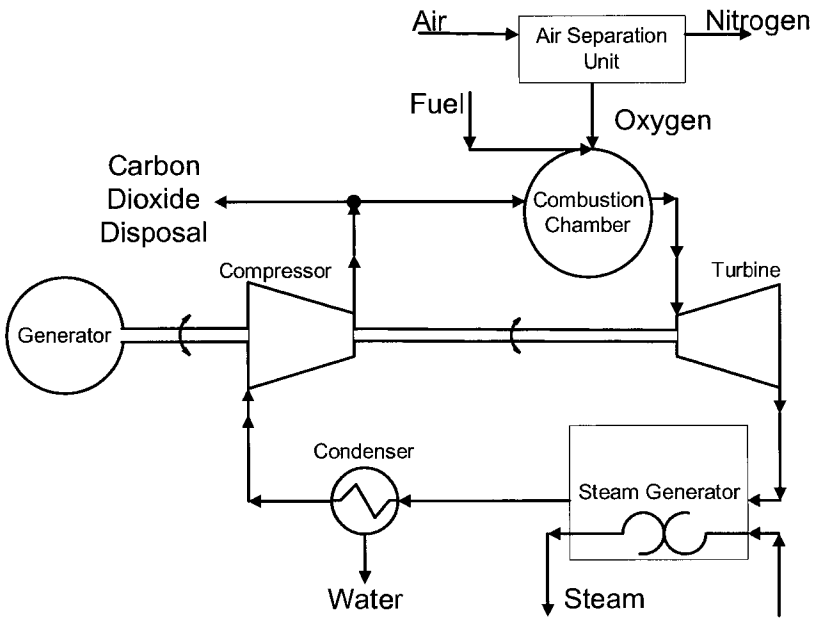

Figure 4-1: Cycle 1; Simplified schematic of simple gas turbine in combined cycle

and this will be injected around the fuel nozzle. The oxygen for combustion is separated from the atmospheric air by an air separation unit, and then passed through a compression train which raises the pressure of the oxygen to the value required for injection to the combustor. The combustor outlet flow will then expand through the turbine. This expansion process results in mechanical work which drives the compressor and the electrical generator. The flow exiting the turbine is at a reduced but still a high temperature. Some of this thermal energy is captured by using it to raise steam in the steam generator. The relatively cool gas flow then enters the condenser, where the mixture is cooled to near ambient conditions by cooling water, and water from the combustion process is condensed

4.2.2 Recuperative Gas Turbine in Combined Cycle Once-Through Reheat Steam Generator

A simplified schematic of Cycle 2 is shown as Figure 4-2. The process flow of Cycle 2 is similar to that of Cycle 1 with the exception of the change due to the recuperator. The recuperator is a non-contact heat exchanger which serves to pre-heat the flow entering the combustor using energy from the hot turbine exhaust gases. This change significantly alters the temperature of the working fluid at the combustor entrance and steam generator entrance.

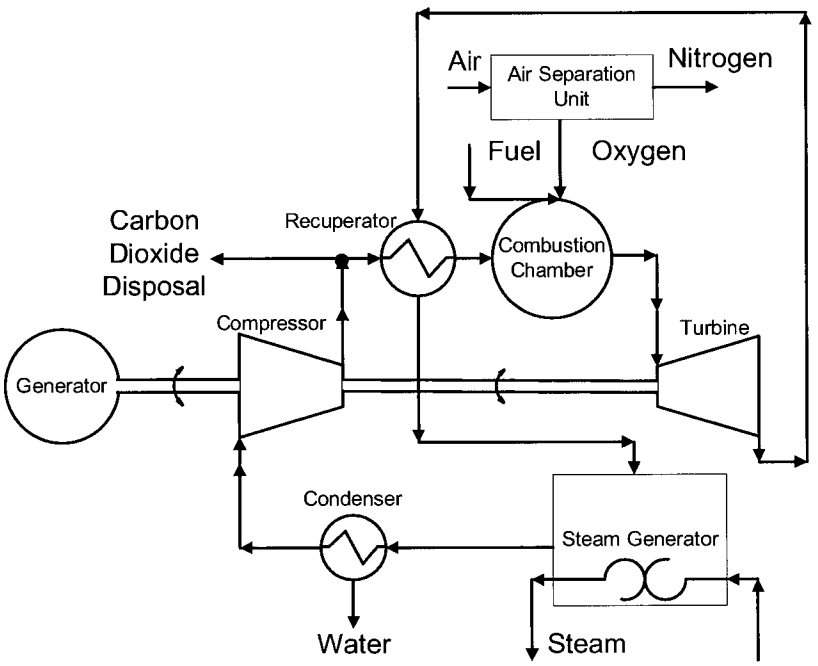

Figure 4-2: Cycle 2; Simplified schematic of recuperative gas turbine in combined cycle

Later sections will often refer to the *hot side* and *cold side* of the recuperator. The recuperator's hot side is the side containing flow which is to give up energy. In this case, the hot side flow is the flow from the turbine outlet. Similarly, the cold side is that which is about to accept energy. The recuperator's cold side flow has just exited the compressor, and will pass through the recuperator on its way to the combustion chamber.

4.3 Cycle Specifications

The overall plant size is to have an electrical power output of 100 MW. This size specification is a key factor to the component efficiency assumptions. The component efficiency assumptions are valid for specific component sizes only. As well, some technology choices will be made based on size. This may include the choice of the type of air separation unit technology. Typically, large machines are at an advantage due to their size. Large components can be more efficient, leading to a larger machine being the most efficient machine.

All cycle specifications are from a review of the following papers: Cau and Cocco (2000), Gabbrielli and Singh (2002), Kenny (2003), Yadav (2003), Bourgeois et al. (2004).

The specification must also include the temperature limits, or maximum cycle temperatures. These maximum cycle temperatures are some of the main factors

determining plant performance. There are two key temperatures in zero-emission semi-closed combined cycles. The first one refers to the temperature of the hot gas at the inlet to the turbine section, the *turbine inlet temperature*. The maximum turbine inlet temperature is based on material capabilities and the extent of cooling being used. The temperature is selected at a value which provides a balance of power and efficiency versus component life. Manufacturers are in a constant quest to find new materials, component coatings, and cooling schemes which allow higher turbine inlet temperatures. For this study, the design turbine inlet temperature was selected as 1723 K (1450°C). This value represents approximately the maximum value used in current industrial gas turbines (GTW, 2004). The effect of turbine inlet temperature on performance will be further discussed in Chapter 5, along with a comparison between the selected temperature and other current and previous gas turbines. The second key temperature limit is that for the steam turbine inlets. In a combined cycle plant, the steam systems are commonly large in comparison with the gas turbine system. This large size is permitted by employing one of the lowest cost materials which can meet the purpose, which is typically steel. The steel must contain steam at high-pressure. The strength of steel begins to decrease with increasing temperature. For this reason, high-pressure steam systems are typically limited to around 873 K (600°C). The steam generator selected for this thesis is constructed of an alloy. The steam generator is capable of producing steam at

temperatures in excess of 1073 K (800°C) (Tangney, 2005). To take advantage of this capability, the steam turbine inlet temperature limit is set to 1073 K (800°C). Steam pressures were limited to 165 bar.

Where needed, ambient conditions are taken as specified by the International Standards Organization (ISO): an ambient temperature of 288 K (15°C) and ambient pressure of 101.325 kPa. The cycles are semi-closed systems which have two low-point temperatures. The first is at the gas turbine compressor inlet, and the second is the steam system's condenser outlet temperature. Since the systems are not open to atmosphere, then heat exchangers determine the low-point temperatures. The heat exchangers must reject energy to the external environment by means of a cooling water source or cooling tower. The external environment is considered to be at the ISO temperature; however, it is anticipated that these plants will have access to a cooling water supply. It is assumed that for a 288 K (15°C) day, the cooling water source will be such that the compressor entry temperature and condenser outlet temperatures will be 298 K (25°C).

Similarly, the condenser temperature is set to 298 K (25°C). The condenser pressure is set to 0.1 bar.

Other specifications are summarized in Table 4-1. Air separation units producing two levels of oxygen purity were considered. For an air separation unit (ASU) producing 95.5 volume % (94.4 % by mass) oxygen, the primary energy cost

was assumed to be 0.87 MJ/kg of oxygen and that a steam energy flow rate of 65.51 kJ/kg O_2 would be required (Smith and Klosek, 2001). Smith and Klosek (2001) do

Table 4-1: Cycle specifications

Gas Turbine		
Power	100	MW net elec.
Turbine Inlet Temperature	1723	K
Compressor Inlet Temperature	298	K
Compressor Inlet Pressure	Variable (~0.5 to 4)	bar
Total Turbine Cooling Flow	6.2	% of inlet
Combustor Efficiency	Gibbs Free Energy - Unspecified	
Oxygen Purity	95.5 or 99.5	Vol. %
Steam System		
Max Acceptable Steam Temperature	1073	K
Max Acceptable Steam Pressure	165	bar
Reheat Steam Pressure	Not Specified	bar
Max OTSG Inlet Temperature	1089	K
Minimum OTSG Outlet Temperature	393	K
Minimum Steam Turbine Outlet Quality	93.5	%
Condenser Temperature	298	K
Condenser Pressure	0.1	bar
Heat Exchanger Hot In – Cold Out Temperature Difference	25	K
Auxiliaries		
Intercooler Hot In - Cold Out Temperature Difference	20	K
House Load (Lights, Etc.)	0	MW
Carbon Dioxide Storage Pressure	80	bar
Air Separation Unit, Delivery Temperature	298	K
Air Separation Unit, Delivery Pressure	1.01	bar

not describe how the steam is used in the process, but it is also mentioned that a significant amount of cooling water is required as well. The ASU producing oxygen

kJ/kg O_2 would be required (Smith and Klosek, 2001). The ASU producing oxygen at 99.5 volume % (99.4 % by mass) purity was assumed to require 1.088 MJ/kg of oxygen (Zanganeh et al, 2004) and a steam energy flow rate of 65.51 kJ/kg O_2. The steam flow is not specified by Zanganeh et al. (2004), but in making the low-purity oxygen and high-purity oxygen air separation units comparable, the steam requirement was added to the energy requirements of the high-purity oxygen air separation unit. Other authors specifying steam energy requirements for cryogenic air separation units were not found; however, the paper by Smith and Klosek (2001) is popular. Thus, this information was adopted as the basis for specifying the air separation unit.

4.4 Component Efficiencies

The component efficiencies of the rotating machinery are detailed in Table 4-2. All component efficiencies are from a review of the following papers: Cau and Cocco (2000), Gabbrielli and Singh (2002), Kenny (2003), Yadav (2003), Bourgeois et al. (2004).

The compressor efficiency is specified as a polytropic efficiency, rather than as an isentropic efficiency. Polytropic efficiency can reasonably be assumed to remain constant over a wide range of pressure ratios, whereas isentropic efficiency

Table 4-2: Rotating machinery efficiencies

Gas Turbine Efficiencies	**%**
Compressor (Polytropic)	91.0
Turbine (Isentropic)	89.0
Mechanical	99.0
Generator (Electrical)	98.5
Steam System Efficiencies	**%**
High Pressure Turbine (Isentropic)	90.0
Low Pressure Turbine (Isentropic)	90.0
Boiler Feed-Water Pumps (Isentropic)	76.0
Generators (Includes electrical + mechanical losses)	97.5
Electrical Drives (Includes electrical + mechanical losses)	95.0
Auxiliary Efficiencies	**%**
Oxygen Compressors (Isentropic)	78.0
Carbon Dioxide Compressors (Isentropic)	83.0
Electrical Drives (Includes electrical + mechanical losses)	95.0

inherently decreases with increasing pressure ratio. Thus, it is convenient to use polytropic efficiency in parametric studies in which the compressor pressure ratio is going to be varied. Unfortunately, the same argument can be made for the turbine efficiency; however, ASPEN PLUS 12.1 does not provide the option of specifying polytropic efficiency for a turbine. Definitions and further discussion of the terms polytropic and isentropic will be presented in Section 4.7.1. Electrical drive efficiencies are set to 95%. This estimate is an average between standard efficiency and premium efficiency motors in the medium voltage but large 300-5000 HP size category. The losses included are transformer losses, variable-frequency drive

losses, electric motor losses, and turbine mechanical losses. The generator efficiencies are set to 98.5%. The oxygen and carbon dioxide compressors have relatively low efficiencies because they are much smaller than the rest of the equipment. The efficiency of the boiler feed-water pump is set to 76%, which is typical of a centrifugal high-pressure water pump.

4.5 Loss Assumptions

Loss assumptions, such as duct pressure losses and heat losses, are presented in Table 4-3. Pressure losses are given in percent (%) of inlet total pressure. The heat

Table 4-3: Loss assumptions

Gas Turbine	**%**
Combustion Chamber Pressure Losses	5.0
Oxygen Injection Pressure Drop	20
Recuperator Pressure Loss – Cold-Side	1.5
Recuperator Pressure Loss – Hot-Side	1.5
Steam Generator to Condenser Duct	0.20
Condenser Hot-Side Pressure loss	2.0
Condenser to Gas Turbine Inlet Duct	0.80
Steam System	**%**
Steam Generator High Pressure - Cold Side Pressure losses(Steam)	5.0
Steam Generator Low Pressure - Cold Side Pressure losses(Steam)	5.0
Steam Generator Hot Side Pressure Losses	2.0
Exhaust Gas Duct Heat Loss (Temperature)	10 K
Auxiliaries	**%**
Oxygen Intercooler Pressure Losses	1.0
Carbon Dioxide Intercooler Pressure Losses	1.0

loss for the exhaust gas duct is assumed to correspond to a fixed temperature drop of 10 K. All loss assumptions are from a review of the following papers: Cau and Cocco (2000), Gabbrielli and Singh (2002), Kenny (2003), Yadav (2003), Bourgeois et al. (2004). No fuel injection pressure drop is specified. It is assumed that high-pressure natural gas will be available for a plant with an output of 100 MW.

4.6 Fuel Composition

The fuel considered in the simulations is natural gas (NG). Many different compositions for NG are possible. The composition available from Duke Energy's Union Gas website was selected (Union Gas Ltd., 2004). This composition is very representative of the fully refined gas which has low propane content and high methane content. The site only quotes higher-heating value (HHV) on a per volume basis. It is preferable to use lower-heating value (LHV) on a per mass basis because it provides a conservative efficiency estimate. The composition and LHV are shown in Table 4-4.

In the modeling, the fuel composition matching lower heating value as calculated for Table 4-4 was specified in ASPEN. The calculations for overall thermal efficiency were then calculated based on the lower heating value from Table 4-4.

Table 4-4: Selected natural gas composition and lower-heating value (LHV)

	Mole %
Methane	94.9
Ethane	2.5
Propane	0.2
iso - Butane	0.03
normal - Butane	0.03
iso - Pentane	0.01
normal - Pentane	0.005
Hexanes plus	0.005
Nitrogen	1.6
Carbon Dioxide	0.7
Oxygen	0.02
LHV Gas (MJ/kg)	**47.602**

4.7 Component Modeling

4.7.1 Compressor

The gas turbine compressor was modeled as three individual compressors, using polytropic efficiencies. There are two alternative methods available for specification of a compression or expansion process efficiency. These are *isentropic efficiency*, and *polytropic efficiency*. The isentropic efficiency is the ratio of isentropic power to actual power for a compressor. The term isentropic power refers to the quantity of power achieved when considering an ideal process, or a process which is reversible. Reversible processes show no entropy change. Entropy is a

measure of the availability of a fluid's energy (Taftan, 1998). Thus, the isentropic compressor efficiency is defined as the ratio of the shaft powers required to produce the same pressure ratio in the ideal and actual machines. Figure 4-3 shows this with distances labelled ideal and stagnation enthalpies, in alignment with Equation 4-1 (Saravanamuttoo et al., 2001).

$$\eta_c = \frac{\dot{W}_{ideal}}{\dot{W}_{actual}} = \frac{\dot{m}\Delta h_{0,ideal}}{\dot{m}\Delta h_{0,actual}} = \frac{\Delta h_{0,ideal}}{\Delta h_{0,actual}} \qquad (4\text{-}1)$$

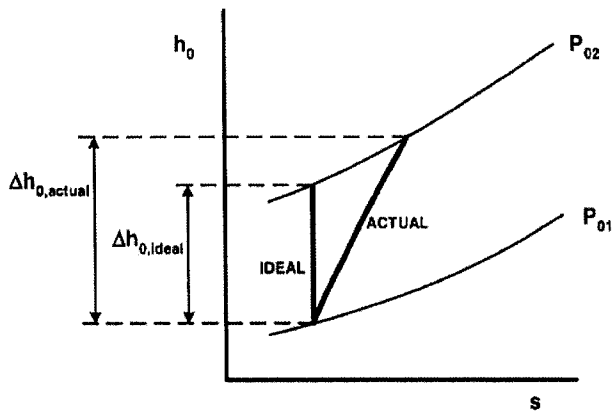

Figure 4-3: Ideal and actual stagnation enthalpies for a compressor on a stagnation enthalpy-entropy (h_0-s) diagram (Sjolander, 2003)

Assuming the working fluid to be a perfect gas gives $h_0 = C_p T_0$. It is common to show the isentropic efficiency of a compressor as follows:

$$\eta_c = \frac{C_p \Delta T_{0,ideal}}{C_p \Delta T_{0,actual}} = \frac{T'_{02} - T_{01}}{T_{02} - T_{01}} \qquad (4\text{-}2)$$

Also important is the relationship between pressures and temperatures in a compression process involving a perfect gas. For isentropic processes involving a perfect gas (Saravanamuttoo et al., 2001),

$$\frac{P}{\rho^{\gamma}} = const. \tag{4-3}$$

and as such:

$$\frac{T'_{02}}{T_{01}} = \left(\frac{P_{02}}{P_{01}}\right)^{\frac{\gamma-1}{\gamma}} \tag{4-4}$$

Figure 4-4 depicts the parameters in Equation 4-4 on a temperature-entropy (T-s) diagram.

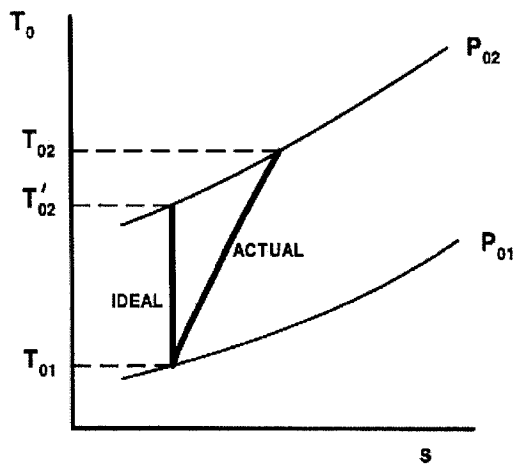

Figure 4-4: Temperature-entropy diagram for a compressor (Sjolander, 2003)

Polytropic efficiency is different than isentropic efficiency. In fact, isentropic efficiency varies with pressure ratio for both compressors and turbines. Figure 4-5

shows the trend of how an isentropic efficiency changes with pressure ratio. The concept of polytropic efficiency, η_∞, has been introduced to address this issue. The polytropic efficiency is defined as the isentropic efficiency of an elemental stage in the process such that it is constant throughout the whole process (Saravanamuttoo et al., 2001). For a compressor, the appropriate formulae are Equations 4-5 and 4-6, using numbering consistent with Figure 4-4. An explanation of the physics responsible for the trends shown in Figure 4-5 is available in Saravanamuttoo et al. (2001).

$$\eta_{\infty c} = \frac{dT_0'}{dT_0} = \frac{\ln(p_{02}/p_{01})^{(\gamma-1)/\gamma}}{\ln(T_{02}/T_{01})} \tag{4-5}$$

and

$$\frac{T_{02}}{T_{01}} = \left(\frac{p_{02}}{p_{01}}\right)^{(\gamma-1)/\gamma\eta_{\infty c}} \tag{4-6}$$

Polytropic efficiency is only valid if the machine can be considered to employ comparable technology and produce comparable performance as the pressure ratio is varied (Sjolander, 2003). For this reason, it should be applied only to explore the influence of pressure ratio on performance of multistage machines (Sjolander, 2003). It is assumed that the pressure ratio is varied by adding or removing comparable stages (Sjolander, 2003). It is more appropriate to use isentropic

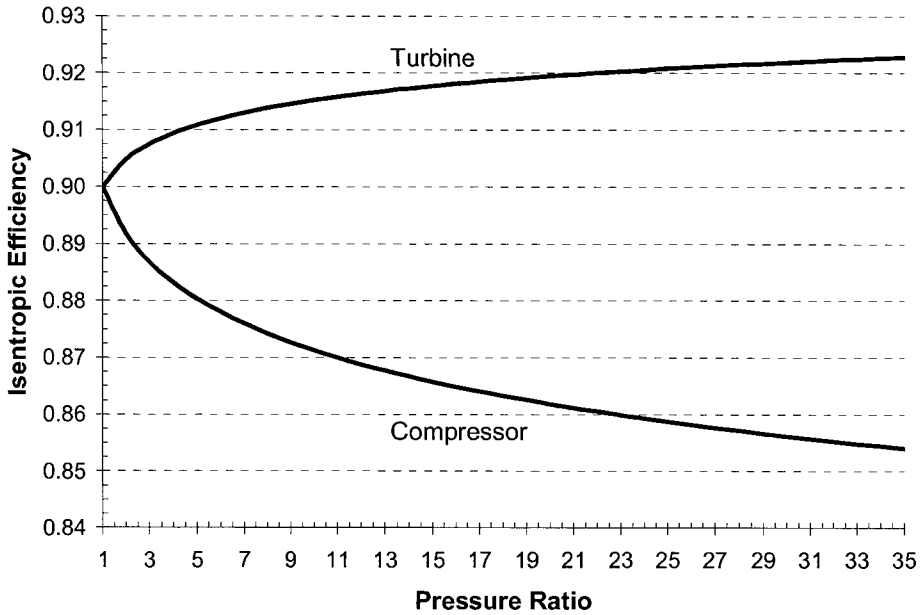

Figure 4-5: Variation of isentropic efficiency with pressure ratio for multi-stage compressors and turbines operating with a CO_2 working fluid

efficiencies when determining the performance of a single cycle of interest or analyzing engine test data (Saravanamuttoo et al., 2001).

There are three types of polytropic methods available for compressors in ASPEN; polytropic using the American Society of Mechanical Engineers (ASME) method, polytropic using the Gas Processors Suppliers Association (GPSA) method, and polytropic using piecewise integration. Polytropic using the ASME method was selected as it is the most rigorous of the three and is recommended in the ASPEN help file. Details on this method are presented in Schultz (1962). The method is similar to common polytropic, but with the addition of two compressibility

correction functions in addition to the commonly used compressibility factor Z, which are referred to as X and Y. The compressibility factor, Z, and the compressibility functions, X and Y, are defined in Equations 4-7, 4-8, and 4-9 (Schultz, 1962).

$$Z = \frac{P \cdot V}{R \cdot T} \qquad X = \left(\left(\frac{T}{V} \right) \cdot \left(\frac{\partial V}{\partial T} \right)_P \right) - 1 \qquad Y = -\left(\frac{P}{V} \right) \cdot \left(\frac{\partial V}{\partial P} \right)_T \qquad \text{(4-7, 4-8, 4-9)}$$

The title of Schultz's paper refers to centrifugal compressors, but the text goes on to state that the material is applicable to any compressor or turbine. The method was validated against centrifugal compressor data.

In ASPEN, fluid cannot be bled from the interior of a compressor. Fluid can be bled before or after a compressor. Thus, the only way to provide cooling air to the turbine, some of which is normally bled at interior stages in the compressor, is to use multiple compressors in series and bleed from between the compressors. The pressure ratio was not divided evenly among the compressors, as this would not lead to required pressures for the cooling gas. Half the pressure ratio is assigned to the first compressor, 3/10s of the pressure ratio is assigned to the 2nd compressor, and 1/5th of the pressure ratio is assigned to the 3rd compressor. This is more accurate than dividing the pressure ratio evenly among the three ASPEN compressor blocks, which would result in bleed pressures of 33%, 66% and full pressure ratio. Bleed

flow at 1/3 pressure ratio pressure is of little to no use. Bleed flow available 50%, 80%, and 100% of the overall compressor pressure ratio is more representative.

4.7.2 Combustor

The gas turbine combustor was modeled using an ideal reactor in combination with a heater block. The ideal reactor used is known in ASPEN as the RGIBBS reactor. The RGIBBS reactor uses the Gibbs Free-Energy method to determine the equilibrium composition of the mixture at the combustor outlet, and also the amount of heat release to the fluid. The released heat is transferred from the reactor to the heater block where the energy balance is completed. A detailed explanation of the Gibbs Free-Energy method can be found in Turns (2000).

4.7.3 Turbine

The turbine of the gas turbine side of the plant was modeled using the isentropic efficiency method as presented in Saravanamuttoo et al. (2001). The definition for the isentropic efficiency of a turbine is similar to that of the isentropic efficiency of a compressor as presented in Section 4.7.1. The formula is presented below as Equation 4-10 and is accompanied by Figure 4-6.

Cooling flow amounts were selected based on the 2004 undergraduate Gas Turbine Project report (McDowell, 2004). In McDowell's report, it was found that

6.2 % of total compressor inlet mass flow would be required for adequate cooling of the turbine section for a turbine inlet temperature of 1723 K (1450°C).

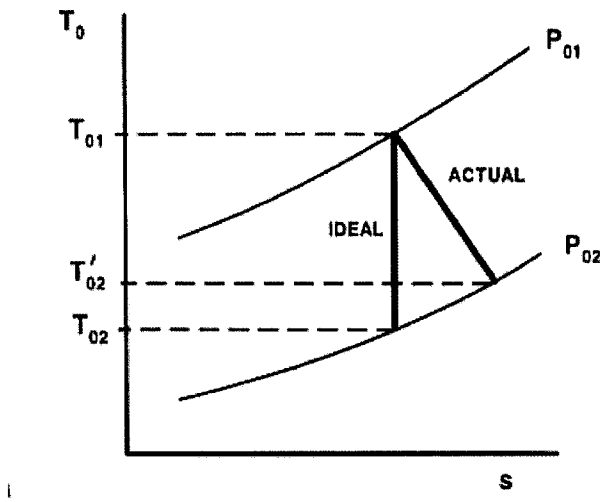

Figure 4-6: Temperature-entropy diagram for a turbine (Sjolander, 2003)

$$\eta_t = \frac{\dot{W}_{actual}}{\dot{W}_{ideal}} = \frac{\dot{m}\Delta h_{0,actual}}{\dot{m}\Delta h_{0,ideal}} = \frac{\Delta h_{0,actual}}{\Delta h_{0,ideal}} = \frac{T_{02} - T_{01}}{T'_{02} - T_{01}} \qquad (4\text{-}10)$$

The method of cooling integration into the turbine consisted of mixing part of the cooling fluid for that stage into the turbine inlet fluid stream upstream of the stage, similar to that described as method #2 in Jordal et al. (2003), but with a significant modification. The modification was to divert a portion of the cooling mass flow to downstream of the component which the flow was cooling. This

method was adopted because perfect mixing does not occur in a real turbine. The perfect mixing of cooling streams was resulting in a 70+K reduction in turbine inlet temperature upstream of the first stage nozzle. The modification results in the flow which is cooling the blades to be mixed after the blade row. The flow which is cooling the stationary vanes is mixed upstream of the vanes. This spreads out the temperature reduction due to cooling along more of the turbine section.

4.7.4 Steam Turbines

The steam turbines were specified using isentropic efficiencies. Turbine exit steam quality was monitored to ensure it stayed above 0.935. The low-pressure turbine exit pressure is fixed at the condenser inlet pressure of 0.1 bar.

4.7.5 Steam Generator

The steam generator selected for the models is of the once-through type. The once-through steam generator (OTSG) differs from a conventional drum boiler by its lack of reliance on natural circulation. The outlet steam temperature is controlled by varying the boiler feed-water flow rate. As the flow rate is changed, the location of vaporization will change along with the outlet steam temperature.

Although single-pressure OTSG's are normally adequate, the low steam quality at the turbine outlet for Cycle 2 necessitated the use of a reheat steam system. Cycle 1 was modeled with the same configuration to ensure comparability of the

cycles. The simplified model separates the carbon dioxide gas flow into two separate streams which pass through the low pressure (LP) and high pressure (HP) superheaters. From there, the gas streams mix and flow through the HP economizer as shown in the Figure 4-7. The HP and LP turbines of the steam system are not

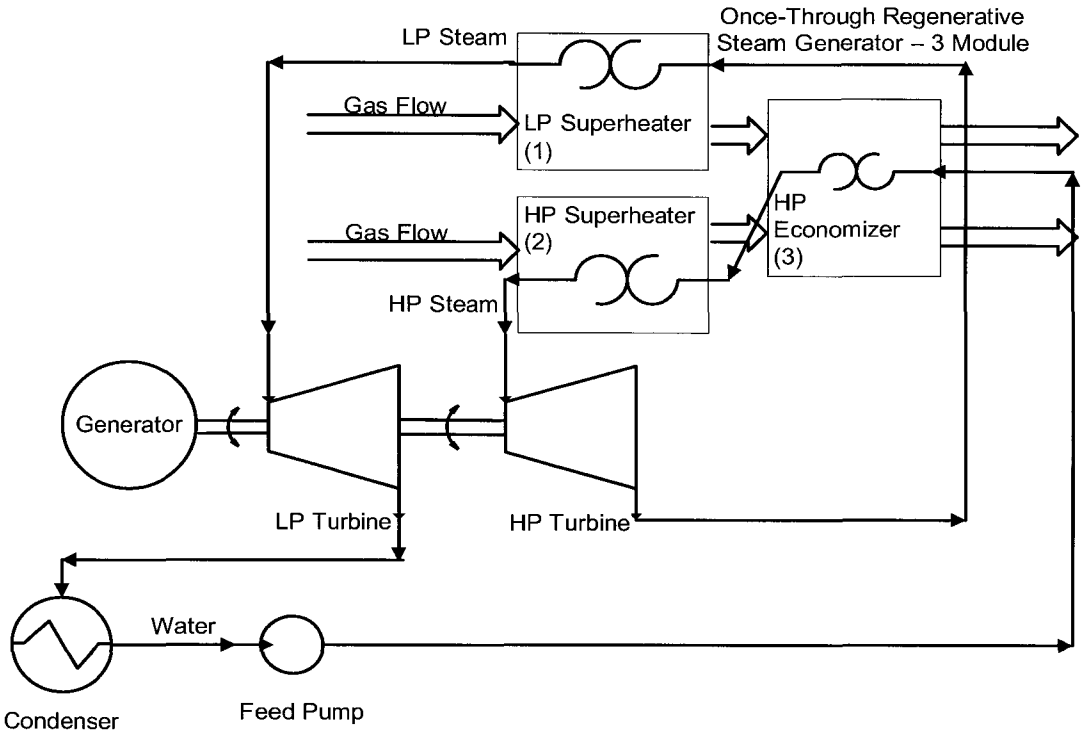

Figure 4-7: Simplified schematic of once-through steam generator and steam system

necessarily operating at the same speed, as this is an undesirable constraint for the design of the turbines. Since the mass flow for each of the turbines is identical, the LP steam turbine will have a much larger diameter than the HP turbine and must have a lower shaft speed in order to meet material stress limits.

Figure 4-7 shows 3 heat exchanger modules in the once-through steam generator (OTSG). Two of the heat exchangers are on the high pressure portion of the loop, while the third exchanger functions as the reheat module for the low pressure portion of the loop. These modules are a high-pressure superheater, high-pressure economizer, and low-pressure superheater. All the heat exchangers are specified identically using a hot-inlet, cold-outlet temperature difference of 25 K in countercurrent configuration. This results in the steam temperature at the OTSG outlet set to 25 K below the steam generator gas inlet temperature. The steam mass flow rate is varied in order to achieve a set steam generator gas flow exit temperature. For comparability between the cycles, the steam generator gas flow exit temperature was held constant at 393 K (120°C). This value was arrived at by reviewing the outlet temperatures of other OTSG configurations as described in Andan and Tangney (2004). In this paper, it was presented that with cold feed-water, a single pressure series OTSG configuration could achieve a gas outlet temperature of 427 K (154°C), while a dual pressure series configuration could achieve gas outlet temperatures as low as 368 K (95°C). The OTSG used in the models is in effect a parallel/series hybrid with a single continuous loop, which easily achieved predicted outlet temperatures of 370 K (97°C) during testing in ASPEN. A 25 K conservative bias was added to the dual pressure series gas outlet temperature results of Andan and Tangney (2004), thus arriving at 393 K (120°C).

These temperatures may be lower than what can be expected from a typical steam generator. They are achievable using cold feed-water at a temperature of 298 K. Using feed-water at this temperature is possible when employing vacuum dearation. Potential corrosion issues at the cold-end of the steam generator on the gas side are eliminated by the choice of alloy materials.

A steam generator will lose energy through its walls. To include this loss in the cycle models, a temperature reduction of 10 K was applied to the steam generator gas inlet stream. It was initially attempted to apply a temperature reduction factor to the stream within the code, but this method caused simulation instability and had to be removed. The root of the instability is that the temperature reduction factor is ignored during sequential modular (SM) initialization. This leads to a SM converged solution which gives a poor starting point for the equation oriented (EO) solver. If there are any changes when switching from the SM solver to the EO solver, the EO solution will diverge.

4.7.6 Recuperative Heat Exchanger

The recuperator is a non-contact countercurrent heat exchanger which transfers energy from the hot turbine outlet fluid to the cooler compressor outlet fluid. The raising of the combustor inlet temperature results in a reduction in the fuel requirement. The recuperator is modeled as a non-contact counterflow heat exchanger with a specified temperature difference between the hot-inlet and cold-

outlet of 25 K. This specification fixes the combustor inlet fluid to be 25 K below the turbine outlet fluid temperature. All of the methods available for specifying heat exchangers in ASPEN use temperature differences, or the fixing of absolute temperatures of outlets. These specification options are not compatible with specifying *Heat Exchanger Effectiveness,* which is the normal method of specifying heat exchanger performance. Heat exchanger effectiveness is defined as the ratio of the energy rate received to energy rate available for transfer, usually expressed as a percentage as follows; with Figure 4-8 showing the numbering scheme. The letter 'h' is to be read 'hot', and letter 'c' is to be read 'cold'. Equation 4-11 shows the definition of heat exchanger effectiveness (Saravanamuttoo et al., 2001).

$$\eta_{HE} = \left(\frac{\dot{m}_c \cdot C_{Pc} \cdot (T_{ch} - T_{cc})}{\dot{m}_h \cdot C_{Ph} \cdot (T_{hh} - T_{cc})} \right) \qquad (4\text{-}11)$$

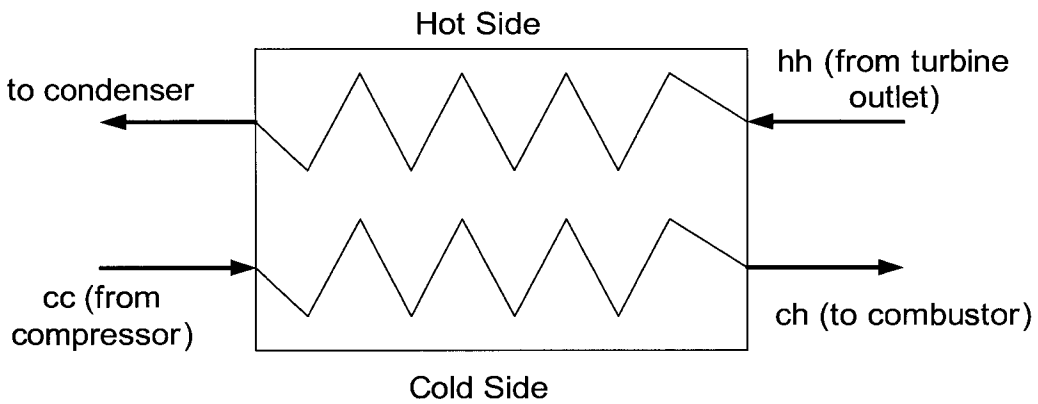

Figure 4-8: Ideal recuperator showing numbering scheme

In the calculation of heat exchanger effectiveness for gas turbines using air as the working fluid, the mass flow terms are sometimes neglected. In zero-emission semi-closed combined cycles, the mass flows cannot be neglected as they are not at all equivalent. In an air gas turbine, the difference in mass flows is a result of the fuel flow. The fuel is injected into the combustion chamber, which is downstream of the compressor. In a zero-emission semi-closed combined cycle, the fuel again contributes to the turbine mass flow being greater than the compressor mass flow; however, the oxygen flow is also injected into the combustion chamber. The zero-emission semi-closed combined cycle's turbine mass flow is greater than the compressor mass flow by the appropriate amounts of fuel and oxygen. Depending on the gas turbine engine's specifications, the turbine mass flow can be 20% greater than the compressor flow.

The specification of the heat exchanger by the hot-inlet, cold-outlet temperature difference of 25 K results in an implied heat exchanger effectiveness which varies with the specification of the cycle. The variation of heat exchanger effectiveness has been examined over the full range of pressure ratios and exhaust gas temperatures encountered in the cycle calculations. Figure 4-9 shows the variation of heat exchanger effectiveness with compressor pressure ratio for the turbine inlet temperature of 1723 K (1450°C). The heat exchanger effectiveness is seen to decrease with increasing pressure ratio. The trend is the result of the changes

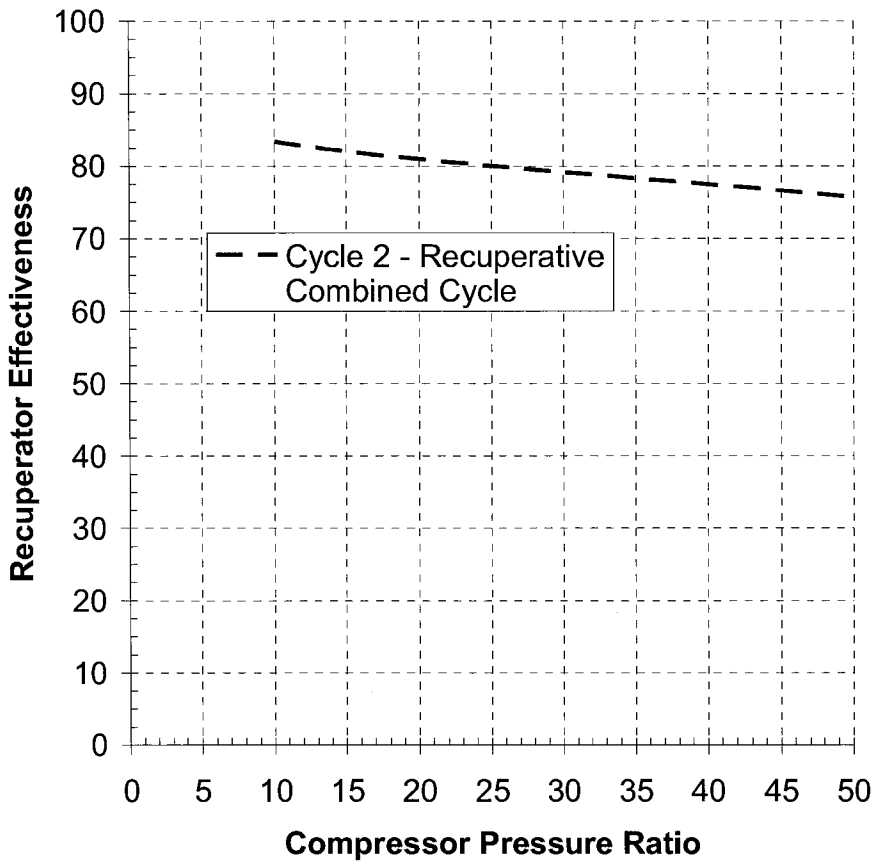

Figure 4-9: Recuperator effectiveness vs. compressor pressure ratio for constant hot-inlet, cold-outlet temperature difference specification of 25 K

in compressor discharge temperature and turbine outlet temperature with pressure ratio. As the pressure ratio increases, the compressor-discharge temperature increases and the turbine outlet temperature decreases. The turbine outlet temperature decreases because of the increased expansion while the expansion begins from a constant turbine inlet temperature. However, the difference between the combustor inlet temperature and the turbine outlet temperature is fixed at 25 K.

As the compressor discharge temperature increases, the recuperator effectiveness decreases. This is because the difference between the compressor discharge temperature and the combustor inlet temperature shrinks in comparison with the difference between the compressor discharge temperature and the turbine outlet temperature. The heat exchanger effectiveness value varies about 8% over the full range of compressor pressure ratios. This will affect the performance of the gas turbine, but the effect will be small over the range of primary interest. For example, later results will show the optimum pressure ratio to be in the 22.5 to 25 range. The range of concern then could be regarded as between compressor pressure ratios of 20 and 30, over which the heat exchanger effectiveness decreases from 80.9% to 79.1%. The effect on the overall cycle thermal efficiency will be smaller than the effect on the gas turbine thermal efficiency. An increase in the outlet temperature of the gas turbine corresponds to an increase in the steam generator's inlet temperature. Increasing the steam generator's inlet temperature increases the steam system's performance. It will be shown that changes in the temperature at the location between the gas turbine and steam system tend to balance one another.

Figure 4-10 shows the variation of implied recuperator effectiveness with turbine inlet temperature. The trend is not linear and appears to have a maximum at about 1450 K (1170°C). The reason for this is not clear. The recuperator effectiveness varies 5% over the entire turbine inlet temperature range considered.

Near the design point turbine inlet temperature of 1723 K, a 50 K change in turbine inlet temperature results in a 1.1% change in recuperator effectiveness. This change will have only a small effect on the overall cycle performance.

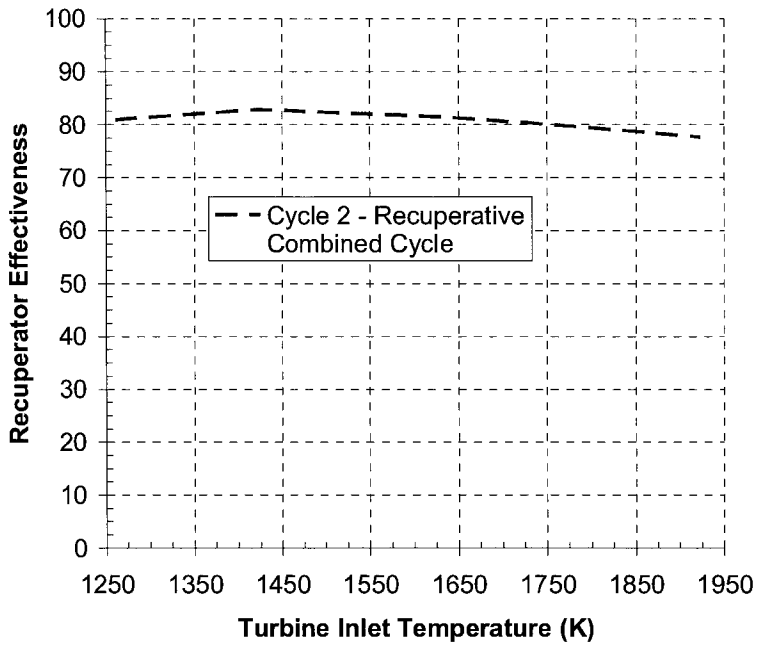

Figure 4-10: Recuperator effectiveness vs. turbine inlet temperature for constant hot-inlet, cold-outlet temperature difference specification of 25 K

If the method for specifying the heat exchanger performance in ASPEN was heat exchanger effectiveness, then the value specified would likely have been on the order of 85%. Figures 4-9 and 4-10 show implied heat exchanger effectiveness values which are less than 85%, but are typically around 80%. The implied values of heat exchanger effectiveness are reasonable and somewhat conservative.

Pressure losses must also be specified for the recuperator. Losses of each the hot-side and cold-side were set to 1.5 % of the inlet total pressure.

4.7.7 Boiler Feed Pump

The boiler feed pump is modeled using a pump. The outlet pressure, isentropic efficiency, and electrical efficiency were specified as required.

4.7.8 Air Separation Unit

In the ASPEN model, the oxygen enters the flow-sheet at an assumed temperature of 298 K (25°C) and pressure of 1.01 bar and is compressed using an inter-cooled centrifugal compressor train to a pressure 20% higher than the combustor pressure. Since the model is designed for ranges of pressure ratio, a calculator block is used to evenly split the pressure change among the three compressors in the train. The isentropic efficiencies of the compressors are set to 78%, and the electrical drive efficiency is set to 95%. The electrical drive efficiency figure of 95% includes mechanical losses for the electrical motor and turbine, electrical and aerodynamic losses in the electric motor, and electrical losses in the variable frequency drive.

Excess oxygen is delivered in the combustor to help ensure complete combustion. The level of oxygen in the working fluid is set to 1 % by mass, upstream of the combustor. This level of excess oxygen in the working fluid is

maintained by an excess in the amount of oxygen injected in the combustor. Ulfsnes et al. (2003b) investigated the physical properties of the CO_2 mixtures in zero-emission semi-closed combined cycles and verified that excess oxygen is required to minimize the production of carbon monoxide. Ulfsnes et al. (2003b) suggest that when the fuel is pure methane, and the oxygen stream is also pure, a 10% excess in oxygen mass flow supplied to the combustor will result in an oxygen concentration in the working fluid of 1.5% upstream of the combustor. This analysis assumes a 1% by mass oxygen concentration in the working fluid is sufficient to minimize the production of carbon monoxide.

4.7.9 CO_2 Storage Compression Unit

The carbon dioxide storage compressor train is designed to pressurize the sequestered carbon dioxide from discharge pressure of the compressor in the gas turbine to carbon dioxide storage pressure of 80 bar. A system was selected consisting of five inter-coolers feeding into five compressors. Since the model is designed for a range of pressure ratios, a calculator block is used to split the pressure rise evenly among the five compressors in the train.

The pressure at the inlet to the compressor train will vary with pressure ratio from about 10 bar to 50 bar. The number of stages in the compressor train is high for the purposes of compressing the carbon dioxide from 10 bar to 80 bar. Five stages are not needed to perform this compression, but five intercoolers greatly reduce the

power required for that compression. In the design process of zero-emission semi-closed combined cycles, once the compressor pressure ratio has been selected, further optimization of the carbon dioxide compression system is recommended. The carbon dioxide in the compression process in these simulations did not exit the compression train in the liquid phase. There is potential for the final stage of compression to be done with a pump if the intercooler cooling fluid is suitably cold. The compression of carbon dioxide in liquid phase requires much less power than the compression of carbon dioxide gas phase.

4.8 Conclusions

Details on the construction of the cycle models have been presented. Various ideas have been presented throughout the chapter. These ideas are summarized in the following list:

- The implied heat exchanger effectiveness corresponding to a hot-inlet, cold-outlet temperature difference of 25 K at about 80% effectiveness is conservative. The implied heat exchanger effectiveness varies a small amount with changes in cycle specification.
- There is room for optimization of the carbon dioxide storage compressor. This could include reduction of stages and the final stage being a pump as the carbon dioxide can be in liquid phase.

- It is not acceptable to model turbine cooling by injecting all the component cooling air upstream of that component because ASPEN assumes two fluids which are combined are mixed perfectly. Steps were taken to better represent the effect turbine component cooling flow on the gas turbine's thermodynamics.
- Multi-stage axial compressor and turbine components blocks with built-in cooling flow ports could be a helpful addition to the ASPEN component list.

Chapter 5 – Cycle Optimization

5.1 Introduction

One of the main goals of this thesis is maximizing the performance of zero-emission semi-closed gas turbine combined cycles. This effort cannot be complete without an optimization study. Two cycles are to be optimized. They are titled Cycle 1, the simple combined cycle, and Cycle 2, the recuperative combined cycle. The two cycles are identical with the exception of Cycle 2's recuperator. A recuperator is a large non-contact heat exchanger which transfers energy from the high-temperature turbine outlet fluid into the relatively low-temperature compressor discharge fluid, thus pre-heating the flow entering the combustor. This decreases the requirement for fuel. In semi-closed cycles, the oxygen requirement will decrease

proportionally with the decrease in fuel. The reduction in required fuel and oxygen correlates to an increase in overall thermal efficiency.

To enable an effective optimization, it is best to understand the effects of each parameter on cycle performance. This verification of parameter effects is best accomplished by a sensitivity study, which is presented in Section 5.2. The appropriate optimization objective must also be determined. There is more than one parameter which could be selected as the criterion suitable for an optimization study of zero-emission semi-closed gas turbine cycles. In the author's experience, given the current high costs of fuel, gas turbine combined cycle plants consume their entire new capital asset value in fuel every year or two when under continuous operation. Plant life spans often exceed 25 years. Thus, this author prefers to focus on the reduction of fuel gas usage. The appropriate criterion for this cycle optimization study is then the *overall thermal efficiency*, as thermal efficiency best encompasses the reduction of fuel gas use. Thermal efficiency is defined as the amount of usable net power out of the system, divided by the total power input to the system, and multiplied by 100. In this case, it is the gross electricity generated minus the loads of all auxiliaries, divided by the energy input of the fuel burned, and multiplied by 100.

There may be other performance criteria which deserve mention, but this study is limited to two, thermal efficiency and one other. This additional value, called *specific work,* is useful when concerned with minimizing capital costs. Specific

work is the value obtained by dividing the power output from the equipment by the mass flow of the working fluid. Considering a low value of specific work, in comparison to a high value, the cycle with the low value must circulate more working fluid to create the same net output as the cycle with the high value of specific work. The size of the fluid moving equipment is proportional to the mass flow rate passed. Large mass flows will require larger equipment. Specific work is thus a measure of plant size. In this study, the specific work was calculated separately for the gas turbine and the steam systems. The ASPEN PLUS OPTIMIZER solver software was not used to determine optimum specific work, since the specific work did not reach a maximum for any of the cases within the allowable design parameter range.

In presenting details on the performance of zero-emission semi-closed combined cycles similarities are often drawn to gas turbine cycles using air. This thesis is not a comparison of air gas turbine performance and semi-closed O_2/CO_2 gas turbine performance. The differences have been presented in previous work at Carleton (Sjolander et al., 2003), and thus will not be presented here.

Section 5.2 presents the trends resulting from varying single variables of the cycle. The results of the optimization study are tabulated and discussed in Section 5.3. Conclusions are summarized in Section 5.4.

5.2 Sensitivity Studies

5.2.1 Presentation Approach

This section details the results of sensitivity studies for various parameters. Each trend was created by holding all other parameters fixed, with the exception of the working fluid mass flows. The working fluid mass flows are free to change as required by the solver to satisfy the target plant net power output of 100 MW. In most cases, thermal efficiency is taken as the criterion of merit and plotted against the variable parameter; in addition, select charts show specific work.

To demonstrate trends over a wide operating range, changes had to be made to the specifications of the steam system. The energy available in the steam generator inlet gas flow must be sufficient to superheat all the feed-water, since the flow at the steam turbine inlet must be dry steam. Most of the heat transfer is occurring from the high-temperature gas to the feed-water at the feed-water saturation temperature. The heat transfer is a function of the temperature difference between the hot gas and the saturated feed-water; thus, the steam generator inlet temperature must be suitably above the saturation temperature. If the feed-water pressure is increased, its saturation temperature is also increased. Since varying cycle parameters can result in a decrease of the steam generator inlet temperature, certain combinations of parameters can lead to insufficient steam generator inlet

temperatures. To expand the operational range, the steam system was specified with relatively low pressures, allowing lower steam generator inlet temperatures, and a wider range for cycle parameter variation. Although these operating points may be far from the optimum, they allow solution convergence and demonstration of trends.

Most charts show comparative performance trends for the simple-combined cycle and the recuperative-combined cycle, known as Cycles 1 and 2, respectively, versus a specified parameter. The parameter of focus is given in the section title and on the x-axis of the plots. All trend lines show the overall quantities, such as overall thermal efficiency, unless otherwise noted in the key and explained in the text. For example, if the key reads 'Gas Turbine Only,' then the quantity is that corresponding only to the gas turbine section of the cycle. Further explanations are given as required. The trends for Cycles 1 and 2 are compared and contrasted for each Figure. Section 5.2 also details the performance trends with the aim of directing and validating the optimization study.

5.2.2 Effect of Overall Compressor Pressure Ratio

Compressor pressure ratio refers to the pressure difference produced across the compressor while operating at its steady-state design speed. Pressure ratio is defined as the pressure at the compressor exit divided by the pressure at the compressor inlet. The gas turbines considered in this thesis are large-scale power generation units and thus assumed to be of *single-shaft* configuration. The term

s*ingle-shaft* means the compressor and turbine are connected to the same shaft and spin at the same speed. If the gas turbine is an industrial engine, then the unit will either be directly coupled to the generator, or coupled through a *reduction gearbox.* If the gas turbines roots are in aero-engines, then the engine, commonly called a *gas generator*, will be aerodynamically coupled to a *free power-turbine*, which is directly coupled to the generator. In this thesis, the assumed configuration is *single-shaft.* In North America, alternating current electricity is distributed at 60 cycle-per-second (Hz). A two-pole generator must rotate at precisely 3600 revolutions-per-second (RPM) to produce 60 Hz electricity. When a gearbox is not used, the 60 Hz electricity fixes the speed of the gas turbine's compressor; thus, the pressure ratio of concern is at precisely one speed. With only one speed to consider, specifying a component efficiency and pressure ratio defines the compressor sufficiently to meet the needs of design point thermodynamic modeling. The investigations presented in this thesis will not be restricted by the single-shaft fixed configuration assumption. This assumption serves as a starting point for the investigation. The final configuration may be different. Changes to the configuration may be needed to meet the optimum specifications. Specific details on those changes will be addressed further along in the design process, which is outside the scope of this thesis.

Table 5-1 shows various gas turbine gen-set models, their key specifications, and performance parameters. These values are power output, thermal efficiency,

pressure ratio, mass flow, and gas generator or gas turbine spool speed. The twin-spool, or dual-shaft, machine speeds are presented with the low-pressure spool speed first, followed by the high-pressure spool speed, separated by a forward slash (/). The models are sorted by power output, and the type is noted as *Ind.*, denoting an industrial style unit, or *Aero.D.*, denoting an aero-derivative unit. Aero-derivative gas turbines are those whose designs were borrowed from aircraft engines. Typically, the fan, corresponding low-pressure turbine, and shaft are removed from the aircraft, or aero, turbofan. The remaining component can be called a gas generator, because its exhaust is a high-temperature fluid at pressure. This fluid is

Table 5-1: Popular gen-sets; simple-cycle specifications

Manufacturer	Model	Type	Output (MW)	Efficiency (%)	Pressure Ratio	Mass Flow (kg/sec)	GG/GT Speed (RPM)
Solar Turbines	Mars 100	Ind.	10.7	32.4	17.4	42	11168
General Electric	LM2500+DLE	Aero.D.	30.5	38.5	22.6	87	10500
Rolls-Royce	RB-211-6761DLE	Aero.D.	32.1	39.3	21.5	94	5250/7500
General Electric	LM6000PD sprint	Aero.D.	45.8	40.9	30.0	130	6000/10500
Siemens-Westinghouse	W251B12A	Ind.	49.5	32.7	15.3	175	5427
Rolls-Royce	Trent 60 DLE	Aero.D.	51.7	41.9	34.0	155	-
General Electric	LMS100	Aero.D.	100.0	45.1	40.0	-	-
Siemens-Westinghouse	501D5A	Ind.	120.5	34.7	14.2	385	3600
General Electric	7FA	ind.	171.7	36.5	16.0	445	3600
Siemens-Westinghouse	501G	ind.	266.3	39.3	20.1	602	3600
Mitsubishi Heavy Ind.	M701G2	ind.	334.0	39.5	21.0	738	3000

then expanded through a free power-turbine, which is connected to the load. Turbojets, or aero-gas turbines which are characterized by having all flow pass through the combustor, also can be converted into industrial aero-derivative gas turbines. Aero-derivative gas turbines, like their aero-engine cousins, are extremely lightweight. Industrial engines differ from aero-derivative engines in many ways. Industrial engines were designed from original conception for ground-based purposes, which have a different set of requirements than those of aircraft gas turbines. Industrial gas turbines can be heavy, and it is desirable to minimize their inlet and exhaust flow velocities to minimize total-pressure losses. In review of Table 5-1, notice the reduction in speeds with increases in power output. For machines of 100 mega-Watt (MW) and larger, the speed can be 3600 RPM. Machines which are significantly smaller than 100 MW output will require a reduction gearbox. The Mars 100 operates at 11168 RPM producing 10.7 MW, the W251B12A operates at 5427 RPM producing 49.5 MW, while the 501D5A and 501G both operate at 3600 RPM, but produce 120.5 MW and 266.3 MW, respectively. It is anticipated that the theoretical gas turbines considered in this thesis will operate at 3600 RPM as the plant's overall power output is to be 100 MW. The gas turbine will not produce 100 MW exactly, as the steam system will have some contribution. The cycles have large auxiliary loads which typically exceed the

steam systems contribution to the overall output. The gas turbines itself will produce about 100 MW.

The compressor pressure ratio is varied here to identify the optimum value which gives the best thermal efficiency. If the resulting value is very high, it may not be feasible or desirable to use the optimum value in practice. There are many challenges associated with high pressure ratios. High pressure ratios require many stages of compression, with each stage very highly loaded. To achieve high efficiency across highly loaded stages, the blade tip clearance must be minimized. Typical single-shaft industrial gas turbines have two bearings supporting the entire shaft. The bearings are located on the outboard positions of the turbomachinery. This can result in the shaft spanning a large distance, with the compressor blade tips which would benefit the most from small tip clearances forced to operate with the greatest clearances. There is a configuration change which can address this issue. It involves splitting up the compression to different shafts. A high-pressure compressor can be driven from a high-pressure turbine. The blade height on the high-pressure compressor is short due to the small area requirements for the flow as a result of the high density. The high-pressure compressor can operate at a higher speed because it is not restricted by the low-pressure portions of the compressor and turbine. Proper blade speeds can be met with a high-pressure turbine of smaller diameter. All of these attributes work together to allow compressors to yield high

pressure ratios and high efficiencies. Table 5-1 shows an assortment of gas turbines. Many are single-spool, while others are multi-spool. The single-spool units show lower compressor ratios. For example, the Mars 100, LM2500+, W251B12A, 501D5A, 501G, and M701G2 are all single-shaft machines with pressure ratios ranging from 14.2 to 22.6, with the LM2500+ is showing the highest pressure ratio. Review of the multi-spool machines shows capabilities of much higher pressure ratios. The LMS100 aero-derivative gas turbine is showing the highest pressure ratio at 40.0. This is about the maximum compressor ratio which can be found in use in land or marine applications. Some current aircraft turbofan offerings use overall compressor pressure ratios higher than 40.0. This includes pressure ratios by the EA GP7277 at 45.6 (2 spool), the GE90-115B at 42.0 (2 spool), the PW4098 at 42.8 (2 spool), RR Trent 762 at 43.2 (3 spool), and the RR Trent 890-17 at 42.7 (3 spool) (Meier, 2005). High compressor pressure ratios must be accompanied by high turbine inlet temperatures. There is an optimum pressure ratio for any turbine inlet temperature. Thus, as turbine inlet temperatures continue to increase, so too will compressor pressure ratios. Current maximum compressor pressure ratios are thus selected on the basis of optimum pressure ratio for the achievable turbine inlet temperature, and also mechanical considerations.

Multi-spool arrangements adapt well to the challenges of high pressure ratios. Not only does multi-spooling allow decreasing tip clearances and increasing blade

speeds with decreasing diameters in the high-pressure section, it also works to overcome compressor surge challenges. It takes great care to startup a single-shaft compressor designed to make a high pressure ratio. The flow conditions in a high pressure ratio single-shaft gas turbine during start-up are such that, if preventative measures are not taken, the flow conditions at the high-pressure end of the compressor will force the flow to separate from the individual airfoils. If the flow separates from too many blades in multiple stages, the compressor will not be able to support the pressure built-up in the combustion chamber. This can result in periodic complete flow reversal in the compressor, a phenomenon known as *surge*. Since the speeds between the high- and low-pressure compressors can vary independently, they work to naturally avoid surge when used in combination with compressor bleeding. Compressor bleed reduces the pressure at an intermediate stage and/or after the final stage of compression by venting air from the recessed bleed cavity to atmosphere. Review of the high pressure ratio aero-derivative and turbofan engines may yield the observation that all of the turbofan engines mentioned show overall pressure ratios above 40, but only the two RR Trents implement true multi-spooling. The difference is that if the fans were removed from all the turbofans, the pressure ratios would drop to the mid and low 30s, much lower than the GE LMS100. The GE LMS100 and the RR Trent industrial engines operate safely at high-pressure ratios using similar dual-spool configurations. The remaining turbofans employ

booster stages on their fan shaft, with many rows of variable geometry stators to allow safe operation with similar pressure ratios. By inspection of Table 5-1, single-spool compressors are limited to pressure ratios around 22-25, true dual-spool compressors can achieve pressure ratios of 35, while the GE LMS 100 configuration suggests that variable stator geometry may be helpful in achieving or exceeding pressure ratios of 40. Increasing the pressure ratio makes the compressor more prone to surge; as a result, variable geometry and other features must be included to allow stable operation particularly during start-up and shut-down. These features include variable compressor inlet guide vanes, variable stators on the early stages of the compressor, as well as bleed valves. Pros and cons to these configurations are beyond the scope of this thesis, but good discussions are available in Saravanamuttoo et al. (2001).

In the following studies, it will become apparent that in the high pressure ratio range, only marginal increases in performance are achieved with increasing pressure ratio. Thus, it was decided to place an upper limit on the pressure ratio at a reasonable value. Increases in compressor pressure ratio beyond 40 may be possible with improved design; however, pressure ratios above 50 were not considered. Similarly, pressure ratios below 10 were not considered since the optimum value was not expected to be below that value.

Figure 5-1 shows a plot of the overall plant thermal efficiency versus pressure ratio for both the cycles considered. The trend for Cycle 1, the simple combined cycle, shows increasing thermal efficiency with increasing pressure ratio. Cycle 1's efficiency trend does have a peak, but its peak occurs at a pressure ratio much greater than 50. Each trend has an optimum value because there is an optimum pressure ratio for each turbine inlet temperature, and Figure 5-1 shows results for one turbine inlet temperature (Saravanamuttoo et al., 2001). The trend for Cycle 2, the recuperative combined cycle, shows an optimum pressure ratio at about 22.5. Table

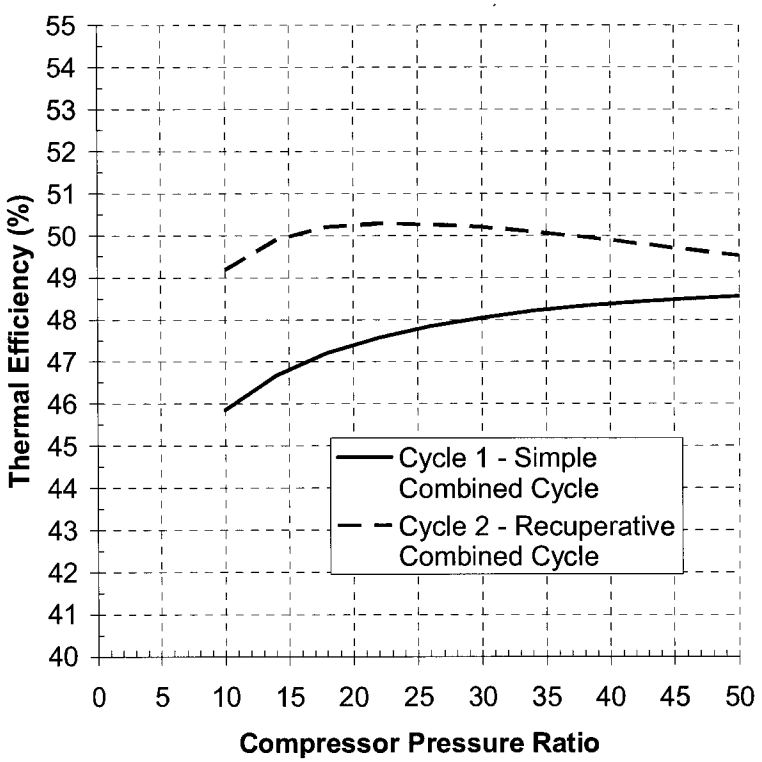

Figure 5-1: Overall thermal efficiency vs. compressor pressure ratio

5-2 shows the main inputs to the simulation involved in the creation of the data for Figure 5-1. In the table, pressure ratio is presented in bold-face type as it is the main specification being varied to create data for Figure 5-1. The remaining parameters which are not fixed are the working fluid mass flows in the gas turbine and steam generator. These vary as required to meet the overall net power output specification of 100 MW. Table 5-2 is valid for all of Figures 5-1, 5-2, 5-3, and 5-4.

The difference in optimum pressure ratios in Figure 5-1 results from the recuperator in Cycle 2, which is the principal difference in configuration between the two cycles. A recuperator is a non-contact heat exchanger which transfers energy from the hot turbine outlet flow to the relatively cool combustor inlet flow. The addition of the recuperator alters the temperatures throughout the cycle, and in particular, increases the gas temperature at the combustor inlet. This affects the overall thermal efficiency. The purpose of the recuperator is to decrease the engine's fuel requirement by preheating the combustor inlet flow. This results in an efficiency increase in the gas turbine section of the plant. On the other hand, the gas inlet temperature to the steam system is correspondingly reduced by the recuperator. This temperature reduction decreases the efficiency of the steam system; however, the decrease in steam system performance is more than offset by the increase in gas turbine performance, as can be seen in Figure 5-1. Over the entire pressure ratio

range, the thermal efficiency of Cycle 2, the recuperative combined cycle, is greater than that of Cycle 1, the simple combined cycle.

Table 5-2: Model specifications for Figure 5-1, 5-2, 5-3, and 5-4

	Gas Turbine					
	Compressor Inlet Pressure (bar)	**Pressure Ratio**	Oxygen Purity (Mole %)	Turbine Inlet Temp. (K)	CO_2 Mass Flow (kg/s)	Net Power Output (MW)
Cycle 1 - Simple Combined Cycle	1.01325	**Design Variable**	95.5	1723	Variable	100
Cycle 2 - Recuperative Combined Cycle	1.01325	**Design Variable**	95.5	1723	Variable	100
	Steam System					
	Steam Mass Flow (kg/s)	Steam Generator Mass Split Ratio	Steam Temp. (K)	Steam Generator Gas Outlet Temp. (K)	Low-Pressure Steam (bar)	High-Pressure Steam (bar)
Cycle 1 - Simple Combined Cycle	Variable	0.5	S.G. inlet - 25 K	393.15	14.7	170.0
Cycle 2 - Recuperative Combined Cycle	Variable	0.5	S.G. inlet - 25 K	393.15	8.00	50.0
* Temp. = Temperature						
** S.G. = Steam Generator						

Figure 5-2 shows the influence of the overall pressure ratio on the steam generator inlet temperature. The trend for Cycle 1, the simple combined cycle, shows steam generator inlet temperatures decreasing with increasing pressure ratio. The trend for Cycle 2, the recuperative combined cycle, is unlike the first in that it

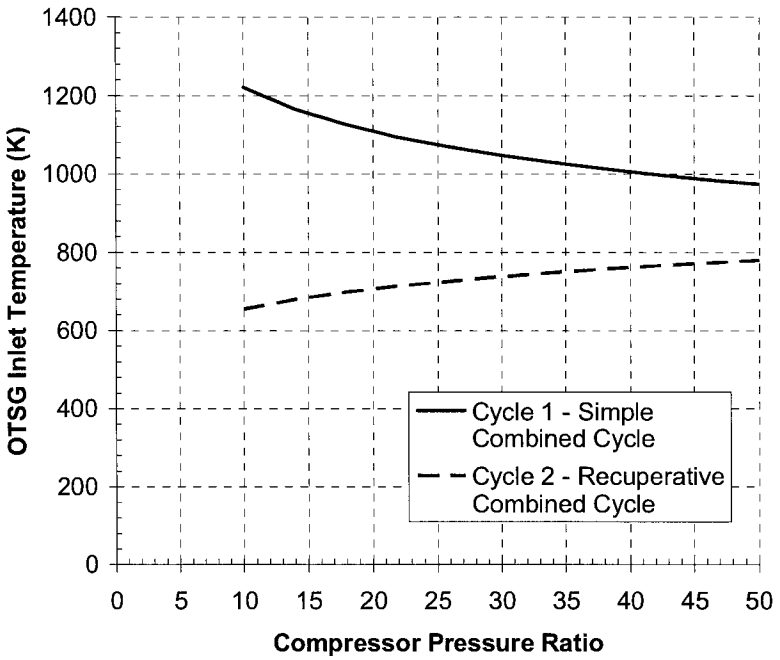

Figure 5-2: Once-through steam generator (OTSG) inlet temperature vs. compressor pressure ratio

shows increasing steam generator inlet temperatures with pressure ratio. The difference is due to the presence of the recuperator in Cycle 2. This difference is most pronounced in the lowest pressure ratios due to the difference between the lowest and highest temperatures for the streams entering the recuperator. Figure 5-3 shows compressor and turbine outlet temperatures and the resulting recuperator outlet temperatures for Cycle 2, the recuperative combined cycle. Again, the comparably large spread between the curves on the left side of the plot shows that the recuperator has its greatest effect on the cycle when the pressure ratio is low. At

low pressure ratios, the turbine exhaust temperature is at its highest, and the compressor outlet temperature is at its lowest. In Figure 5-3, the recuperator outlet temperature is the steam generator inlet temperature, as the hot-side of the recuperator is before the steam generator. Since the cool compressor outlet flow is receiving heat from the turbine outlet gases, the hot-side recuperator outlet flow will be affected by the compressor outlet temperature. Thus, the steam generator inlet temperature is low because the compressor outlet temperature is low.

In Figure 5-2, it is shown that Cycle 1's steam generator inlet temperature decreases with increasing compressor pressure ratio. This is best explained by considering the conditions in the turbine section. The turbine inlet temperature is fixed at 1723 K as per Table 5-2. As the pressure ratio across the compressor is increased, so too does the pressure ratio across the turbine. The increased pressure ratio across the turbine results in an increased expansion of the flow. As the amount of expansion increases, more power is extracted by the turbine. The result is a decreasing turbine outlet temperature. The turbine outlet temperature and the steam generator inlet temperature are generally the same in a simple-cycle gas turbine combined cycle, differing only due to the assumed steam generator heat loss. The steam generator heat loss assumption takes into account the energy which is transmitted through the insulated walls of the steam generator.

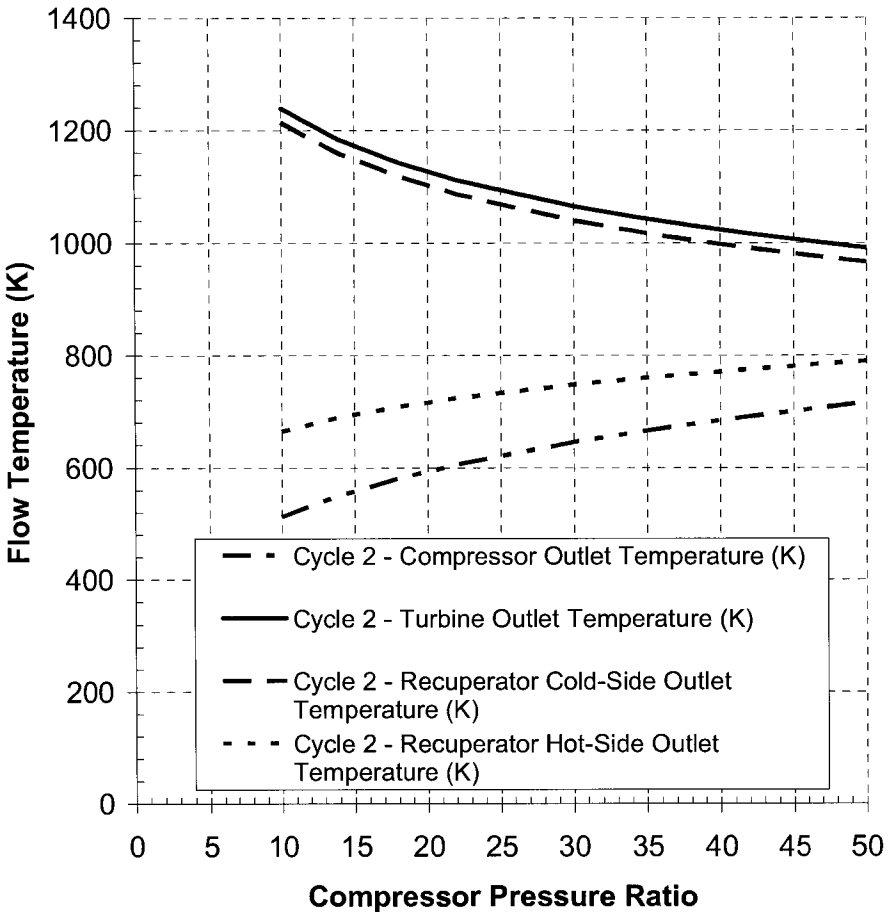

Figure 5-3: Recuperator flow temperatures vs. compressor pressure ratio for Cycle 2, the recuperative combined cycle

Figure 5-4 shows trends of specific work produced by the steam cycle when varying the compressor pressure ratio. The specific work for the gas and steam sides of the plant are calculated separately; thus, Figure 5-4 shows the output of the steam turbine divided by the mass flow rate of steam. The selection of pressure ratio for

optimum efficiency will have an effect on the size of the steam system. Specific work is an indicator of plant size. The greater the value of specific work, the smaller

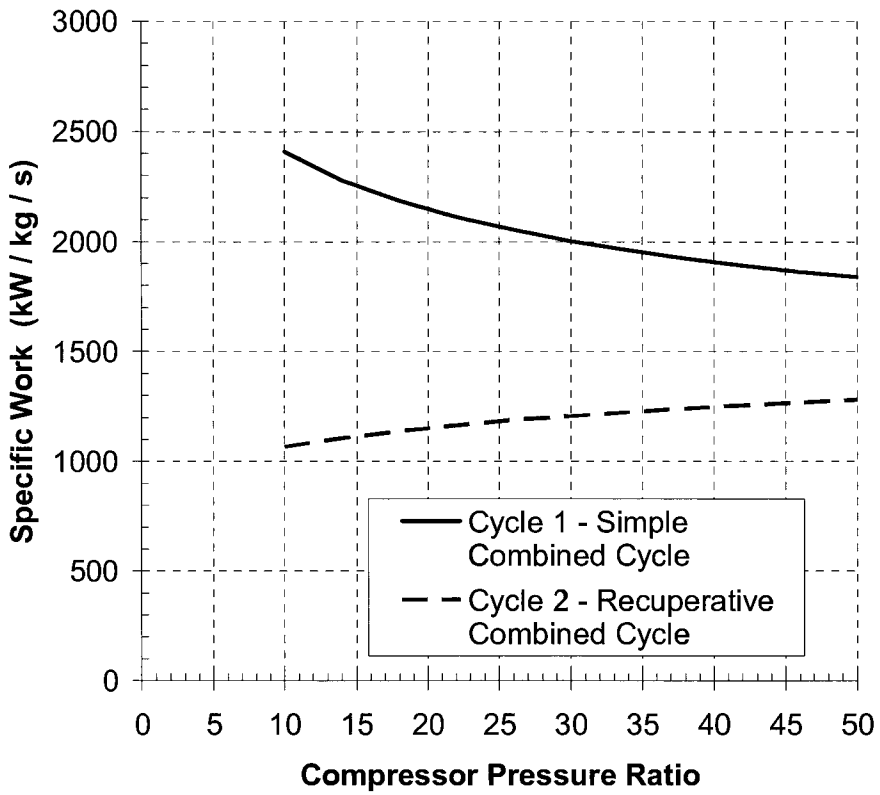

Figure 5-4: Curves of steam system specific work vs. compressor pressure ratio

the cycle's mass flow can be, while smaller mass flow means a smaller plant. For Cycle 1, the simple combined cycle, in comparing Figures 5-1 and 5-4, the increase in pressure ratio towards the pressure ratio which gives optimum thermal efficiency yields a decrease in steam cycle specific work, which is undesirable as the steam system will be larger and more expensive. In Cycle 2, the recuperative combined

cycle, increases in pressure ratio have positive effects on the steam system's specific work value; however, the optimum thermal efficiency is attained at a pressure ratio of about 22.5.

In the preceding discussion of Figure 5-2, it was mentioned that the steam generator inlet temperature affects the efficiency of the steam system. Similarly, the steam system specific work is also affected by the steam generator inlet temperature. This can be seen by comparing Figure 5-2 and Figure 5-4. The slopes of the Cycle 1 and Cycle 2 trends have the same sign between the two charts. The trends are the result of varying only one parameter, the compressor pressure ratio. The mass flow rates through each the gas turbine and steam system will also vary to make the specified power. Specific details on cycle specifications are given in Table 5-2. Changes in compressor pressure ratio result in changes in the steam generator inlet temperature which in turn leads to changes in steam system specific work. Steam generator inlet temperature is therefore a dominant factor in the steam system efficiency and specific work.

Figure 5-4 shows the curves of specific work achieved by the steam cycle while Figure 5-5 shows the corresponding values of specific work for the gas turbine when varying the compressor pressure ratio. The specific work for the gas and steam

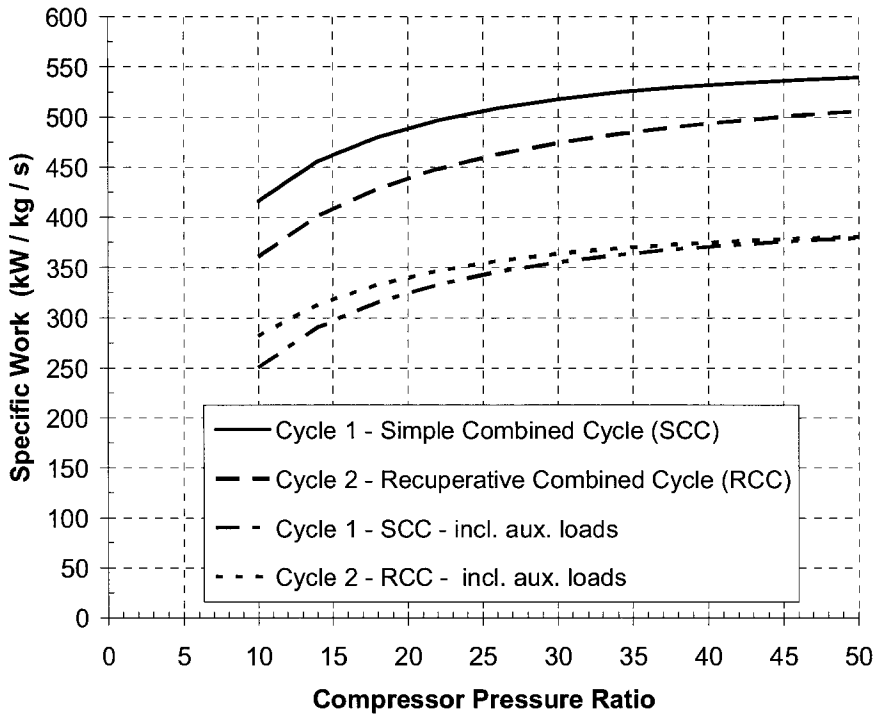

Figure 5-5: Gas turbine specific work vs. overall compressor pressure ratio

sides of the plant are calculated separately; thus, Figure 5-4 shows the output of the steam turbine divided by the mass flow rate of steam. Similar to the previous figures, data is presented for both cycles; Cycle 1, the simple combined cycle, and Cycle 2, the recuperative combined cycle.

In Figure 5-5, two sets of data are presented for each cycle. The second dataset, those which titles in the chart's key include 'incl. aux. loads,' are specific work trends including all auxiliary loads. Review of the curves reveals that gas turbine specific work is maximized for both Cycles 1 and 2 at highest pressure ratio.

Cycle 2 again shows that, in reference to Figure 5-1, the desirable high specific work is not at the same overall pressure ratio as its thermal efficiency optimum. It is evident that the designer has the option to trade-off thermal efficiency and specific work for both Cycles 1 and 2.

It is noticeable that, when considering gas turbine specific work including auxiliary loads, the specific work values begin to match between the two cycles. It seems that the cycle with the stronger specific work without auxiliaries has a higher auxiliary load which results in its specific work being at an identical value to the other cycle. It is not clear whether or not this is coincidence.

The results of sensitivity studies into the effects of compressor pressure ratio on overall thermal efficiency and specific work have been presented. Compressor pressure ratio has significant effects on cycle performance. The peak thermal efficiencies and peak specific works do not match for both cycles. Considering thermal efficiency as the criteria of merit, sensitivity studies show that for Cycle 1, the simple combined cycle, the theoretical optimum overall pressure ratio is greater than 50. For the recuperative combined cycle, the optimum overall pressure ratio is approximately 22.5.

5.2.3 Effect of Turbine Inlet Temperature

Another factor which dominates gas turbine performance is the *Turbine Inlet Temperature*. The turbine inlet temperature is the name given to the mean

temperature of the high-pressure high-temperature gas flow in the transition region between the combustion chamber and the inlet to the turbine. The inlet to the turbine is the location immediately upstream of the turbine's first row of stationary airfoils. As the flow at this location is high temperature and non-uniform, it is not often measured in production gas-turbines. The commonly used alternative is a select number of evenly spaced temperature measurement probes in the turbine outlet blade path, or also measurement probes which span the exhaust duct further downstream. The gas turbine's control system can keep the turbine inlet temperature within limits by controlling the fuel flow based on the turbine outlet temperature. As measurement of the turbine outlet temperature is done with the aim of providing information for turbine inlet temperature control, it is best to communicate in terms of the turbine inlet temperature when discussing theoretical gas turbine performance

Figure 5-6 is a chart showing thermal efficiency versus turbine inlet temperature. Two sets of data are presented for each of Cycle 1, the simple combined cycle, and Cycle 2, the recuperative combined cycle. The first set is presenting the cycle's overall thermal efficiency, while the second set presents the thermal efficiency calculated considering the gas turbine only. The 'Gas Turbine Only' portion, as named in the figure's key, includes no auxiliary loads and is simply the power extracted from the gas turbine's generator divided by the fuel power input to the combustor. This second data series helps to determine whether varying a

parameter increases or decreases the performance of the gas turbine. It can also help isolate any variable which affects the steam system performance only. As with the other figures in Section 5.2 and its sub-sections, Figure 5-6 was generated by means of sensitivity study. This means all other parameters were held constant with the exception of the working fluid mass flows.

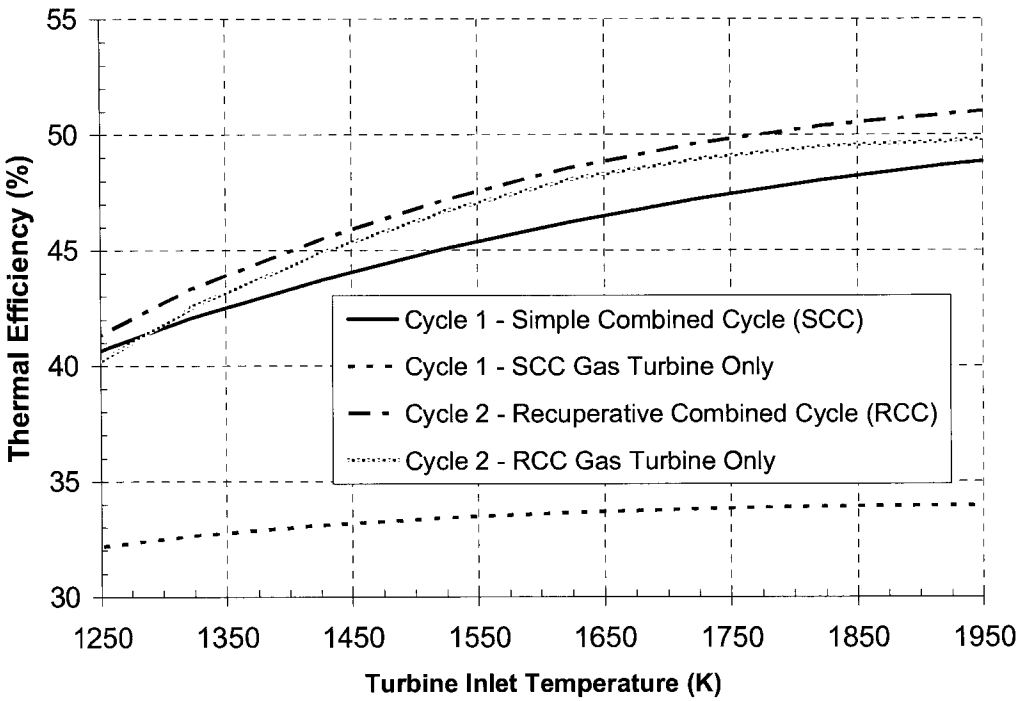

Figure 5-6: Thermal efficiency vs. turbine inlet temperature

Specific details describing the cycle parameters are shown in Table 5-3. The turbine inlet temperature is labelled as the Design variable in bold-face type. The gas turbine working fluid and steam system working fluid are also labelled as

Table 5-3: Model specifications for Figure 5-6

	Gas Turbine					
	Compressor Inlet Pressure (bar)	Pressure Ratio	Oxygen Purity (Mole %)	**Turbine Inlet Temp. (K)**	CO_2 Mass Flow (kg/s)	Net Power Output (MW)
Cycle 1 - Simple Combined Cycle	1.01325	22.5	95.5	**Design Variable**	Variable	100
Cycle 2 - Recuperative Combined Cycle	1.01325	22.5	95.5	**Design Variable**	Variable	100
	Steam System					
	Steam Mass Flow (kg/s)	Steam Generator Mass Split Ratio	Steam Temp. (K)	Steam Generator Gas Outlet Temp. (K)	Low-Pressure Steam (bar)	High-Pressure Steam (bar)
Cycle 1 - Simple Combined Cycle	Variable	0.5	S.G. inlet - 25 K	393.15	10.0	125.0
Cycle 2 - Recuperative Combined Cycle	Variable	0.5	S.G. inlet - 25 K	393.15	4.29	28.0
* Temp. = Temperature						
** S.G. = Steam Generator						

variable. The fixed values are given for the remaining parameters. Figure 5-6 is a plot of turbine inlet temperature performance with pressure ratio fixed at 22.5 for both cycles.

The effect of increasing the turbine inlet temperature on both overall thermal efficiency and gas turbine thermal efficiency is shown in Figure 5-6. The results are in alignment with ideal cycle theory, which demonstrates that maximizing the cycle's highest temperature is key to achieving high efficiency when the cycle's lowest temperature is fixed (Moran and Shapiro, 1996). The turbine is a cooled unit; thus, the trend was created by assuming the cooling flow increases linearly from 1200 K to 1723 K (927°C to 1450°C). Figure 5-6 is useful in showing approximate thermal efficiencies for a given achievable turbine inlet temperature. The comparatively low slope of Cycle 1's 'Gas Turbine Only' trend demonstrates the importance of adding a bottoming cycle to a system using a carbon dioxide working fluid. The steam system's contribution is responsible for raising Cycle 1's slope to thermal efficiency magnitudes approaching those of Cycle 2. The ratio of specific heats for carbon dioxide is such that the difference between the turbine inlet and outlet temperatures is smaller in comparison with air, meaning that much more energy would leave the cycle as waste, if not for the steam generator. The efficiencies achieved by Cycle 2's 'Gas Turbine Only' trend, in comparison to Cycle 1's 'Gas Turbine Only' trend, shows the recuperator is effective in increasing the thermal efficiency of the gas turbine.

The turbine inlet temperature selected for the cycles in this thesis is 1723 K (1450°C). This turbine inlet temperature should be achievable using super-alloy

materials with proper attention to component cooling. Turbine inlet temperature data for gas turbines is commonly not readily dispersed by manufacturers. From time to time, data is published, but often the best sources is those who work closely with the engines and interface with the manufacturers. Table 5-4 presents the turbine inlet temperatures of a few previous gas turbines. Figure 5-7 is a plot of thermal efficiency versus turbine inlet temperature for the engines presented in Table 5-4. Two of the engines are aero-derivatives while the others are industrials. All the gas turbines in the table show turbine inlet temperatures below the selected 1723 K with

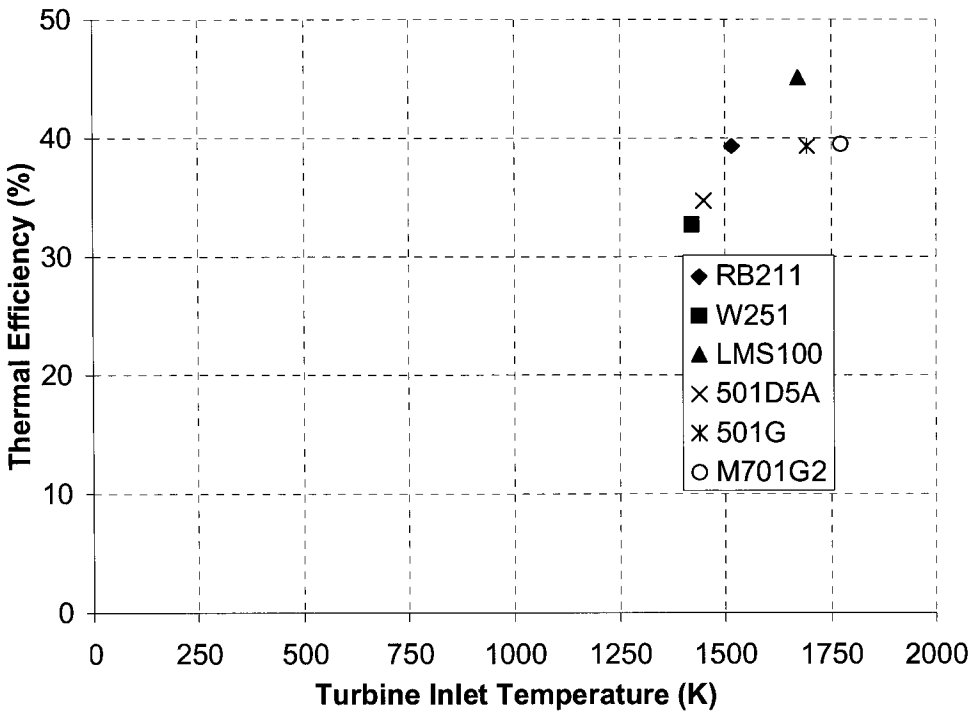

Figure 5-7: Thermal efficiency vs. turbine inlet temperature for gas turbine engines in Table 5-4

the exception of the M701 G2. This author has no familiarity with the M701 G2 in order to suggest this value as accurate or erroneous. The target turbine inlet temperature for the cycles in this thesis is 135 K above the average of the turbine inlet temperatures shown in the Table 5-4. This is not cause for alarm as many of these engines were released many years ago. The newest engine in the table is the LMS 100, but this engine is mainly the combination of a previous core with the addition of a new low-pressure compressor and intercooler. The intercooler helps

Table 5-4: Turbine inlet temperatures for previous gas turbines

Manufacturer	Model	Type	Output (MW)	Efficiency (%)	Pressure Ratio	Turbine Inlet Temperature (K)
Rolls-Royce	RB-211-6761DLE	aero.D.	32.1	39.3	21.5	**1516**
Siemens-Westinghouse	W251B12A	ind.	49.5	32.7	15.3	**1422**
General Electric	LMS100	aero.D.	100.0	45.1	40.0	**1672**
Siemens-Westinghouse	501D5A	ind.	120.5	34.7	14.2	**1450**
Siemens-Westinghouse	501G	ind.	266.3	39.3	20.1	**1693**
Mitsubishi Heavy Ind.	M701G2	ind.	334.0	39.5	21.0	**1773**

give a very high efficiency, while the turbine inlet temperature is adequate but is not pushing boundaries. The 1723 K target turbine inlet temperature is a worthy target which will yield class leading performance.

The results of sensitivity studies into the effect of turbine inlet temperature on thermal efficiency have been presented. Results show that maximizing the turbine inlet temperature is important when attempting to maximize thermal efficiency.

5.2.4 Effect of CO_2 Loop Gas Turbine Compressor Inlet Pressure

One controllable parameter in a semi-closed gas turbine cycle is the gas turbine compressor inlet pressure. Varying the compressor inlet pressure has benefits and potential challenges. One potential benefit is in an operating scenario where the unit must produce less than full power, the compressor inlet pressure can be reduced, and the unit's efficiency can be maintained as the turbine inlet temperature is kept constant. There are two potential pitfalls to this scenario. First, operating at a reduced compressor inlet pressure infers that the pressure of the working fluid inside the compressor intake manifold is below atmospheric pressure. In fact, operating at a reduced compressor inlet pressure may result in the entire loop from the gas turbine outlet all the way to the compressor inlet being below atmospheric pressure. There will be flanges and joints which may leak due to the presence of a pressure gradient. Operating with a compressor inlet pressure below atmospheric pressure opens the system to the potential of contamination by air. Air

could leak past any of the flanges where the pressure inside is below atmospheric. This pitfall is not immediately dangerous, but could be difficult to detect and even more challenging to locate. The symptom may be excess nitrogen or oxygen in the sequestered carbon dioxide, but this gives no indication of the leak location. To find the leak, the pressure at the compressor inlet could be raised to some level above atmospheric pressure. This can be done during operation. The intake manifold flanges could then be taped and sniffed using the appropriate gas detection equipment for conditions which are not identical to ambient air. The taping of the flanges forces the leaking fluid to exit through a single puncture in the tape. This increases the likelihood of finding the leak. The leak may not be immediately offensive to the instruments so it could prove challenging to find. Also, the pressure required to force the leak may be different for the different directions. Thus, the leak may not be present in the configuration which allows it to be investigated. The second potential pitfall relates to the fluid which is bled from the various compressor bleed cavities for use in cooling the turbine. Reducing the compressor inlet pressure results in pressure reductions at all bleed locations. There will continue to be a pressure differential to drive cooling flows through the cooling system; however, the reduction in pressure will result in a reduction in mass flow through the cooling system. Turbine cooling systems are designed such that there is no extra cooling. Thus, with any reduction in cooling mass flows, adverse effects can be expected in

the form of increased component distress and reduced reparability. At the very worst, component failure can occur before the appropriate repair interval. Detailed calculations should be satisfactory in predicting a suitable reduced compressor inlet pressure operating curve; however, the balance of turbine inlet temperature reduction and resulting efficiency loss may exceed the benefits of reduced compressor inlet pressure operation.

The second interesting operating mode for a semi-closed cycle gas turbine is the raising of the compressor inlet pressure. This could be advantageous when excess power production is desired. Operating with the compressor inlet pressure above atmospheric pressure means that system leaks do not risk contamination of the working fluid. There are many challenges associated with this operating mode. First, the unit's cooling system and generator will need to be sufficient for the extra load. The increase in compressor inlet pressure will ensure a proportional increase in the mass flow through the turbine cooling system. It is this author's opinion that turbine cooling should function sufficiently so long as the turbine inlet temperature is held at its normal maximum; however, further investigation is recommended to quantify the component temperatures which can be expected. The generator should have sufficient cooling as long as the load does not exceed its nameplate load. It may be necessary to exercise caution in approaching the nameplate load on days of high ambient temperatures. Typical gas turbines produce net power outputs

significantly below nameplate generator loads on hot days. Some manufacturers may have included this fact in approving their generator's cooling system. Any generator which is operated continuously to its nameplate load is being subjected to harsh service in comparison to others in gas turbine service which experience significant reductions in load on warm days. This difference will only reduce the life of the generator. The second challenge associated with this operating mode has to do with the load on the shaft. The increase in mass flow will increase the load on the turbine section and compressor section. These loads transfer directly through the gas turbine main shaft. The main gas turbine shaft must be able to withstand this increase in torque. Finally, the gas turbine's case, or its pressure containment structure surrounding the compressor, combustion chamber, and turbine, must be able to withstand pressure increases which are proportional to the increases in compressor inlet pressure multiplied by the compressor pressure ratio. There are significant roadblocks to operating the semi-closed gas turbine at compressor inlet pressures above atmospheric pressure; however, with extra effort, the benefits of increased production could be realized.

Figure 5-8 is a plot of the overall thermal efficiency versus the compressor inlet pressure. The compressor inlet pressure is varied from 0.5 bar to 4.0 bar. Both cycles show changes in performance when varying the gas turbine compressor inlet

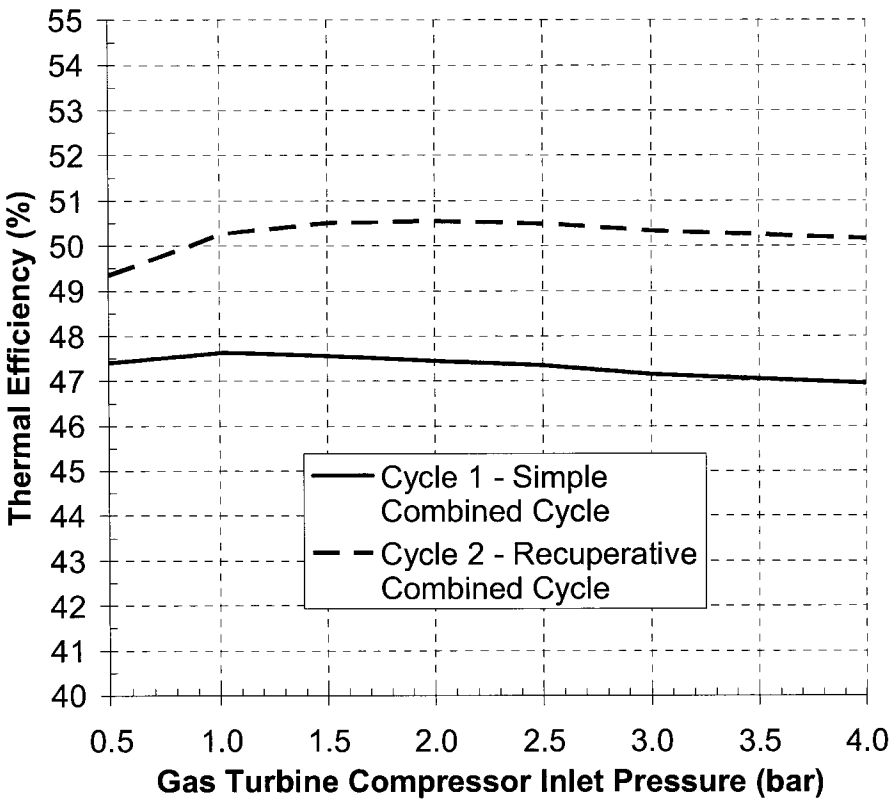

Figure 5-8: Thermal efficiency vs. gas turbine compressor inlet pressure

pressure. These variances are explained when considering the effects of entire cycle. For example, if the gas turbine compressor inlet pressure is reduced, then the compressor discharge pressure is also reduced. The compressor discharge pressure is proportional to the inlet pressure multiplied by the compressor pressure ratio. The compressor discharge pressure and the carbon dioxide sequestration pressure, or the pressure at which the carbon dioxide is bled for storage, is the same; thus, the

pressure with which the carbon dioxide sequestration compressors receive the fluid is reduced. These compressors must continue to pressurize the carbon dioxide to the storage pressure, 80 bar. As the gas turbine compressor inlet pressure is reduced, the power required to compress the carbon dioxide to storage pressure increases.

Similarly, the influence of the oxygen compressor must be considered when explaining the trends found in Figure 5-8. If the gas turbine compressor inlet pressure is increased above the standard atmospheric conditions of 101.325 kPa, then the compressor discharge pressure will increase proportionally to the inlet pressure multiplied by the compressor pressure ratio. The combustor pressure is equal to the compressor discharge pressure minus the aerodynamic pressure losses which are necessary for good combustion, which is normally around 5 % of the inlet pressure. The combustor pressure increases as the compressor inlet pressure increases; therefore, the pressure of the oxygen to be injected must also be proportionally higher. Increased work is then required by the oxygen compressor to suitably raise the oxygen delivery pressure above the combustor pressure.

Close inspection of Figure 5-8 may reveal that the trends for Cycle 1, the simple combined cycle, and Cycle 2, the recuperative combined cycle, differ not only in their achieved overall thermal efficiency, but also in the shape of the curves. Specifically, at the 1.0 bar location the Cycle 1's trend decreases in value with both increasing and decreasing pressure; whereas, Cycle 2's trend passes through the 1.0

bar location with a positive slope and maintains its achieved overall thermal efficiency to the 2.5 bar location before tapering off. This difference between the trends is not well understood. Table 5-5 presents the model inputs which create the data for Figure 5-8. The compressor inlet pressure is marked as the Design variable, with the gas turbine and steam system working fluids permitted to vary also. The remaining parameters are fixed as per the table.

The other notable observation from the trends of Figure 5-8 is the decrease in slope apparent in both trends above the 3.0 bar location. This anomaly is best explained beginning again with review of the pressures in the combustion chamber for Cycle 1, the simple combined cycle. Both cycles where simulated using a compressor pressure ratio of 22.5 for the purposes of creating data for Figure 5-8. If the compressor inlet pressure is considered at 3.0 bar, then the compressor discharge pressure shall be 67.5 bar. The compressor discharge pressure is also the pressure at which the carbon dioxide storage compression train receives the working fluid. Since the carbon dioxide storage pressure is set to 80 bar, then the carbon dioxide sequestration train is required to perform little work. At the next investigation interval, the 3.5 bar location, the carbon dioxide sequestration train will receive the working fluid at 79 bar, thus negligible electrical auxiliary load will be charged against the system's thermal efficiency. If there is no electrical load required by the carbon dioxide storage compressors, then the efficiency curve can be anticipated to

lose slope.

A change in the compressor inlet pressure results pressure changes throughout the cycle. Aside from the direct thermodynamic effects of cycle pressures, pressure changes also have indirect changes on the cycle performance. One example is the effect of pressure on component efficiency. The increase in pressure results in an increase in density. The increasing density feeds an increase in the turbomachinery's Reynolds numbers. Increasing Reynolds numbers yield small increases in the component efficiency (Saravanamuttoo et al., 2001), which then affects the overall cycle performance. The component efficiencies are held constant in the creation of the curves in Figure 5-8; thus, the Reynolds number effects were not taken into account. A second example is the effect of variable specific heats with pressure. The specific heats of a fluid are mainly affected by temperature, but are to a lesser extent affected by pressure. Changing the compressor inlet pressure changes the absolute pressures throughout the cycle. Although the turbine inlet temperature will be held constant, the changes in pressures will change the specific-heats and specific-heats ratios. This means the compressor outlet temperature, and turbine outlet temperature will change. A detailed investigation to quantify this effect has not been undertaken; however, for Cycle 1, the simple combined cycle, a 6-fold increase in pressure resulted in a 1.1% increase in compressor discharge temperature, and a 1.9% decrease in turbine outlet temperature. The change in compressor

Table 5-5: Model specifications for Figure 5-8

	Gas Turbine					
	Compressor Inlet Pressure (bar)	Pressure Ratio	Oxygen Purity (Mole %)	Turbine Inlet Temp. (K)	CO_2 Mass Flow (kg/s)	Net Power Output (MW)
Cycle 1 - Simple Combined Cycle	**Design Variable**	22.5	95.5	1723	Variable	100
Cycle 2 - Recuperative Combined Cycle	**Design Variable**	22.5	95.5	1723	Variable	100
	Steam System					
	Steam Mass Flow (kg/s)	Steam Generator Mass Split Ratio	Steam Temp. (K)	Steam Generator Gas Outlet Temp. (K)	Low-Pressure Steam (bar)	High-Pressure Steam (bar)
Cycle 1 - Simple Combined Cycle	Variable	0.5	S.G. inlet - 25 K	393.15	14.7	170.0
Cycle 2 - Recuperative Combined Cycle	Variable	0.5	S.G. inlet - 25 K	393.15	8.00	50.0
* Temp. = Temperature						
** S.G. = Steam Generator						

discharge temperature is distinctly due to the difference in conditions at the compressor inlet propagating through the compressor, but the change in turbine outlet temperature may be heavily influenced by the turbine cooling flows. These effects are small and thus will not be discussed further.

Certain observations are made for the purposes of guiding the optimization in reference to Figure 5-8. In Cycle 1, the simple combined cycle, the thermal efficiency decreased when the gas turbine compressor inlet pressure was changed in either direction from the standard atmospheric level. In Cycle 2, the recuperative combined cycle, a gain of 0.3% points in thermal efficiency was achieved by raising the gas turbine compressor inlet pressure by 30%.

5.2.5 Effect of Steam Generator High-Pressure and Low-Pressure Steam Pressure

The pressure of the steam in the high-pressure and low-pressure portions of the steam system will affect the performance of the steam system. Since the steam begins as a liquid and then transitions to a gas in the steam generator, the heat transfer process in the steam generator is not uniform. The heat transfer to the fluid occurs in three stages. From the perspective of the feed-water, the first stage involves the heating of the feed-water to the point where it can begin to vaporize. This stage is accomplished by the lowest grade heat which remains in the gas turbine exhaust after it has already given up significant energy to steam production in the second and third stages. The temperature change seen by the feed-water is large in the first stage, with the final temperature equalling the saturation temperature. The saturation temperature is the temperature at which the water will begin to transition to steam. The saturation temperature depends on the pressure of the water, and can

be increased by increasing the pressure of the water. It can occur where the pressure is too high for the required heat transfer, which is when the saturation temperature is too close to the gas turbine exhaust temperature. Reduction in steam temperature or reduction in steam flow rate can both allow successful completion of the second stage of heat transfer. The fluid reaching the saturation temperature in the steam generator denotes the start of the second stage, while the end of the second stage corresponds to fluid being entirely in the vapour phase. The third and final stage is where the steam is raised in temperature, or becomes superheated, above the saturation temperature.

Given the details of steam generation, it should be clear that for a fixed turbine exhaust gas temperature, there will be saturation temperatures which best suit energy extraction. Considering what was presented in the previous paragraph, it might seem that the lowest saturation temperature would be the optimum, but this is not the case. By reviewing the steam tables, it can be seen that the enthalpy values rise with pressure and temperature. Thus, with increasing pressure and temperature of the steam, there is more energy available for removal. It requires very little energy to compress liquid water, thus the benefits of increasing the steam pressure more than offsets the additional energy required for the increased compression of the feed-water. It can be shown that steam cycles, or Rankine Cycles, are such that the available enthalpy change across the steam turbine generally increases with the

temperature and pressure present at the steam turbine inlet. This fact balances the heat transfer benefits with a low saturation temperature, and thus there is an optimum steam pressure.

Figure 5-9 shows a plot of thermal efficiency on the vertical axis against the low-pressure steam pressure. As shown in Section 4.7.5, the steam system considered in this thesis is of the two-pressure variety. There is a high-pressure steam circuit followed by a low-pressure circuit which combines to form a single continuous loop with only one pump and one condenser. To demonstrate the effects of steam pressure on the overall thermal efficiency, curves of high-pressure steam are plotted on the thermal efficiency versus low-pressure steam pressure graph. Three curves of high-pressure steam pressures are presented in Figure 5-9; they are 40 bar, 60 bar, and 80 bar. Each of these curves has a peak. Upon these peaks are plotted square blocks. These blocks represent the optimum low-pressure steam pressure for each of the high-pressure steam curves. For example, looking at the 40 bar high-pressure steam trend, the square block is positioned at the peak, which aligns on the horizontal axis showing a low-pressure steam pressure optimum of 8 bar. Another observation is that as the high-pressure steam pressure is increased, the benefit gained in thermal efficiency becomes smaller; however, raising the high-pressure steam pressure continues to produce thermal efficiency benefits even above 175 bar. At very high steam pressures, the mechanical expense serves to place an

upper limit on the design specifications. Industry standard is to pick the high-pressure steam pressure at the point where the increased mechanical costs outweigh the potential benefits from the increase in thermal efficiency, or at some justifiable location near this point.

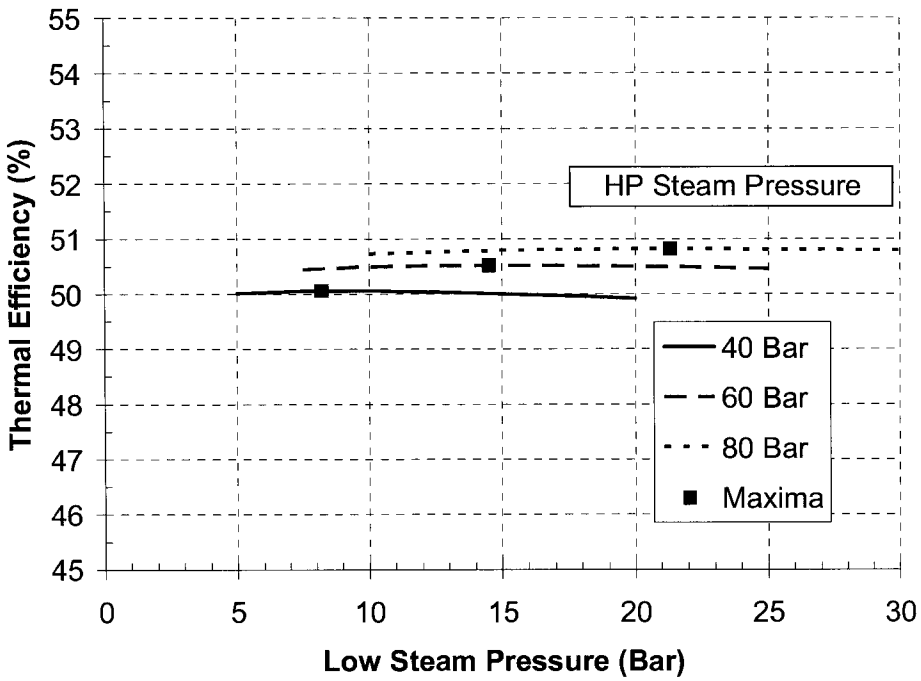

Figure 5-9: Thermal efficiency vs. low pressure steam pressure; contours of high pressure steam pressure

Table 5-6 summarizes the model details used to create the data for Figure 5-9. Cycle 2, the recuperative combined cycle, was the model used. The two main design variables, the high-pressure steam pressure, and the low-pressure steam pressure, are

shown in bold-face type. As with most of the other figures, the mass flows are allowed to vary to meet the plant output specification of 100 MW.

Table 5-6: Model specifications for Figure 5-9

	Gas Turbine					
	Compressor Inlet Pressure (bar)	Pressure Ratio	Oxygen Purity (Mole %)	Turbine Inlet Temp. (K)	CO_2 Mass Flow (kg/s)	Net Power Output (MW)
Cycle 1 - Simple Combined Cycle	N/A	N/A	N/A	N/A	N/A	N/A
Cycle 2 - Recuperative Combined Cycle	1.01325	22.5	95.5	1723	Variable	100
	Steam System					
	Steam Mass Flow (kg/s)	Steam Generator Mass Split Ratio	Steam Temp. (K)	Steam Generator Gas Outlet Temp. (K)	**Low-Pressure Steam (bar)**	**High-Pressure Steam (bar)**
Cycle 1 - Simple Combined Cycle	N/A	N/A	N/A	N/A	N/A	N/A
Cycle 2 - Recuperative Combined Cycle	Variable	0.5	S.G. inlet - 25 K	393.15	**Design Variable**	**Design Variable**
* Temp. = Temperature						
** S.G. = Steam Generator						
***N/A = Not Applicable						

A few final observations are warranted concerning the optimization of steam cycles. First, close inspection of the vertical axis of Figure 5-9 reveals that when optimizing the steam system, the maximum expected benefit is about 1 percentage

point of overall thermal efficiency. It is important to note that most of this benefit is attained by maximizing the high-pressure steam pressure, and in comparison, optimizing the low-pressure steam pressure may contribute only one-tenth the benefit. It may be most beneficial to select the low-pressure steam pressure at a level which is convenient for reasons other than the peak efficiency, as the difference between the optimum and off-design performance is small. In summary, maximizing the high-pressure steam pressure and choosing the low-pressure steam pressure as required is sufficient to obtain maximum performance.

The effect of condenser pressure on efficiency was not investigated by parametric study. The minimum condenser pressure is specific to steam system configuration and available cooling water temperature. As such, the moderately conservative assumption of 0.1 bar condenser pressure, as specified in Chapter 4, was held constant for all cycles during modeling and optimization.

5.2.6 Effects of Steam Generator Steam Temperature

Steam temperature, similar to steam pressure, has an effect on the overall efficiency of the cycle. Figure 5-10 shows a plot of thermal efficiency on the vertical-axis versus steam temperature on the horizontal-axis. The trend was generated considering a single-pressure once-through steam generator (OTSG). In an OTSG, the feed-water is forced through the heat exchanger from the cold end; the end furthest from the turbine outlet. Since the water is forced, there is control over

the flow rate. Increasing the feed-water flow rate decreases the temperature of the steam at the outlet of the steam generator, while decreasing the flow rate increases the steam temperature. The steam temperature can only approach the exhaust gas temperature, and can obviously not exceed it. How close the steam temperature approaches the turbine outlet gas temperature depends on the size of the steam generator. A very large steam-generation heat exchanger

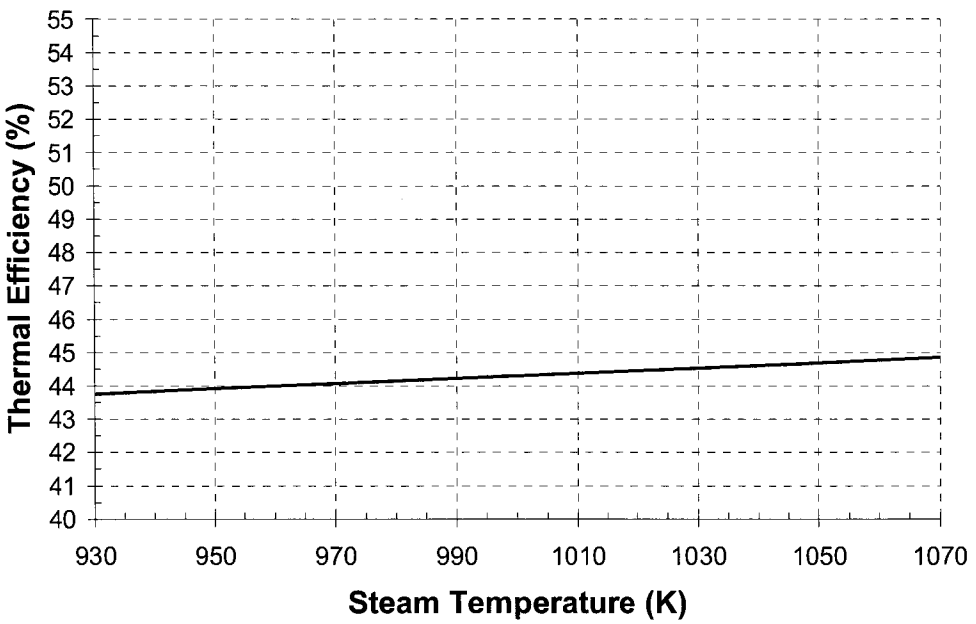

Figure 5-10: Thermal efficiency vs. once through steam generator steam temperature

may be able to create steam at temperatures within 25 K of the gas turbine outlet temperature, while a smaller, low-budget version may achieve a differential greater than 50 K. Figure 5-10 shows the thermal efficiency increasing 1.9% points for

every 200 K (200°C) in temperature. The term *% points,* denotes the subtracted difference between two overall thermal efficiency values. For example: a thermal efficiency of 48.4% subtract a thermal efficiency of 46.7% gives 1.7% *points* in thermal efficiency; however, dividing the two numbers, subtracting 1, and multiplying by 100 shows a 3.6% difference. The 200 K difference in steam temperature was achieved by decreasing the feed-water mass flow rate from its maximum flow by 10%. The 1.9% point thermal efficiency gain is significant. The zero-emission semi-closed combined cycles are able to generate high steam generator inlet temperatures in comparison with current open-cycles which operate on air. This is due to the lower ratio of specific heats value in the turbine flow with respect to open-cycles using air. To capitalize on the performance potential due to the high steam generator inlet temperatures, steam turbines with at least 1073 K (800°C) inlet temperatures should be used.

Table 5-7 presents the specifications which were used to generate the data for Figure 5-10. A simple combined cycle with a single pressure OTSG was used. The Design variable was the steam temperature, which was varied by manipulating the steam generator feed-water mass flow rate. The mass flow rate of the carbon dioxide through the gas turbine was also permitted to vary to meet the power output requirement of 100 MW.

The steam temperature affects the overall cycle efficiency because of the effects it has on the efficiency of the steam cycle. This steam cycle is similar to the standard superheat Rankine cycle, where superheated steam is steam raised to some

Table 5-7: Model specifications for Figure 5-10

	Gas Turbine					
	Compressor Inlet Pressure (bar)	Pressure Ratio	Oxygen Purity (Mole %)	Turbine Inlet Temp. (K)	CO_2 Mass Flow (kg/s)	Net Power Output (MW)
Cycle 1 - Simple Combined Cycle	1.01325	22.5	95.5	1723	Variable	100
Cycle 2 - Recuperative Combined Cycle	N/A	N/A	N/A	N/A	N/A	N/A
	Steam System					
	Steam Mass Flow (kg/s)	Steam Generator Mass Split Ratio	**Steam Temp. (K)**	Steam Generator Gas Outlet Temp. (K)	Low-Pressure Steam (bar)	High-Pressure Steam (bar)
Cycle 1 - Simple Combined Cycle	Variable	0.5	**Design Variable**	393.15	N/A	170.0
Cycle 2 - Recuperative Combined Cycle	N/A	N/A	N/A	N/A	N/A	N/A
* Temp. = Temperature						
** S.G. = Steam Generator						
***N/A = Not Applicable						

temperature above its saturation temperature, and the Rankine cycle refers to the fluid cycle where a liquid is compressed, vaporized by heat, and then expanded to convert the energy into mechanical energy. In the superheated Rankine cycle, a high superheat temperature results in a high efficiency.

5.2.7 Effects of Steam Generator Outlet Gas Temperature

The temperature of the gas flow leaving the steam generator has a significant effect on the overall thermal efficiency. This *waste heat* refers to the amount of heat contained in the flow between its temperature at the steam generator exit and the temperature of the flow at the compressor inlet. For a given gas turbine mass flow and turbine outlet temperature, three main attributes affect the temperature of the gas leaving the steam generator. The first is the size of the heat exchanger. The largest heat exchanger is best at minimizing the temperature of the exhaust gas flow. The second and third attributes affecting the temperature of the gas flow leaving the steam generator are the feed-water temperature and the feed-water mass flow rate. The steam generator outlet temperature can only be so low as to approach the feed-water temperature. An increase in feed-water temperature would result in an increase in steam generator outlet temperature. The feed-water mass flow is limited by the amount of energy available to the feed-water vaporization process, thus it cannot be increased at will to satisfy the desires of minimizing the steam generator outlet gas temperature.

The main function of the steam generator is to capture the waste heat from the gas turbine. The steam generator's performance is maximized when the steam generator outlet temperature is being minimized. Figure 5-11 is a plot of thermal efficiency versus the steam generator outlet gas temperature, which is shown in the absolute units of temperature, K. Data is shown for Cycle 1, the simple combined cycle, and Cycle 2, the recuperative combined cycle. The data trends are shown over different ranges as different steam generator outlet temperatures are achievable given the large difference in the steam generator gas inlet temperatures. Cycle 2, with its

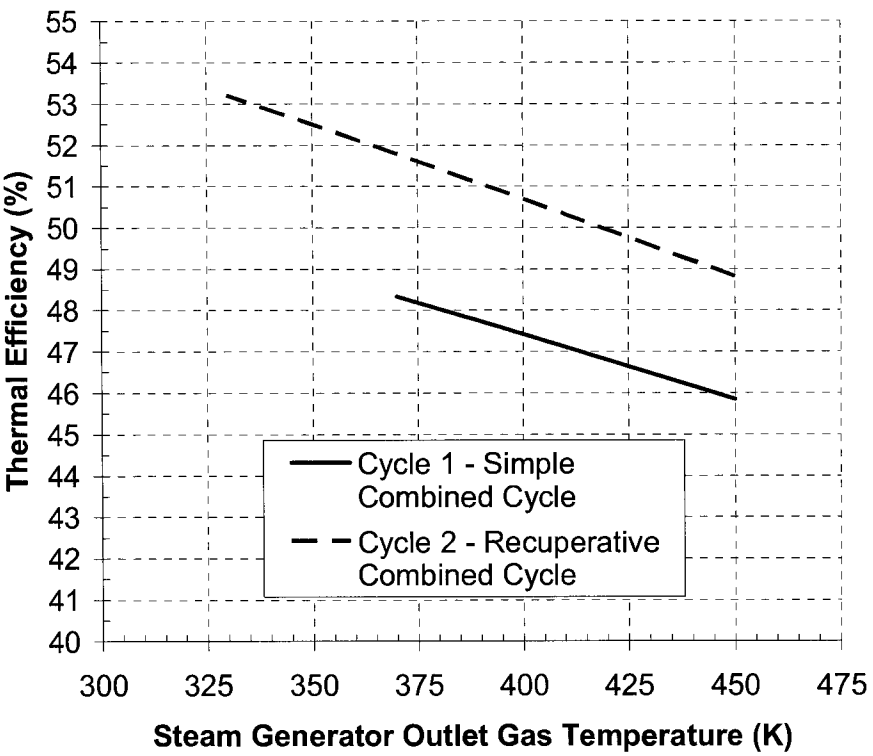

Figure 5-11: Thermal efficiency vs. once-through steam generator outlet gas flow temperature

lower steam generator gas inlet temperature, is able to achieve lower steam generator gas outlet temperatures, even though Cycle 1's feed-water temperature is identical. Data from each cycle shows an approximately 30 K reduction in steam generator outlet gas temperature can result in a 1% point increase in overall thermal efficiency. Table 5-8 shows the model specifications used to create the data for Figure 5-11. The steam generator gas outlet temperature is the Design variable and is shown in bold-face type. The gas turbine and steam generator working fluid mass flow rates are permitted to vary to meet the power output requirement of 100 MW. The steam generator gas outlet temperature is a direct specification in the models.

There is an extra benefit to minimizing the steam generator outlet gas temperature. Upon leaving the steam generator, the gas working fluid moves on to the main cooling condenser. The main condenser's function is to drop the temperature of the working fluid to as close to the ambient temperature as possible while removing excess water which was released during the combustion process. When the steam generator outlet gas temperature is minimized, less cooling is required by the condenser. The result is a smaller required condenser, with less mass flow from the heat sink. Minimizing the steam generator outlet gas temperature not only maximizes the performance of the steam system, but also reduces the size and cost of the main cooling condenser.

Table 5-8: Model specifications for Figure 5-11

	Gas Turbine					
	Compressor Inlet Pressure (bar)	Pressure Ratio	Oxygen Purity (Mole %)	Turbine Inlet Temp. (K)	CO_2 Mass Flow (kg/s)	Net Power Output (MW)
Cycle 1 - Simple Combined Cycle	1.01325	22.5	95.5	1723	Variable	100
Cycle 2 - Recuperative Combined Cycle	1.01325	22.5	95.5	1723	Variable	100
	Steam System					
	Steam Mass Flow (kg/s)	Steam Generator Mass Split Ratio	Steam Temp. (K)	**Steam Generator Gas Outlet Temp. (K)**	Low-Pressure Steam (bar)	High-Pressure Steam (bar)
Cycle 1 - Simple Combined Cycle	Variable	0.5	S.G. inlet - 25 K	**Design Variable**	14.7	170
Cycle 2 - Recuperative Combined Cycle	Variable	0.5	S.G. inlet - 25 K	**Design Variable**	21	80.0
* Temp. = Temperature						
** S.G. = Steam Generator						

5.2.8 Effects of Steam Generator Mass Split Ratio

The once-through steam generator (OTSG) configuration as described in Section 4.3.1 can accommodate various ratios of gas turbine exhaust mass flow split between the high- and low-pressure superheaters. This is not a feature that would be

built as adjustable, but the steam generator could be constructed at a selected mass split ratio. Figure 5-12 is a plot of thermal efficiency versus the mass flow split ratio

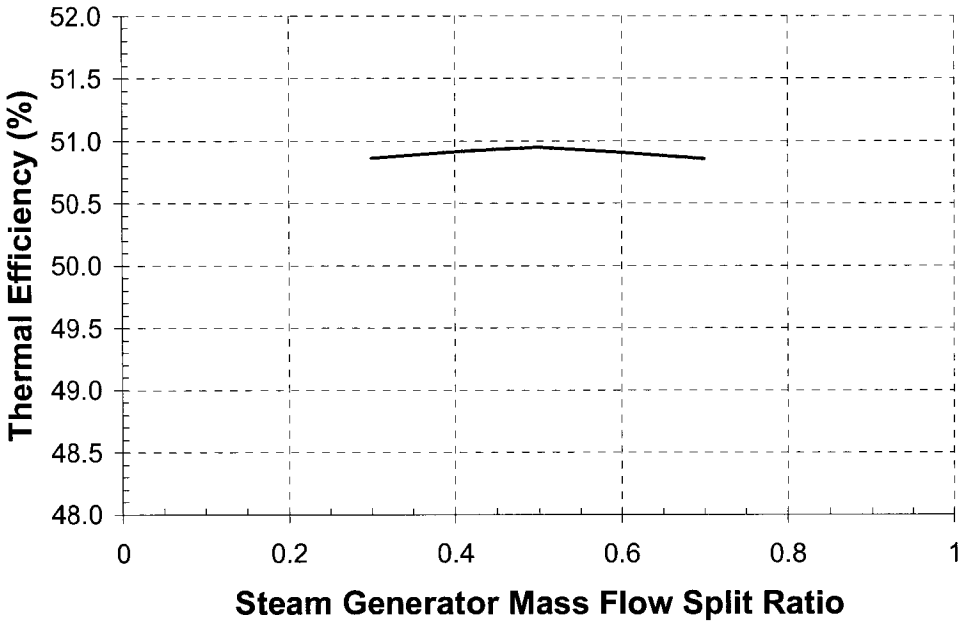

Figure 5-12: Thermal efficiency vs. once-through steam generator mass split ratio for Cycle 2

between the high-pressure and low-pressure superheaters in the steam generator. The flow split ratio of 0.5 infers 50% of the mass flow is sent to each of the high-pressure or low-pressure superheaters. Results show that a balanced OTSG split is the optimum mass flow split value. The thermal efficiency lost by using an uneven split is marginal. Table 5-9 shows the model specifications used to create the data for Figure 5-12. The OTSG mass split ratio is the Design variable and is shown in bold-face type. The gas turbine and steam generator mass flows are allowed to vary to meet the power output specification of 100 MW.

Table 5-9: Model specifications for Figure 5-12

	Gas Turbine					
	Compressor Inlet Pressure (bar)	Pressure Ratio	Oxygen Purity (Mole %)	Turbine Inlet Temp. (K)	CO_2 Mass Flow (kg/s)	Net Power Output (MW)
Cycle 1 - Simple Combined Cycle	N/A	N/A	N/A	N/A	N/A	N/A
Cycle 2 - Recuperative Combined Cycle	1.01325	22.5	95.5	1723	Variable	100
	Steam System					
	Steam Mass Flow (kg/s)	**Steam Generator Mass Split Ratio**	Steam Temp. (K)	Steam Generator Gas Outlet Temp. (K)	Low-Pressure Steam (bar)	High-Pressure Steam (bar)
Cycle 1 - Simple Combined Cycle	N/A	N/A	N/A	N/A	N/A	N/A
Cycle 2 - Recuperative Combined Cycle	Variable	**Design Variable**	S.G. in - 25 K	393.15	21.3	80.0
* Temp. = Temperature						
** S.G. = Steam Generator						
***N/A = Not Applicable						

5.3 Performance Results

Table 5-10 presents the peak overall thermal efficiency values achieved using the ASPEN PLUS OPTIMIZER. The first column in the table is used to show which

cases are low-purity oxygen and which are high-purity oxygen. The peak performance values are presented as thermal efficiency values in the second column. The remaining four columns show the parameters which achieve maximum performance. It takes many parameters to define the cycle; however, of the parameters investigated by sensitivity study in Section 5.2, only the four parameters presented in Table 5-10 have the potential of adding value by being optimized using a optimization algorithm.

Although specific work trends were reviewed during the parametric studies, the cycles where not optimized with the aim of determining maximum specific work. The optimum parameters for maximizing specific work are at the ends of the ranges of the input parameters. Maxima in specific work are not present between the upper and lower limits input parameters. It is for these reasons that the ASPEN PLUS OPTIMIZER was used to determine peak thermal efficiencies only.

Table 5-10: Summary of cycle performance study, optimum parameters

	Oxygen Purity:	Overall Efficiency	Compressor Inlet Pressure	Pressure Ratio	HP Pressure	LP Pressure
	Input	Result	Optimum	Optimum	Optimum	Optimum
	v/v %	%	bar		bar	bar
Cycle 1	95.5	48.4	1.01	40	165	14.6
Cycle 1	99.5	46.7	1.01	40	165	14.2
Cycle 2	95.5	51.5	1.29	25	150	49.3
Cycle 2	99.5	50.1	1.29	25	140	47.4

For Cycle 1, the simple combined cycle, the compressor pressure ratio was limited to 40, the high-pressure steam pressure was limited to 165 bar, and the

compressor inlet pressure was set to 1.01 bar. Also shown in Table 5-10, the optimizer found a low-pressure optimum of 14.6 bar and 14.2 bar for the low- and high-purity oxygen cases, respectively. For Cycle 2, the recuperative combined cycle, the optimizer found the pressure ratio optimum at 25, which allowed high-pressure steam pressures of 150 bar and 140 bar, respectively, for the low and high oxygen purity cases. The high-purity oxygen case used a lower high-pressure steam pressure as the steam generator inlet temperature was lower. The high-pressure steam pressure was lowered for the feed-water to vaporize. The compressor inlet pressure was above atmospheric pressure to capture the benefits of the 'Cycle 2 – Recuperative Combined Cycle' trend shown in Figure 5-8. The optimizer yielded the optimum low-pressure steam pressure at 49.3 bar and 47.4 bar, respectively, for the low and high oxygen purity cases.

Comparing the peak performance values for pressure ratio for Cycle 2 from Table 5-10 and Figure 5-1 shows a small discrepancy which demonstrates the importance of using optimization software in lieu of sensitivity study. Figure 5-1 shows that sensitivity study predicts optimum overall pressure ratio to be about 22.5. Table 5-10 shows the ASPEN PLUS OPTIMIZER predicting the optimum overall pressure ratio to be 25. Figure 5-1 shows the trend to be very flat from the overall pressure ratio figures of 20 to 25. This fact allows the optimum to be easily affected. There are no influences present in the sensitivity study as the intent is to hold as

many parameters constant as possible. This is not true when using the ASPEN PLUS OPTIMIZER, which can vary multiple parameters when determining the optimum. In the case of optimum pressure ratio for Cycle 2, the optimizer recognizes that the gas turbine outlet temperature increases with pressure ratio. This can be seen in Figure 5-2. The increase in gas turbine outlet temperature allows higher steam pressures and steam temperatures. This has favourable effects on the overall thermal efficiency. Thus, the ASPEN PLUS OPTIMIZER finds the optimum pressure ratio to be 25, which is higher than the 22.5 as predicted by sensitivity analysis.

Further review of Table 5-10 shows the low oxygen purity cases outperform the high-purity cases by 1.7% points and 1.5% points for Cycles 1 and 2, respectively. The recuperative combined cycle, Cycle 2, outperforms the simple combined cycle, Cycle 1, by 3.1% points for the low oxygen purity case, and 3.4% points for the high purity oxygen case.

Determining the optimum pressure ratios at 25 and 40 will have an effect on the configuration of the gas turbine. Gas turbine compressors can produce high pressure ratios over wide operating ranges only with the help of variable stator geometry or multiple shafts. The baseline assumption for the models was a single-shaft gas turbine. Further design stages of a Cycles 1 and 2 would revisit this assumption.

In Section 2.5, it was determined by review of the literature that open-cycle gas turbine combined cycles which release emissions to the atmosphere can achieve overall thermal efficiencies of about 60%. The zero-emission semi-closed combined cycles of comparable technology presented in Table 5-10 achieve overall thermal efficiencies between 46.7% and 51.5%. Thus, this study shows the semi-closed oxy-fuel cycle method for achieving zero atmospheric emissions costs about an 8.5% point to 13% point reduction in overall thermal efficiency. The variance of 4.5% points between the 8.5% points and 13% points is due to the use of different levels of oxygen purity and different cycle configurations.

5.4 Conclusions

The cycle of highest thermal efficiency is Cycle 2, the recuperative combined cycle, which achieves 51.5% overall thermal efficiency when using low-purity oxygen. Cycle 1 trails Cycle 2 by only 3.1% points. This performance gap widens to 3.4% points when considering the high-purity oxygen case.

Sensitivity studies show that the cycle designer has the opportunity to trade-off thermal efficiency for specific work for both cycles when selecting operating specifications.

The ASPEN PLUS OPTIMIZER yields results which are superior to those generated from sensitivity studies due to the OPTIMIZER's ability to take advantage of synergistic parameter relationships.

The relatively high overall pressure ratio values determined in the optimization process will result in increasing the complexity of the compressor during future design iterations.

Chapter 6 – Investigations of Detailed Plant Issues

6.1 Introduction

Aside from the need to make specific cycle performance estimations, there is also a need to quantify the influence of various inputs on the cycle. The composition of the cycle working fluid is the result of the composition of the fuel, natural gas, and the oxygen streams. The fuel is burned with the oxygen in the combustion chamber, and the resulting products of combustion are primarily carbon dioxide and water. The water is then removed by the main cooling condenser. Thus, the working fluid which remains is primarily carbon dioxide. This chapter investigates the effects of: oxygen purity on the working fluid composition; fuel purity on the working fluid composition; working fluid composition on plant performance; and the effect on

performance of operating with excess oxygen in the working fluid. The final investigation reviews the performance potential of steam injection for the purposes of power augmentation.

6.2 The Effects of Oxygen Purity on Working Fluid Composition

Two factors affect the composition of the carbon dioxide working fluid: the purity of the two cycle inputs, the fuel and the oxygen. This section reviews the effect of varying the oxygen purity on the working fluid composition. Section 6.3 reviews the effects of fuel purity on working fluid composition. Section 6.4 evaluates the cost of producing high-purity carbon dioxide by investigating the effects of working fluid composition on plant performance.

Plant designers must select a level of oxygen purity to be produced by the cycle's air separation unit. This selection will be based on a balance of costs, performance, and the desired purity of the working fluid. Of course, the excess working fluid is continuously captured and compressed to a high pressure, which makes it convenient for transportation to its final destination. If the end use of the carbon dioxide is oil well or ocean injection, then purity would be less of a concern. For industrial use requiring high carbon dioxide purity, it may be most effective to

meet the industry specification directly by ensuring high-purity carbon dioxide is produced by the cycle. This can be done by maximizing the purity of the oxygen and the fuel. It is also possible to use a carbon dioxide cleanup capture process. This system would process the flow leaving the cycle; ensuring high-purity carbon dioxide is captured. Investigation of the performance of post-combustion cleanup processes was beyond the scope of this thesis.

Table 6-1 compares the composition of the working fluids at the compressor inlet as a result of using low-purity and high-purity oxygen. The approximate compositions of low- and high-purity oxygen are 94.4 mass % and 99.4 mass % respectively. The oxygen flow's balance of composition is assumed to be pure argon. This assumption was made because no references were found which present a common air separation unit oxygen stream concentration for the oxygen purities mentioned above. The location of the working fluid in the cycle which is presented in Table 6-1 is the compressor inlet. The concentration of the oxygen in the working fluid at that location is set to 1.0 mass % and held to this value by varying the oxygen mass flow rate entering the combustor from the air separation unit. The value of 1% oxygen in the working fluid is used to help ensure complete combustion.

The working fluid is assumed to be made of 18 components; however, the concentration of most of the components is small. A table listing the concentrations of all components is presented in Appendix D. The use of low-purity oxygen results

in the working fluid reaching a steady-state composition of 90 mass % carbon dioxide. High-purity oxygen is needed to achieve carbon dioxide with a purity of 97 mass %. Working fluid composition is also a function of fuel composition. The effect of the fuel composition on the working fluid is investigated in the following section.

Table 6-1: Working fluid compositions as a function of oxygen purity at the gas turbine compressor inlet

	(Mass %)	(Mass %)
Inputs:		
Oxygen flow:	**94.4 (Low)**	**99.4 (High)**
Oxygen	94.4	99.4
Argon	5.6	0.6
Fuel Flow:	natural gas	natural gas
Working fluid:		
Argon	7.7	0.84
Carbon Dioxide	**90.1**	**96.9**
Nitrogen	0.90	0.97
Oxygen (fixed)	1.0	1.0
Water (post-condenser)	0.293	0.286

For some industrial applications, 98 mass % and higher purity carbon dioxide is required. Since such high purity is not reasonably achievable in the bleed stream from the zero-emission plant, an additional carbon dioxide purification system would be required. This can take the form of an amine scrubber system. These systems are in use today around the world in various applications. Amine scrubbers are a mature

technology but have many undesirable characteristics, commonly suffering high equipment corrosion rates and significant energy requirements (Fulkerson et al, 1990).

6.3 The Effects of Fuel Composition on Working Fluid Composition

Three fuel compositions are used to investigate the effects of fuel composition on working fluid composition. The compositions of the three fuels, as well as the fuels lower-heating values, are shown in Table 6-2. The first fuel is natural gas. The second fuel is similar to the first except that all the non-hydrocarbon components are removed. Typical non-hydrocarbon components in natural gas, such as nitrogen, carbon dioxide, oxygen and water add no value to the gas. These components effectively degrade the quality of the gas. During the refining stages of natural gas, these elements are present at the refining plant's inlet. Both carbon dioxide and water are actively removed from the gas; however, the extent to which it is removed varies. Often carbon dioxide and water are side-slipped, or allowed to continue into the natural gas produce stream. For most users of the natural gas, this is of little cause for concern, except when buying gas on a per-cubic-foot basis. Purchasing natural gas on a volume basis may result in the buyer

Table 6-2: Three fuel compositions and lower-heating values (LHV)

Composition #	1	2	3
	Natural Gas	Pure Hydrocarbons	Methane
	(Union Gas)	(Ideal clean NG)	(Ideal)
Component:	(Mass %)	(Mass %)	(Mass %)
Methane	94.9	97.2	100
Ethane	2.50	2.56	
Nitrogen	1.60	0	
Carbon Dioxide	0.700	0	
Propane	0.200	0.205	
Iso-Butane	0.0300	0.0307	
N-Butane	0.0300	0.0307	
Oxygen	0.0200	0	
I-Pentane	0.0100	0.0102	
N-Pentane	0.0050	0.0051	
N-Hexane	0.0050	0.0051	
Argon	0	0	
Water	0	0	
Carbon Monoxide	0	0	
Hydrogen	0	0	
LHV (MJ/kg)	**47.602**	**49.854**	**50.018**

being short-changed due to the lower heating value of the gas. In zero-emission semi-closed cycles, impurities which enter the cycle from the gas will decrease the purity of the working fluid. The second fuel, with only hydrocarbon components, is used to quantify the result of the fuel impurities on the composition of the working fluid. The third fuel investigated is pure methane. This fuel is often used in cycle simulation as a simple representation of natural gas. In zero-emission semi-closed combined cycles, the fuel composition has an effect on the working fluid. This third

fuel may provide insight into the relevance of representing natural gas by using pure methane.

The change in fuel composition affects the plant's overall efficiency due to the corresponding change in working fluid composition; however, the small changes in the lower heating value do not significantly affect the overall thermal efficiency. The work required by a fuel gas compressor would change when the mass flow of fuel required changes due to a change in fuel heating value. This would affect the overall efficiency if there was a fuel compressor in the cycle; however, no fuel gas compressor has been included in the present plant model. It is assumed that high-pressure natural gas would be available to a plant of this size.

The effect of the change in fuel composition on the working fluid is presented in Table 6-3. Surplus oxygen is set at 1% by mass to ensure sufficient oxygen for combustion for reasons presented in Section 4.7.8. The oxygen stream is assumed to be oxygen and argon; therefore, no nitrogen is present in the cycle when considering either of the ideal fuels. Reducing the amount of nitrogen entering the cycle is an effective method of increasing the carbon dioxide concentration in the working fluid. The reduction in nitrogen is the primary difference between the first and second fuel composition as described in Table 6-2. The water concentration is similar for all three cases as the carbon dioxide leaves the condenser at a fixed temperature and 100% humidity. The natural gas case does hold 8% more water by mass than the

Table 6-3: Working fluid composition as a function of fuel composition at the gas turbine compressor inlet

	(Mass %)	(Mass %)	(Mass %)
Inputs:			
Oxygen flow:	**94.4 (Low)**	**94.4 (Low)**	**94.4 (Low)**
Oxygen	94.4	94.4	94.4
Argon	5.6	5.6	5.6
Fuel Flow:	natural gas (1)	ideal natural gas (2)	ideal Methane (3)
Working fluid:			
Argon	7.7	7.8	7.9
Carbon Dioxide	**90.1**	**90.9**	**90.8**
Nitrogen	0.90	0.00	0.00
Oxygen (fixed)	1.0	1.0	1.0
Water (post-condenser)	0.293	0.269	0.269

other two cases. In changing the fuel composition from natural gas, the cycle overall thermal efficiency decreases by about 0.08% points. The ideal methane case out-performs the ideal natural gas fuelled case by 0.012% points in overall thermal efficiency. Considering working fluid composition, the result of using an idealized natural gas or pure methane in zero-emission semi-closed cycle simulation is identical.

6.4 The Effect of Excess Oxygen on Overall Thermal Efficiency

As described in Section 4.7.8, the oxygen concentration in the loop is controlled to provide a small excess to promote complete combustion. Figure 6-1 shows the effect of excess of oxygen in the working fluid on the overall thermal efficiency.

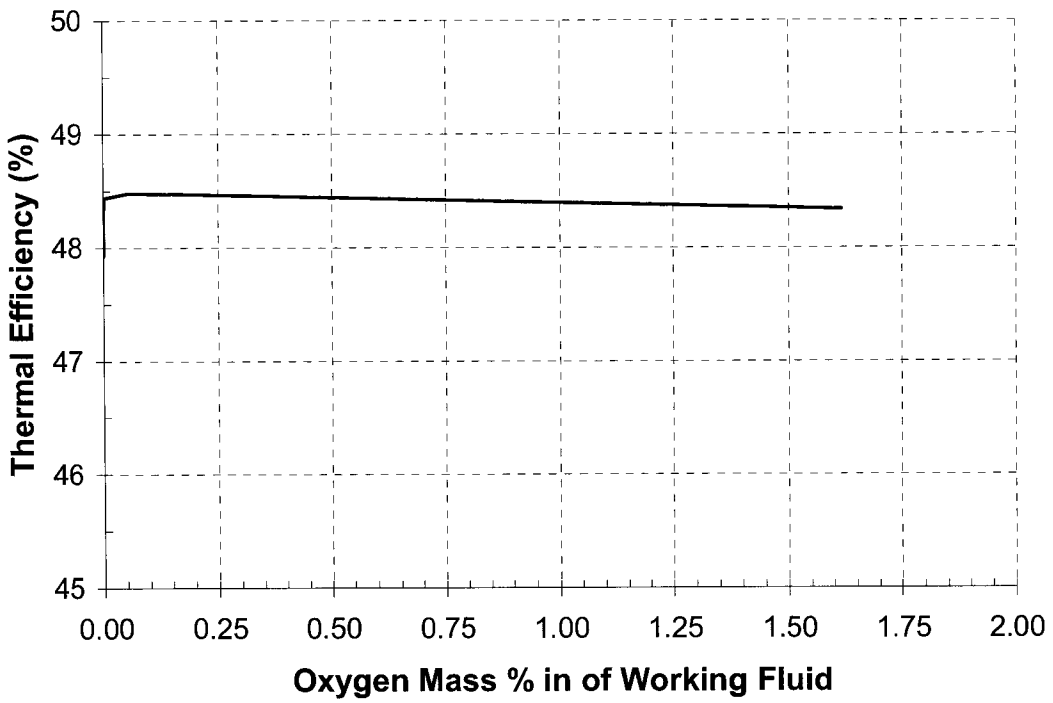

Figure 6-1: Overall thermal efficiency vs. oxygen concentration in working fluid

The cost of operating a working fluid with an oxygen concentration of 1% by mass is an overall thermal efficiency decrease of 0.08% points compared with the

case of no excess oxygen. This value is small because of the steady-state characteristics of the cycle, which deem that the concentrations of non-reacting species in the semi-closed loop will generally follow the combined concentrations of all the inlets, with changes due to the combustion process. In this case, a 0.65% increase in oxygen mass flow rate above stoichiometric results in a 1% by mass excess of oxygen in the working fluid. The increase in oxygen production by the air separation unit will detract from the overall cycle thermal efficiency as shown in the negative slope of Figure 6-1.

6.5 The Effects of Working Fluid Properties on Performance

This section reviews the effects of the changes of the working fluid composition on cycle performance. Results show that increasing the oxygen purity from 94.4 mass % to 99.4 mass % results in a decrease in cycle efficiency. The cause of this net efficiency reduction can be attributed to changes in the powers required by individual components. The effect of power required for particular components are shown in Figures 6-2 and 6-3 for Cycle 1, the simple combined cycle, and Cycle 2, the recuperative combined cycle, respectively. From left to right, the first four data bars are the efficiency changes due to changes in power required

for the auxiliaries: the air separation unit (ASU), the oxygen compressor (O_2C), the carbon dioxide bleed compressor (CO_2 C), and the boiler feed pump (BFP). The fifth bar shows the net effect on the overall efficiency of the change in working fluid properties due to change in gas turbine (GT) efficiency, followed by the same effect

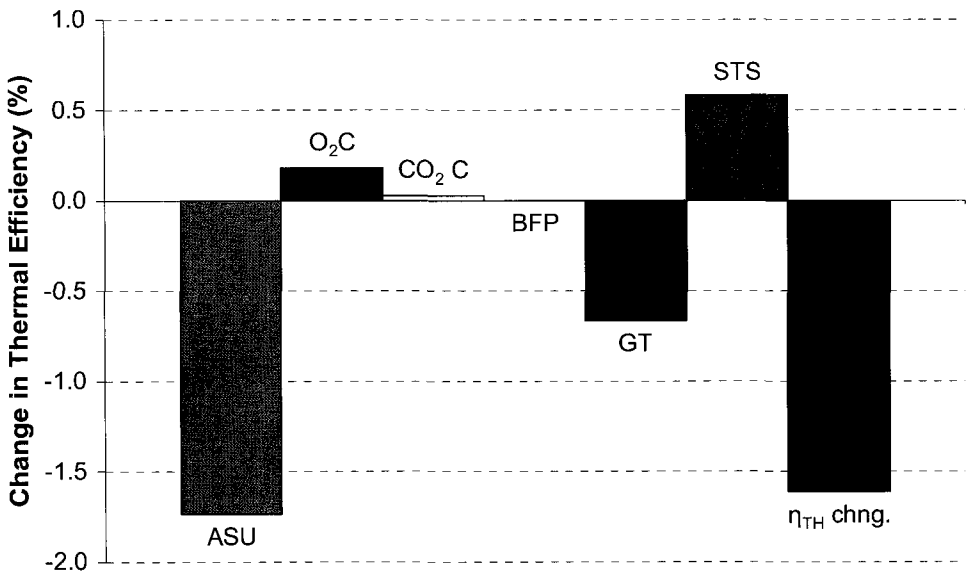

Figure 6-2: Cycle 1: Changes in thermal efficiency with increasing oxygen purity from 94.4 mass % to 99.4 mass %

for the steam system (STS) in the sixth bar. The final bar shows the net change in overall thermal efficiency (η_{th} chng.), the sum of the first six series.

From Figure 6-2, for Cycle 1, as the system moves from low-purity oxygen to high-purity oxygen, the air separation load will increase as more power is needed to increase the oxygen purity, contributing to a reduction in the overall thermal

efficiency from 48.4% to 46.7%. Counteracting this effect, the oxygen compressor and carbon dioxide storage compressor will require less power. Table 6-1 shows the high-purity oxygen case of 99.4 mass % purity contains only 10% as much argon as the low oxygen purity case. This difference in composition affects the properties of the gas being compressed in both the oxygen compressor and carbon dioxide storage compressor. The specific heats and ratio of specific heats for argon are such that it requires more energy to compress argon than it does to compress carbon dioxide. At standard ISO conditions, C_p and γ for argon are 0.5 and 1.67, respectively. For carbon dioxide, at the same conditions, C_p and γ are 0.84 and 1.33, respectively (Toolbox, 2005). Holding these values constant, it can be shown that when compressing these gases to 25 atmospheres, the argon flow would require approximately 28% more power. Thus, Cycle 1's oxygen compressor and carbon dioxide storage compressor will require less power when the amount of argon in the cycle is reduced. The amount of argon decreases significantly when high-purity oxygen is used in the cycle. The change in feed-water pump power is small, but the gas turbine contributes a loss of thermal efficiency of approximately 0.6 % points due to the change in working fluid properties. The increase in carbon dioxide concentration in the working fluid decreases the temperature at the inlet to the combustion chamber and increases the turbine outlet temperature. This change means that more fuel is required in the combustion chamber, and more energy will

leave the gas turbine without being converted to mechanical work. Fortunately, the increased turbine outlet temperature has a positive effect since the steam generator can recover more waste heat. Overall, the contribution of the air separation unit to the reduction in thermal efficiency largely accounts for the net reduction in thermal efficiency, since the effect of the other components largely balance each other.

Figure 6-3 shows the effect of the change of working fluid properties on Cycle 2. The result is similar to Cycle 1, except for the gas turbine and steam system contributions. The change in working fluid properties again results in a decrease in temperature at the outlet of the compressor; however, this decrease and the increased temperature at the turbine outlet favour energy transfer in the recuperator. The greater difference between the two temperatures helps transfer more energy through the recuperator. This favourable adjustment in temperatures results in the gas turbine in Cycle 2 making a positive contribution to the overall thermal efficiency due to the increased oxygen purity and the resulting carbon dioxide concentration in the working fluid. The increase in gas turbine efficiency results in a decrease in gas inlet temperature to the steam system. This decrease negatively affects the steam system's performance, resulting in a negative contribution to overall thermal efficiency from that component. Once again, similar to Cycle 1, the air separation unit makes the main contribution in decreasing the overall thermal efficiency. The effects of other components are approximately in balance.

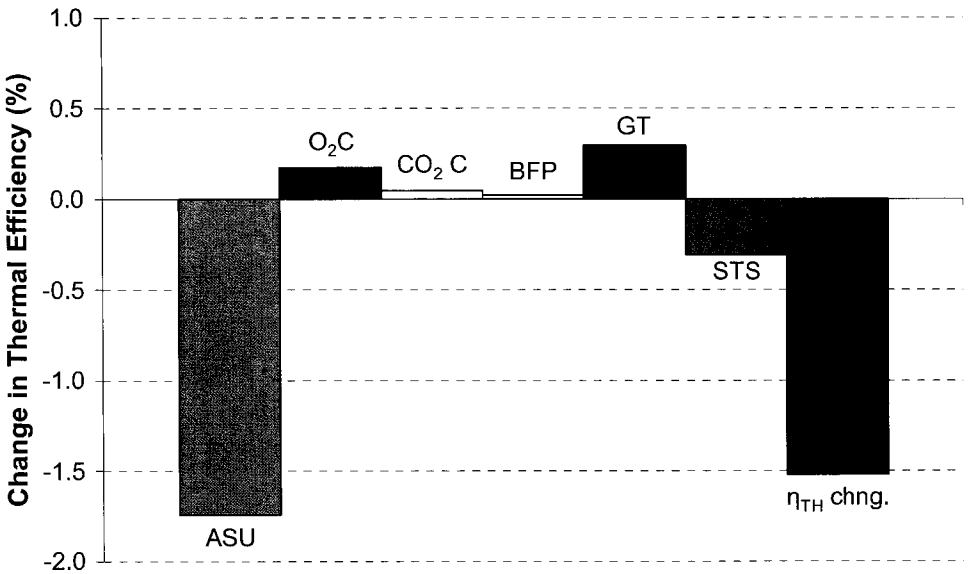

Figure 6-3: Cycle 2: Changes in thermal efficiency with increasing oxygen purity from 94.4 mass % to 99.4 mass %

In summary, for the assumptions presented in Chapter 4; using a natural gas fuel in a zero-emission semi-closed cycle, and changing the oxygen purity from 94.4 mass % to 99.4 mass % will reduce overall plant efficiency by 1.62 % points for Cycle 1, the simple combined cycle, and 1.47 % points for Cycle 2, the recuperative combined cycle. The effects of oxygen purity on the primary component groups of the cycle are summarized in Table 6-4. The four main portions of the plant are shown, and it is indicated whether the effect of an increase in oxygen purity is favourable or unfavourable on cycle performance. Increases in oxygen purity affect the gas turbine and steams systems oppositely for the two cycles, while the air separation load and auxiliary load are affected similarly.

Table 6-4: Summary of effects of raising the oxygen purity on the overall thermal efficiency of the cycles

System	Cycle 1: Simple Combine Cycle	Cycle 2: Recuperative Combined Cycle
	Effect on overall efficiency	Effect on overall efficiency
Air Separation Load	Unfavourable	Unfavourable
Gas Turbine	Unfavourable	Favourable
Remaining Auxiliary Load	Favourable	Favourable
Steam System	Favourable	Unfavourable

6.6 The Effect of Steam Injection Power Augmentation on Performance

Steam power augmentation involves injecting steam into the combustor of the gas turbine to increase the gas turbine's power output. It has been used successfully in many open-cycle gas turbines, but open-cycle power augmentation by steam injection suffers one main drawback; the requirement for a large quantity of treated water, as the injected steam is expelled in the gas turbine's exhaust. Semi-closed cycle gas turbines have a potential advantage over open-cycle gas turbines in this respect as the water will be recovered from the gas turbine's exhaust in a semi-closed cycle. The water recovery will take place in the main carbon dioxide cooling condenser, which is designed to cool the flow and remove the water which is a product of combustion. The water recovered in the condenser will likely require

some form of treatment, but the treatment may be less involved than treating water directly from the environment.

A previous study at Carleton reviewed water and steam injection in zero-emission semi-closed cycle gas turbines (Shan, 2003). It was determined that three mechanisms are responsible for the increase in power output from the gas turbine. Each mechanism will be explained in turn.

The first mechanism deals with the effects of steam addition on the turbine section of the gas turbine. In steady-state operation without power augmentation, the mass flow through the turbine section is equal to the mass flow of working fluid entering the compressor, plus the mass flows of the fuel and oxygen. In applying steam power augmentation, the mass flow through the turbine section is increased. The steam can be injected directly into or immediately upstream of the combustion chamber. The increased mass flow through the turbine section will help produce more power as it is expanded. Since the mass flow through the compressor is unchanged, the ratio of power required by the compressor versus power supplied by the turbine decreases favourably. Thus, the first mechanism responsible for the increase in power output from the gas turbine is the increase in mass flow through the turbine section due to the addition of steam.

The second mechanism by which steam power augmentation increases power output is related to the temperature at which the steam is injected. The steam

generated for injection is usually produced in a waste-heat recovery boiler. Except for the condition where there is supplementary firing of the boiler, which is when fuel burners operate in the space between the gas turbine outlet and the steam generator's heat exchanger elements, the steam will always be at a temperature which is lower than the turbine outlet temperature. The turbine outlet temperature is lower than the turbine inlet temperature due to the expansion process which takes place through the turbine. Thus, the maximum steam temperature is significantly less than the turbine inlet temperature. As steam is introduced to the gas turbine, the turbine inlet temperature will tend to decrease as the steam temperature is much lower than the turbine inlet temperature. The fuel mass flow must then increase to hold the turbine inlet temperature constant. This increase in fuel increases the mass flow rate passing through the turbine section, which will contribute to increased gas turbine overall power output. Thus, the second mechanism which increases the gas turbine's power output during power augmentation is the increase in mass flow due to the increase in fuel required to maintain the turbine inlet temperature.

The third mechanism which increases the gas turbine's power output during power augmentation is a result of the changes in the working fluid properties. The addition of steam to the primarily carbon dioxide working fluid will change the specific heat capacity and ratio of specific heats. At turbine inlet temperatures, the specific heat capacity and ratio of specific heats are much higher for steam than they

are for carbon dioxide. When mixing the steam and carbon dioxide, the result is that the temperature difference across the turbine will become larger, which means the enthalpy change across the turbine is larger. Both the specific heat capacity and ratio of specific heats contribute to this result; however, the influence of the specific heat capacity is dominant. Figure 6-4 shows the effect of changes of specific heat

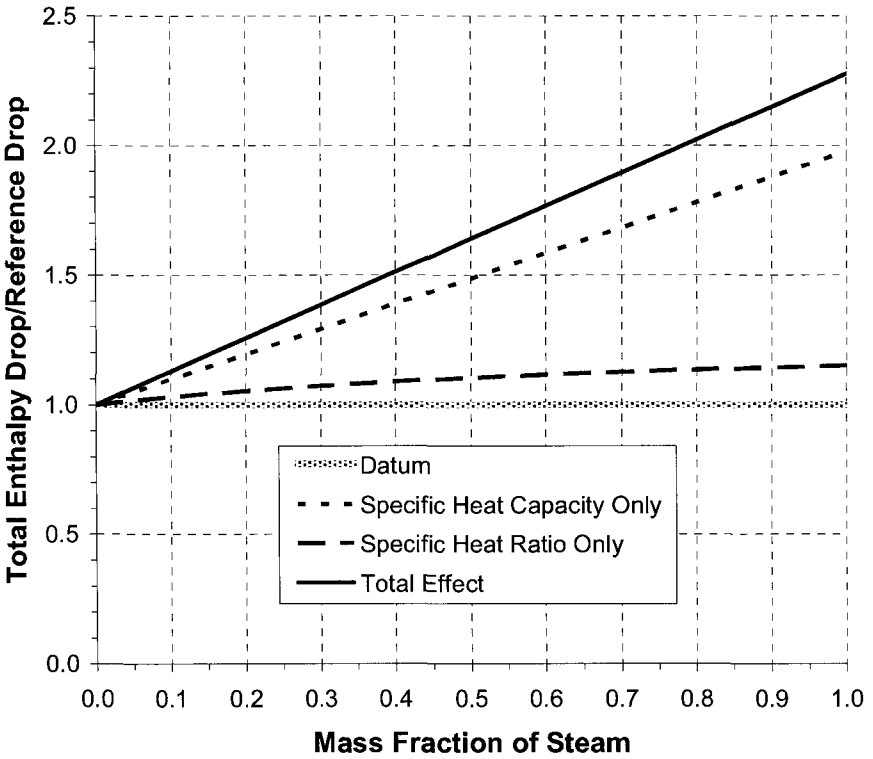

Figure 6-4: Normalized gas turbine enthalpy drop for range of mass fractions of steam in carbon dioxide

capacity and specific heat ratio due to increasing mass % of steam in a carbon dioxide mixture on the enthalpy extracted from a turbine. The results are normalized

to a datum at 1.0 which represents a pure carbon dioxide working fluid. The specific heat capacity is responsible for more than 2/3s of the change in enthalpy available. Thus, the third mechanism which increases the gas turbine's power output during power augmentation is the favourable expansion properties that the steam brings to the working fluid. Specifically, the addition of steam increases the mixture's ratio of specific heats.

Considering combined cycle plants, it is best to inject steam into the gas turbine's combustor at the highest possible temperature, while minimizing the differential pressure between the injecting steam system and the combustor shell pressure. The pressure energy difference is effectively a loss, as the steam throttles to the shell pressure during the injection into the combustor. This mechanism contributes to the fact that, during power augmentation, even though the gas turbine efficiency increases, the overall combined cycle efficiency decreases. Figure 6-5 is a plot of thermal efficiency versus the steam-to-fuel ratio. Steam-to-fuel ratio is defined as the mass flow of steam divided by the mass flow of fuel. Steam-to-fuel ratio is useful when quantifying the maximum steam injection which can be applied without impeding combustion in an open-cycle gas turbine. In semi-closed cycle gas turbines, if the combustor is designed to handle a high mass flow of steam, the steam flow will not necessarily inhibit the combustion process. The steam-to-fuel

ratio remains a valid parameter as it puts the magnitude of the mass flow of the steam into context. Figure 6-5 shows the effect of minimizing the differential pressure

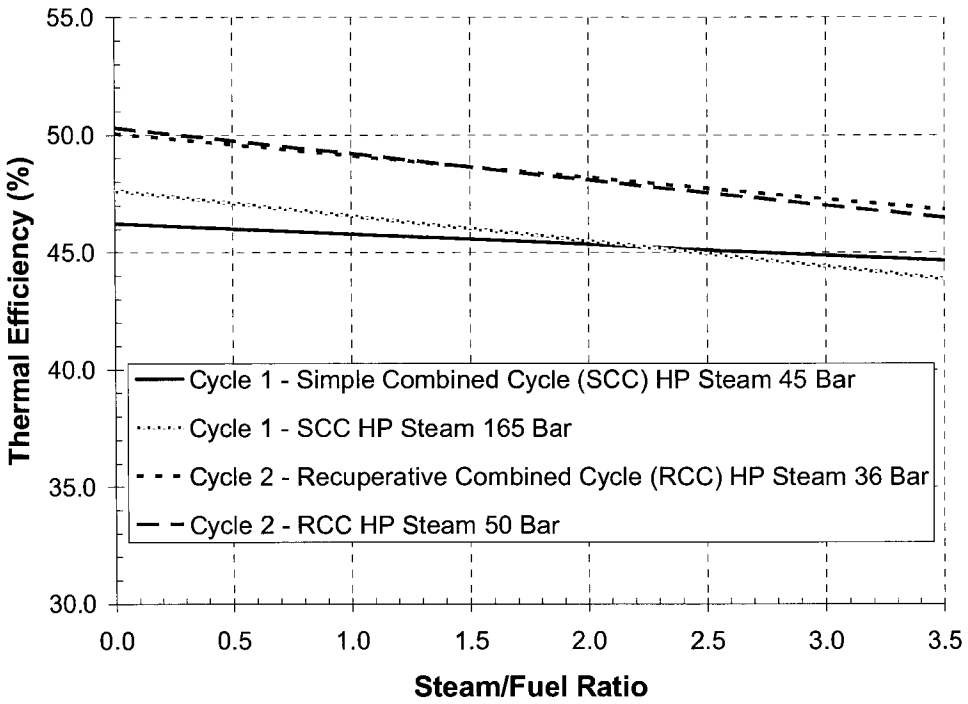

Figure 6-5: Overall thermal efficiencies vs. steam/fuel ratio for two steam power augmentation steam injection pressures

between the injecting steam system and the combustor shell pressure for both cycles. This effect is shown in the slopes, as the minimized pressures have reduced slopes. As expected, when the injection pressure differential is minimized, the reduction in overall efficiency with increasing steam flow is minimized.

Figure 6-6 is a plot of thermal efficiencies for the plant as a whole and for the gas turbine only as a function of steam-to-fuel ratio. In the figure, the trends show

the gas turbine efficiency increases with increasing steam injection while the overall efficiencies of the plant decreases. The 'Gas Turbine Only' efficiency curves neglect all auxiliary loads. The important conclusion to draw from Figure 6-6 is that when the steam-to-fuel ratio is increased, the overall thermal efficiency, that is the efficiency including all the auxiliary loads, losses, and waste heat captured in the steam generator, decreases. The decrease may be the result of a few mechanisms. Firstly, the isentropic efficiency of the steam turbines is assumed to be 90%, while

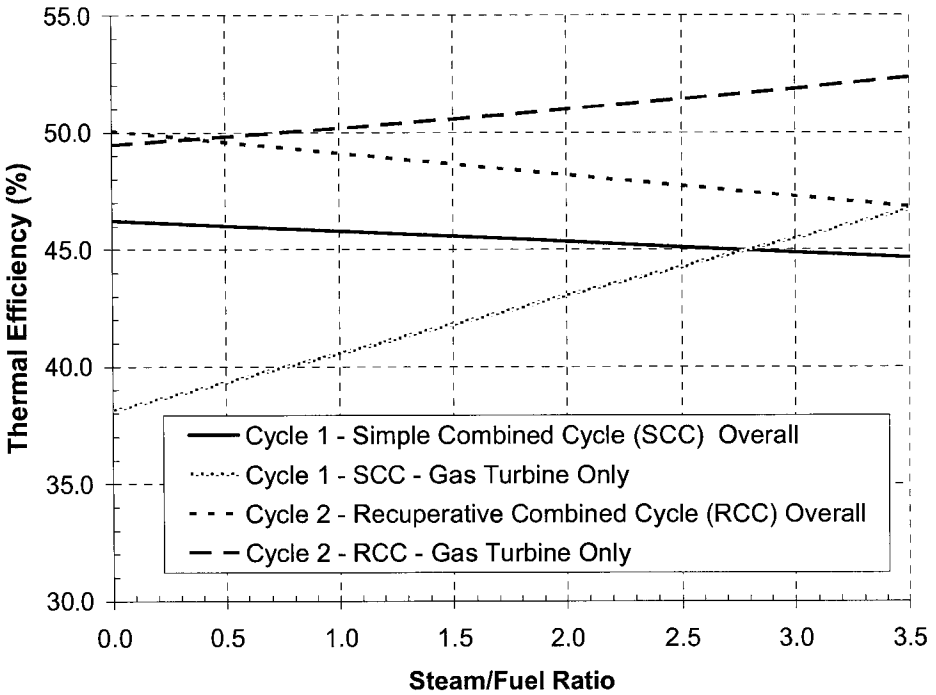

Figure 6-6: Simple and overall thermal efficiencies vs. steam/fuel ratio

the isentropic efficiency for the gas turbine is assumed to be 89%. These values were selected based on a review of parameters selected by other authors as presented in Section 4.3. The result is that expanding steam in the gas turbine will not be as efficient as expanding the steam in the steam turbines. Secondly, it is not possible to eliminate the pressure difference between the steam and the combustor shell. Thus, some efficiency is lost when throttling the steam to the combustor shell pressure. Thirdly, the change in working fluid properties has an undesirable effect on the steam generator inlet temperature. As discussed previously in this section, steam power augmentation in a primarily carbon dioxide working fluid reduces the temperature at the turbine outlet when the turbine inlet temperature is held constant. In the previous discussions it was mentioned that this phenomenon had a positive result on the gas turbine's power output. The same temperature decrease at the steam generator inlet decreases the steam temperatures. This decreases the efficiency of the steam system. These three mechanisms lead to the decrease in overall efficiency which can be seen in the negative slopes of the trends in Figure 6-6.

Figure 6-7 is a plot of net power output versus steam-to-fuel ratio. The trends for each the cycles, Cycle 1, the simple combined cycle, and Cycle 2, the recuperative combined cycle, show increases in power output with increases in steam injection. Note that Cycle 2, the recuperative combined cycle, sees a greater power

increase than Cycle 1, the simple combined cycle. When comparing Figure 6-7 with Figure 6-6, it is apparent that steam power augmentation in zero-emission semi-closed combined cycles increases the power output, but results in a reduction in overall thermal efficiency.

It is important to note that these trends are developed using heat and mass balance software, and not detailed turbine or steam generator models. The results depend on the simplifying assumptions that are made. For example, the steam generator outlet temperature is specified at an assumed constant value. In reality, the

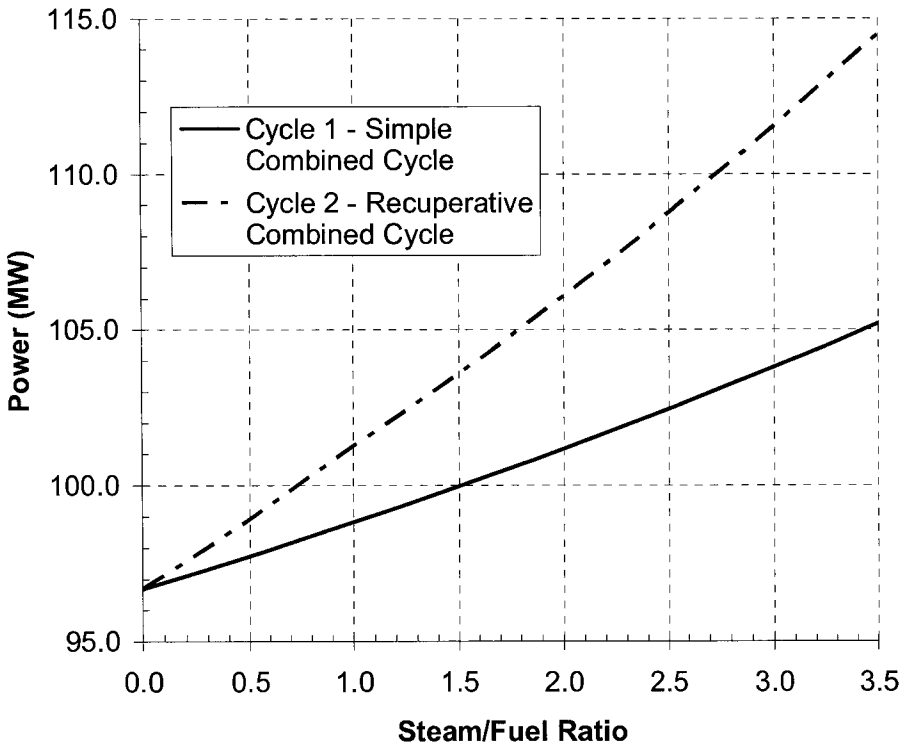

Figure 6-7: Power output increase vs. steam/fuel ratio

steam outlet temperature will change under different levels of steam injection on the gas turbine side of the plant. If the steam generator geometry is fixed, and steam is removed for use in steam injection in the gas turbine then the drop in steam generator inlet temperature may result in a drop in steam generator outlet temperature. The plant model does not take this into account. The model also does not account for changes in turbine efficiency due to changes in fluid properties. As well, the power augmentation will cause the compressor to change its operating point, which would mean some change in pressure ratio it delivers. Detail design calculations can be supported by ASPEN, but flow characteristics for both the compressor and turbine would be required.

The Figures 6-5, 6-6, and 6-7 each show steam-to-fuel ratio on the horizontal axis ranging from 0 to 3.5. This range of steam injection is similar to what can typically be admitted to open-cycle gas turbines which can run into flame stability problems as a result of too much steam. The zero-emission semi-closed combined cycle can be designed to use a wide range of steam-to-fuel ratio. Other authors, including Jerica et al. (2003), Martinas-Frias et al. (2004), and Sanz et al. (2004), have studied zero-emission cycles which have steam acting as the sole thermal ballast limiting the turbine inlet temperature. These cycles show good potential; however, the complete range of steam-to-fuel ratios was not studied as the overall cycle performance was decreasing with increasing steam injection mass flow rates.

Figure 6-8 shows the specific work trends for the gas turbine portion of the plant when injecting steam into the gas turbine combustor. Both trends have positive slopes because steam injection increases the gas turbine's power output. The

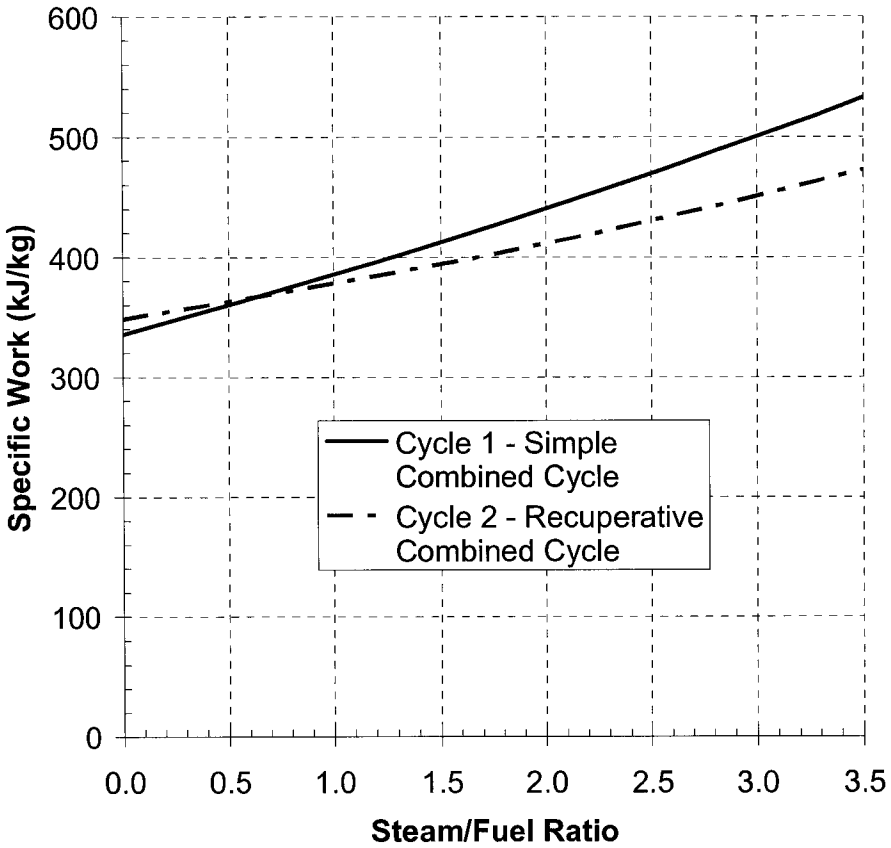

Figure 6-8: Specific work vs. steam/fuel ratio for the gas turbine only

calculations for specific work used the total gas turbine power output divided by the mass flow rate of working fluid at the inlet to the compressor. This calculation method is best because the range of steam-to-fuel ratios presented in the Figure 6-8 can usually be handled by a gas turbine originally designed for no steam injection.

Thus, if the mass flow used in the specific work calculation was taken from the combustor outlet, it would suggest the specific work was only marginally affected by steam injection. This could be misleading because much more work is being produced by a gas turbine of the identical size.

Figure 6-9 shows the trends of specific work vs. steam-to-fuel ratio for the steam system for each of the two cycles. The slopes are strongly negative for two reasons. The first is that the steam system working fluid mass flow is the value of

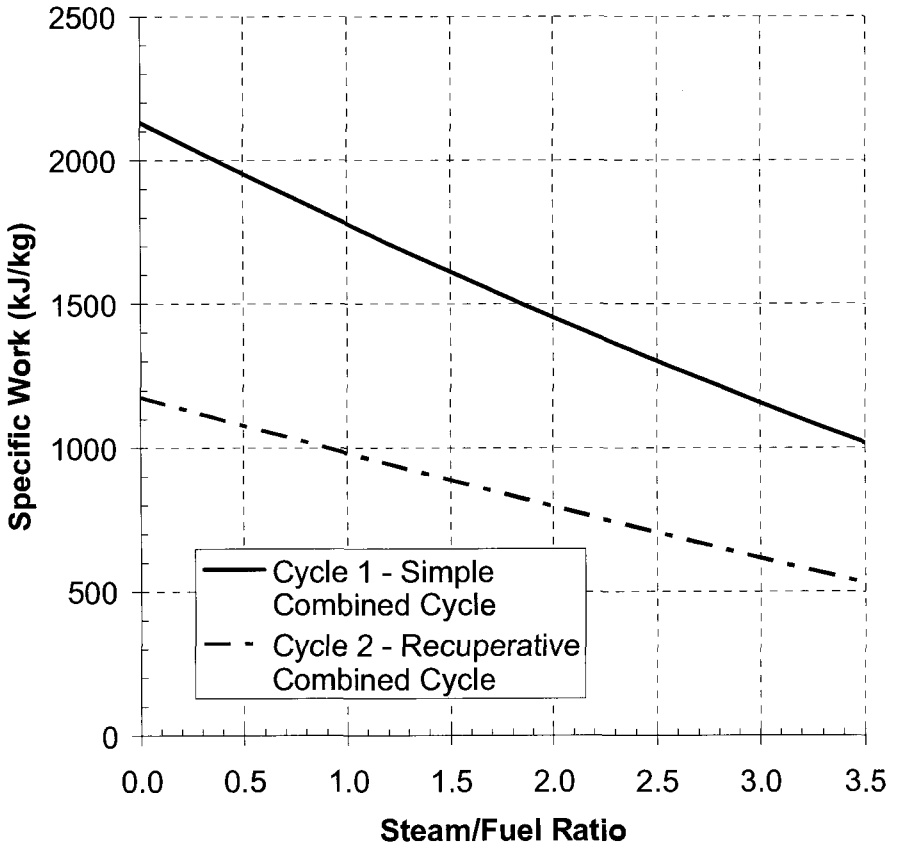

Figure 6-9: Specific work vs. steam/fuel ratio for the steam cycle only

water at the inlets to the boiler-feed pumps. Steam injected into the gas turbine's combustor is taken from the steam system. Less work is produced by the steam turbines in the steam system as the steam-to-fuel ratio is increased. The second reason the trends are negative is that the steam system's working fluid increases when the gas turbine passes increased mass flow to the steam generator. As the steam system working fluid mass flow rate increases, and the mass flow rate of steam expanded in steam turbines decreases, the result is a negative specific work trend with increasing steam-to-fuel ratio. The difference in the slopes of the specific work trends is due to the changes in steam generator inlet temperature. This temperature changes as a result of the fluid property changes due to the gas turbine working fluid composition gaining a significant amount of steam. In Cycle 1, the simple combined cycle, the steam generator inlet temperatures decrease approximately 6 K between steam-to-fuel ratios of 0 and 3.5. In Cycle 2, the recuperative combined cycle, the steam generator inlet temperatures increase approximately 70 K between steam-to-fuel ratios of 0 and 3.5. Increasing steam generator inlet temperature results in increasing specific work. It is for this reason that the slope of the Cycle 2 data is less than that of Cycle 1.

6.7 Conclusions

Results show that increasing the supplied oxygen purity increases the level of carbon dioxide in the working fluid. Simulation results also show that reducing fuel impurities can increase the carbon dioxide concentration in the working fluid. Section 6.4 demonstrates that forcing the semi-closed loop to operate with excess oxygen only marginally affects the overall thermal efficiency. The effect of working fluid properties on performance was reviewed by varying the oxygen purity. The oxygen purity has opposite effects on the performance of the gas turbine and steam system, but in terms of the overall plant performance, these effects largely balance one another. The loss of thermal efficiency by operating with high-purity oxygen is caused by the increased power needed to operate the air separation unit. Steam injection power augmentation increases the efficiency of the gas turbine, but reduces the overall combined cycle thermal efficiency. Steam injection power augmentation does increase combined cycle net power output. Considering a combined cycle, it is best to minimize the pressure difference between the steam pressure and the pressure in the gas turbine combustor shell, as the throttling of the steam to the combustor shell pressure reduces the steam temperature.

Chapter 7 – Application: Semi-Closed O_2/CO_2 Cycle Based on Solar Turbines Mercury 50

7.1 Introduction

This chapter examines the possibilities of using the Solar Turbines Mercury 50 recuperative gas turbine as the basis for the zero-emission power plant. The Mercury 50 has a power output of about 4.6 MW which corresponds closely to the estimated peak power requirement for the new building*. In addition, the novel configuration

* A small group of faculty members in the Department of Mechanical and Aerospace Engineering has submitted a proposal to a competition for external funding for a new building which would augment current facilities at the University. Included in the proposal for this new building is a rotorcraft wind tunnel which would have considerable electrical load requirements during operation. The local utility's pricing structure for purchasing intermittent electricity could result in high costs. Consequently, consideration is being given to installing in the building a small gas-turbine based zero-emission power plant which would produce supplemental electricity for the University and the new

of the Mercury 50 seems to lend itself to incorporation in a semi-closed plant, as required for the zero-emission concept. This investigation concentrates on the performance potential of the Mercury 50 cycle, and not the detailed aspects of the changes required.

7.2 Description of Solar Turbines Mercury 50

Table 7-1 presents performance details and specifications for the Mercury 50 (Gas Turbine World, 2004; Stambler, 2004; Teraji et al., 2005). The Mercury 50 is a recuperative turbogeneration package. This configuration helps produce a high thermal efficiency without cutting-edge turbine inlet temperatures. The turbine section has two stages, with cooling assumed to take place in the row 1 nozzles and blades, and perhaps the row 2 nozzles.

A flow schematic of the Mercury 50 is shown in Figure 7-1. The component placements are not typical as it has been packaged for convenient integration with the recuperator. This involves placing the compressor intake at a mid-engine location, with the compressor outlet at one end. The combustor is placed on the opposite end and feeds into the turbine which is at a central location. This combustor

---

wind tunnel as required, thus reducing dependence on the local utilities. Given that the Kyoto accord is coming into effect in 2012, the objective would be for the new building to be a green facility which generates zero emissions as a result of its power requirements. This would involve integrating a carbon dioxide capture method into whichever gas turbine unit is selected, resulting in an environmentally friendly facility.

Table 7-1: Mercury 50 performance details and specifications using air as working fluid

Solar Turbines Mercury 50	
ISO Power Rating	4.6 MW
Thermal Efficiency	38.5%
Turbine Inlet Temperature	1436 K
Mass Flow	17.78 kg/s
Shaft Speed	14186 RPM
Compressor Pressure Ratio	9.9
Number of Compressor Stages	10
Number of Turbine Stages	2
Generator Speed	1800 RPM

location is convenient for adaptation to zero-emission cycles using a CO_2 working fluid because the combustor needs to be redesigned. The CO_2-cycle combustor may be larger or smaller without affecting the rest of the engine. This layout can also be easily adapted to a semi-closed type system by routing the exhaust flow through a condenser and then back to the compressor intake. The exhaust and intake reside in close proximity to one another. Another advantage to this layout is that the components are in modular form. The combustor, turbine, compressor, and gearbox are all bolted to one another. The result is that should any components need to be redesigned, they can potentially be replaced without major changes to the other components. In replacing any of the components, the component size may change requiring flange location changes. The ducting between most of the components will facilitate changes to the flange locations.

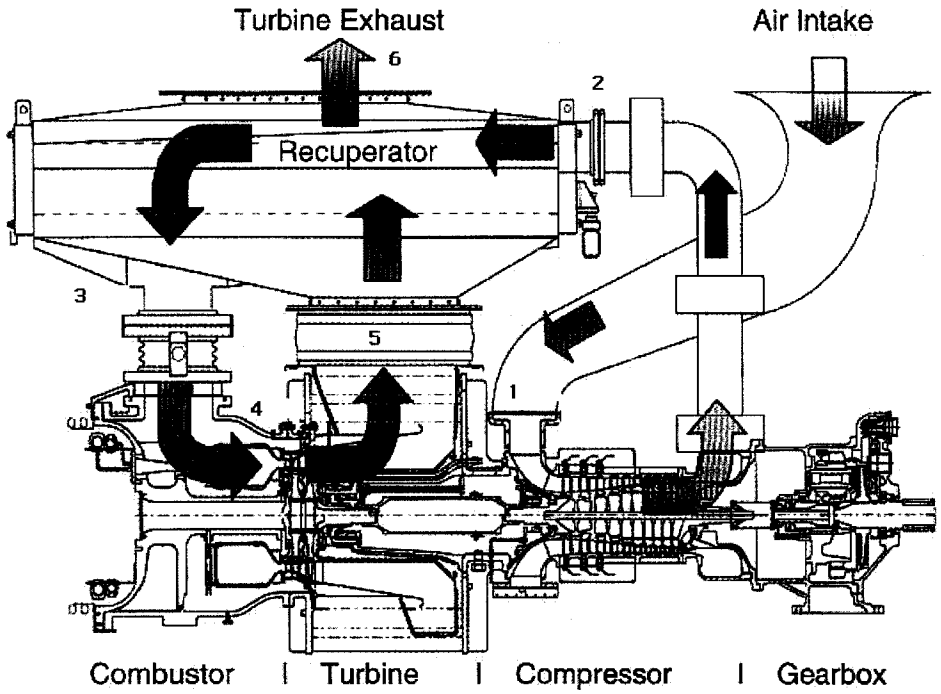

Figure 7-1: Mercury 50 flow schematic (Reference: Gas Turbine World, 2004)

7.3 Required Similarity Criteria and Correction Formulae

One operating point will be investigated for the Mercury 50 in a zero-emission cycle. This operating point involves operating the compressor at a reduced absolute speed, in dynamically similar non-dimensional conditions to the original design conditions. This necessitates a gearing change in the main gear box to make 60 cycle electricity. The investigation of the scenario which requires no gearbox change is an investigation of off-design performance. Detailed compressor performance information is required to analyze off-design operation.

This section presents the similarity criteria and correction formulae required to relate the compressor performance in air to that which will apply with carbon dioxide as the working fluid.

Roberts and Sjolander (2005) discussed the four similarity criteria which apply to turbomachinery operating with perfect gases:

Speed parameter, Π_N:

$$\Pi_N = \frac{ND}{a_{01}} = \frac{ND}{\sqrt{\gamma RT_{01}}} = \frac{N}{\sqrt{T_{01}}}\frac{D}{\sqrt{\gamma R}} \tag{7-1}$$

where N is the shaft rotational speed, D is the diameter of the machine, a_{01} is the sound speed based on the inlet total temperature, γ is the ratio of specific heats, R is the gas constant, and T_{01} is the total temperature at the inlet.

Flow parameter, $\Pi_{\dot{m}}$:

$$\Pi_{\dot{m}} = \frac{\dot{m}}{\rho_{01} a_{01} D^2} = \frac{\dot{m}}{\frac{P_{01}}{RT_{01}}\sqrt{\gamma RT_{01}}D^2} = \frac{\dot{m}\sqrt{T_{01}}}{P_{01}}\sqrt{\frac{R}{\gamma}}\frac{1}{D^2} \tag{7-2}$$

where $\dot{m}$ is the mass flow rate, P_{01} is the inlet total pressure, and ρ_{01} is the inlet total density.

Reynolds number, Re_D:

$$\mathrm{Re}_D = \frac{\rho_{01} N D^2}{\mu} \tag{7-3}$$

where μ is the viscosity.

Specific heat ratio or isentropic exponent, γ:

$$\gamma = \frac{c_p}{c_v} \qquad (7\text{-}4)$$

where c_p is the specific heat capacity at constant pressure, and c_v is the specific heat capacity at constant volume.

To relate the performance of a known machine operating with two different perfect gas working fluids, one first matches the speed and flow parameters. Matching the speed parameter will yield the relationship between the absolute operating speeds for the two machines. Matching the flow parameter will relate the absolute mass flows. It is assumed that at standard atmospheric conditions, the condenser results in a compressor inlet temperature of 10 K above the standard atmospheric temperature of 288 K. Thus, for the zero-emission cycle using CO_2, the temperature at the compressor inlet is assumed to be 298 K. It is also assumed that the compressor inlet pressure in the zero-emission cycle is the same as when the Mercury 50 is operated in air under standard conditions. In this study, the pressure at the inlet to the zero-emission cycle is assumed to be 1.003 bar. Since the zero-emission cycle is a semi-closed cycle, the compressor inlet pressure is not restricted to 1.003 bar. However, this pressure is used for performance comparison purposes. Considering that the density, viscosity, and the specific heat ratio will in general be

different for the two fluids, it is not possible to match the Reynolds numbers once the inlet pressure and temperature are fixed. The effects of differences in Reynolds number and specific heat ratio are taken into account by correction formulae. An empirical correlation is available which will correct compressor efficiency for differences in Reynolds number (ASME, 1965). Correlations for the effects of specific heat ratio on compressor performance have been developed by Roberts and Sjolander (2005) and will be summarized below.

The efficiency correction for Reynolds number, Re, is given in Equation 7-5:

$$\frac{1-\eta_A}{1-\eta_B} = \left(\frac{\mathrm{Re}_B}{\mathrm{Re}_A}\right)^n \qquad (7\text{-}5)$$

where η is the isentropic efficiency and the subscripts A and B denote the two operating conditions that are being related. The ASME Power Test Code (ASME, 1965) suggests $n = 0.2$ for axial compressors if $\mathrm{Re_B} \geq 10^5$, where $\mathrm{Re} = ND^2/\nu$ and ν is the kinematic viscosity.

Roberts and Sjolander (2005) present correlations for the effect of the specific heat ratio on pressure ratio, efficiency, and choking mass flow rate. These correlations are as follows:

For pressure ratio, PR:

$$PR_B = \left[\frac{\gamma_B - 1}{\gamma_A - 1}\cdot\left(\frac{\eta_B}{\eta_A}\right)\cdot\left(PR_A^{(\gamma_A-1)/\gamma_A} - 1\right) + 1\right]^{\gamma_B/(\gamma_B-1)} \qquad (7\text{-}6)$$

where PR is pressure ratio.

For isentropic efficiency, η:

$$\frac{1-\eta_A}{1-\eta_B} = \left(\frac{\gamma_A}{\gamma_B}\right)^n \qquad (7\text{-}7)$$

where n is a value less than 1.0. Based on experimental data, Roberts and Sjolander (2005) suggest a value of $n = 0.8$ be used for carbon dioxide.

For choking mass flow parameter, $\Pi^*_{\dot{m}}$:

$$\frac{\Pi^*_{\dot{m}B}}{\Pi^*_{\dot{m}A}} = \frac{\left(\frac{\gamma_B+1}{2}\right)^{-(1/2)[(\gamma_B+1)/(\gamma_B-1)]}}{\left(\frac{\gamma_A+1}{2}\right)^{-(1/2)[(\gamma_A+1)/(\gamma_A-1)]}} \qquad (7\text{-}8)$$

7.4 Assessment of the Performance Potential of the Mercury 50 Gas Turbine in a Zero-Emission O_2/CO_2 Cycle

7.4.1 Introduction

This section presents the background information necessary to model the Mercury 50 in a zero-emission cycle in ASPEN with the compressor operating at dynamically similar conditions in air and CO_2. The turbine and compressor

efficiencies are not available in the literature. Thus, the Mercury 50 gas turbine was first modeled in its conventional cycle using air as the working fluid. Component efficiencies and losses were adjusted iteratively until the predicted engine performance matched the published operating data. Next, estimates of the compressor and turbine characteristics were made. The compressor characteristic was then corrected for the effects of specific heat ratio and Reynolds number when the working fluid is changed to CO_2.

The turbine performance is also affected by the change in working fluid properties; however, with the exception of the correction for choking mass flow, the correction formulae are not yet available for turbines. The turbine characteristic is corrected for the effects of specific heat ratio on the choking mass flow, but the effects of the change in fluid properties on the turbine power output and isentropic efficiency are neglected in this analysis. As a result, the performance estimates for the zero-emission cycle using CO_2 cycle are not strictly correct.

The corrected estimated maps for the compressor and turbine were matched by hand. The resulting values of compressor pressure ratio and mass flow were then used in the zero-emission model to predict the performance of the Mercury 50 with CO_2 as the working fluid.

The working fluid in the zero-emission cycle is referred to as CO_2. The actual working fluid composition is a mixture of carbon dioxide, argon, nitrogen, oxygen,

water, and trace amounts of unburned hydrocarbons. The working fluid composition is as presented in Table 6-1 of the previous chapter. It is assumed that the oxygen purity is low, and that the fuel is natural gas as described in Table 6-2. Thus, the working fluid is 90.1% CO_2.

7.4.2 Model of Mercury 50 Gas Turbine Using Air Working Fluid

As mentioned, the Mercury 50 was simulated for air using ASPEN to estimate the isentropic efficiency of the compressor, η_c, and turbine, η_t. Table 7-2 shows the results of this simulation.

Table 7-2: Aspen analysis results of Mercury 50 air cycle

Working fluid:	Air
Compressor Isentropic Efficiency - η_c	87.0%
Turbine Isentropic Efficiency - η_t	86.8%

A compressor characteristic was estimated based on the design point. It was assumed that the surge margin would be 25%, and that the constant speed operating line intercepted the surge line at a 90° angle. The term surge margin refers to the distance between the design point and the surge limit line on the compressor characteristic as shown in Figure 7-2. The estimated partial compressor map consisting of the design constant speed line and the surge line is shown in Figure 7-3. The compressor choking mass flow was estimated to be slightly higher than the mass

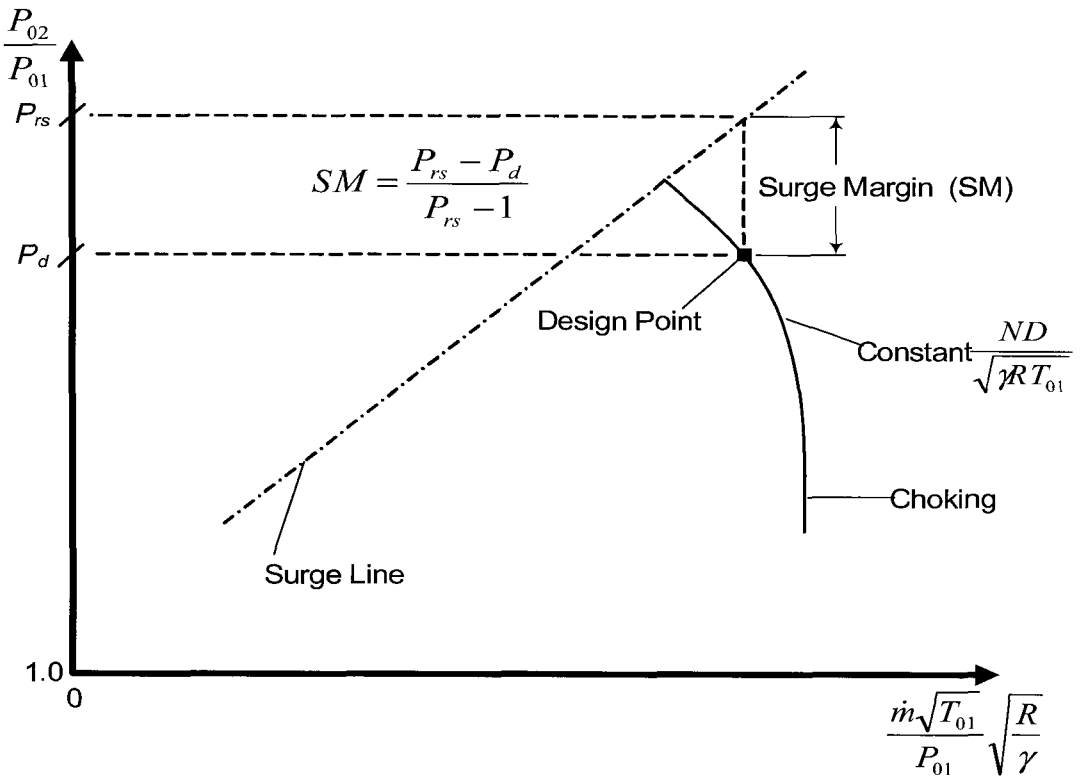

Figure 7-2: Definition of surge margin

flow rate at the assumed design point. The accuracy of choking mass flow for the compressor is not important here as the area of interest for operating points is near the design point and up to the surge line.

The turbine characteristic for the open cycle was estimated using the ASPEN simulation. From the design operating point, shown as compressor operating point 1 on Figure 7-3, the pressure ratio across the turbine and mass flow parameter for this same operating point were predicted as follows:

$$\frac{P_{04}}{P_{05}} = 9.236 \qquad \frac{\dot{m}\sqrt{T_{04}}}{P_{04}}\sqrt{\frac{R}{\gamma}} = 0.009944$$

The estimated turbine characteristic is then as shown in Figure 7-4, with the design point labelled as operating point 1. For gas turbine engines, the turbine is typically choked at the design point for the engine and this is assumed to be the case for the

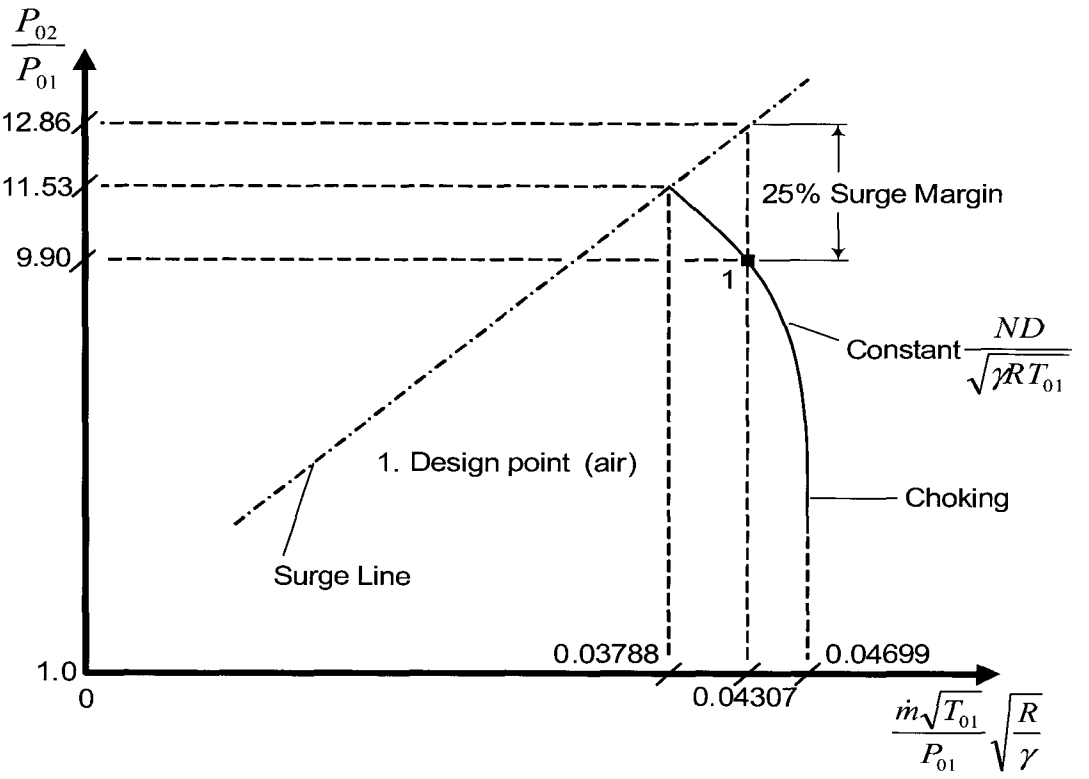

Figure 7-3: Estimated Mercury 50 compressor characteristic using air

Mercury 50. The choking is indicated by the constancy of mass flow parameter with varying pressure ratio. The pressure ratio at which the turbine comes unchoked has been guessed, but the precise location is not important since it is expected that all operating points of interest in the present work will lie in the choked range.

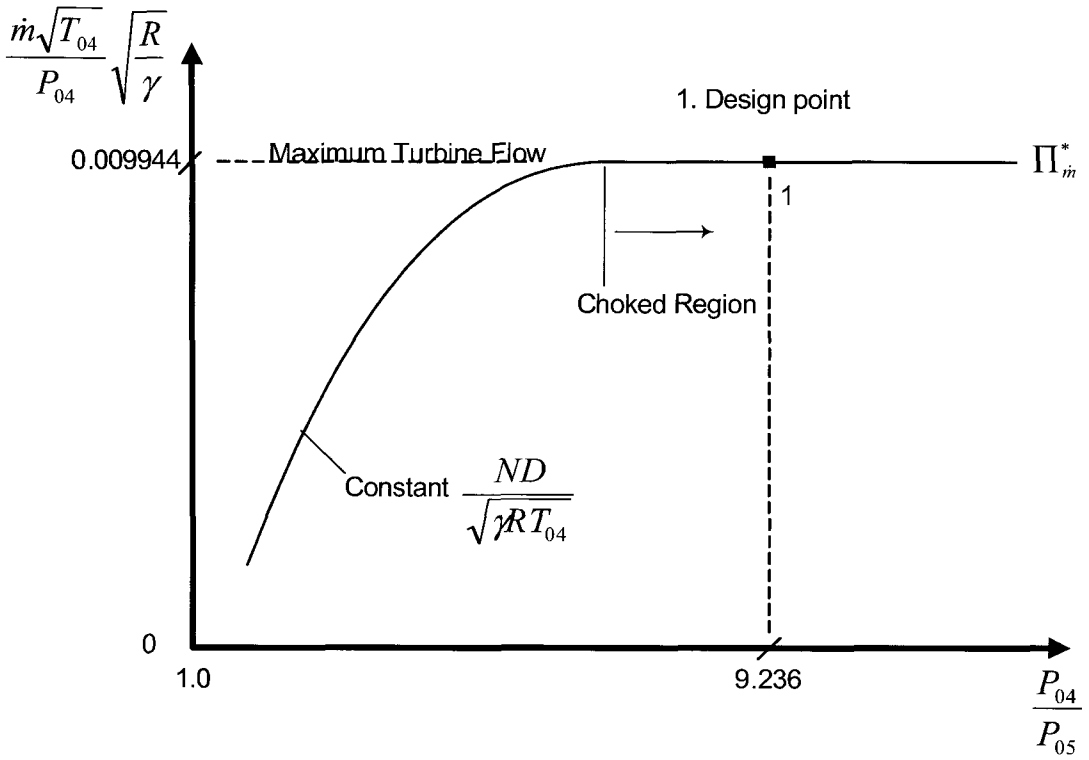

Figure 7-4: Estimated Mercury 50 turbine characteristic using air

7.4.3 Predicted Compressor Performance Map for Carbon Dioxide

Values are used for the ratio of specific heats, γ, and the specific gas constant, R, in many instances in this chapter. These values are shown in Table 7-3. The specific gas constant and the specific heat ratio for air at the compressor inlet were found using White (1994). The remaining specific heat ratios were taken from ASPEN simulations. The specific gas constant for the primarily CO_2 working fluid was calculated from the working fluid composition presented in Table 6-1 for low-purity oxygen and natural gas fuel. This is done by calculating the contribution of

the components of the working fluid to the mixture's molecular weight, then dividing the universal gas constant, 8.314 J/kg-K (White, 1994), by the mixture's molecular weight. The specific gas constant of the mixture is 191.8 J/kg-K, which is higher than the specific gas constant of pure CO_2, 188.9 J/kg-K (White, 1994).

Table 7-3: Values of specific gas constant and specific heat ratio used in this chapter

		Compressor Inlet		Turbine Inlet	
	R (J/kg-K)	T_{01} K	γ	T_{04} K	γ
Air	287.1	288	1.400	1436	1.302
$C0_2$	191.8	298	1.303	1436	1.183

As shown in Table 7-1, the design speed of the Mercury 50 gas turbine operating in air is 14186 RPM. To determine the corresponding absolute speed when using carbon dioxide, the non-dimensional speed parameters defined in Equation 7-1 are equated and solved for the speed in carbon dioxide.

$$\left(\frac{ND}{\sqrt{\gamma RT_{01}}}\right)_{Air} = \left(\frac{ND}{\sqrt{\gamma RT_{01}}}\right)_{CO_2}$$

As mentioned previously, the inlet temperature, T_{01}, for the zero-emission semi-closed gas turbine is assumed to be 10 K higher than the inlet temperature for the open cycle gas turbine using air. The absolute speed for CO_2 is then 11378 RPM or about 20% less than that for air.

The mass flow is determined by equating the flow coefficients defined in Equation 7-2 and solving for the mass flow of carbon dioxide.

$$\left(\frac{\dot{m}\sqrt{T_{01}}}{P_{01}}\sqrt{\frac{R}{\gamma}}\frac{1}{D^2}\right)_{Air}=\left(\frac{\dot{m}\sqrt{T_{01}}}{P_{01}}\sqrt{\frac{R}{\gamma}}\frac{1}{D^2}\right)_{CO_2}$$

As mentioned previously, the value of P_{01} is assumed to be 1.003 bar for both the air and CO_2 cycles. This value is from the air cycle's compressor inlet during operation under standard conditions. The value of 1.003 bar is less than the standard atmospheric pressure of 1.013 bar by the amount of assumed inlet filter, plenum, and duct losses. The same value was adopted for the zero-emission CO_2 cycle for the purpose of comparability. Since the zero-emission cycle is semi-closed, it is not necessary that the pressure be 1.013 bar. Using an inlet pressure below 1.013 bar could lead to contamination of the CO_2 working fluid with air if there is any leakage into the gas path. Using an inlet pressure above 1.013 bar will require the fuel and oxygen compressors to use more power, and result in higher stresses in all of the casings. On the other hand, raised operating pressure would also increase the power output of the plant. For the conditions assumed, the mass flow increases by 16 % from 17.78 kg/s for air to 20.63 kg/s for CO_2.

The next step is to correct the compressor efficiency for the effects of specific heat ratio using Equation 7-7.

$$\frac{1-\eta_A}{1-\eta_B}=\left(\frac{\gamma_A}{\gamma_B}\right)^{0.8}$$

Using γ_A = 1.400 and γ_B = 1.303 from Table 7-3, the isentropic efficiency of the compressor increases from an estimated value of 87% for air to 87.7% for CO_2 due to the effects of specific heat ratio.

Equation 7-5 is used to correct the compressor isentropic efficiency, η, for the effects of Reynolds number, Re. Reynolds numbers must be determined using equation 7-3.

$$\mathrm{Re}_D = \frac{\rho_{01} N D^2}{\mu}$$

At the design point with air as the working fluid, the compressor operates with a Reynolds number of 28.4x10^6. The correction applied above for the effect of γ alone then gives the efficiency that the compressor would have if it were compressing CO_2 and operating at the same Reynolds number of 28.4x10^6. However, at the dynamically similar operating point, the CO_2 compressor is in fact operating at a Reynolds number of 39.2x10^6. Therefore, a second correction must be applied to correct for the effects of the difference in Reynolds numbers on the efficiency of the compressor. The correction formula recommended by the ASME Power Test Code was used (ASME, 1965). The correction formula has been previously introduced as Equation 7-5.

$$\frac{1-\eta_A}{1-\eta_B} = \left(\frac{\mathrm{Re}_B}{\mathrm{Re}_A}\right)^{0.2}$$

The resulting isentropic efficiency for the compressor operating at its design point in CO_2 is $\eta_B = 88.5\%$.

The effects of specific heat ratio and Reynolds number on efficiency where included in Equation 7-6, which corrects pressure ratio, PR, for the effects of specific heat ratio.

$$PR_B = \left[\frac{\gamma_B - 1}{\gamma_A - 1} \cdot \left(\frac{\eta_B}{\eta_A} \right) \cdot \left(PR_A^{(\gamma_A - 1)/\gamma_A} - 1 \right) + 1 \right]^{\gamma_B/(\gamma_B - 1)}$$

The corresponding pressure ratio at the design point will decrease from 9.90 for air to 8.71 for CO_2.

The compressor choking mass flow was corrected using Equation 7-8:

$$\frac{\Pi^*_{\dot{m}B}}{\Pi^*_{\dot{m}A}} = \frac{\left(\frac{\gamma_B + 1}{2} \right)^{-(1/2)[(\gamma_B + 1)/(\gamma_B - 1)]}}{\left(\frac{\gamma_A + 1}{2} \right)^{-(1/2)[(\gamma_A + 1)/(\gamma_A - 1)]}}$$

where the values of the specific heat ratio from Table 7-3 are 1.303 for CO_2 and 1.400 for air. The choking mass flow rate will increase as the correction factor is 1.0110. The new choking mass flow parameter for CO_2 is 0.04751, whereas it was 0.04699 for air.

The corrected operating conditions for the compressor for CO_2 are compared with the original values for air in the Table 7-4. The corrected conditions in Table 7-4 are used as a basis for correcting the estimated partial compressor map from Figure

7-3 as it would apply for CO_2. The corresponding partial compressor map is shown as Figure 7-5. The original surge line has moved to a lower pressure ratio for a given

Table 7-4: Summary of compressor specifications for dynamically similar conditions of an identical compressor design point, corrected for specific heat ratio and Reynolds number

	Air	Carbon Dioxide
Speed (RPM)	14186	11378
η_C	87.0	88.5
Pressure Ratio	9.90	8.71
Mass Flow (kg/s)	17.78	20.63
Choking Mass Flow Parameter $\frac{\dot{m}\sqrt{T_{01}}}{P_{01}}\sqrt{\frac{R}{\gamma}}$	0.04699	0.04751

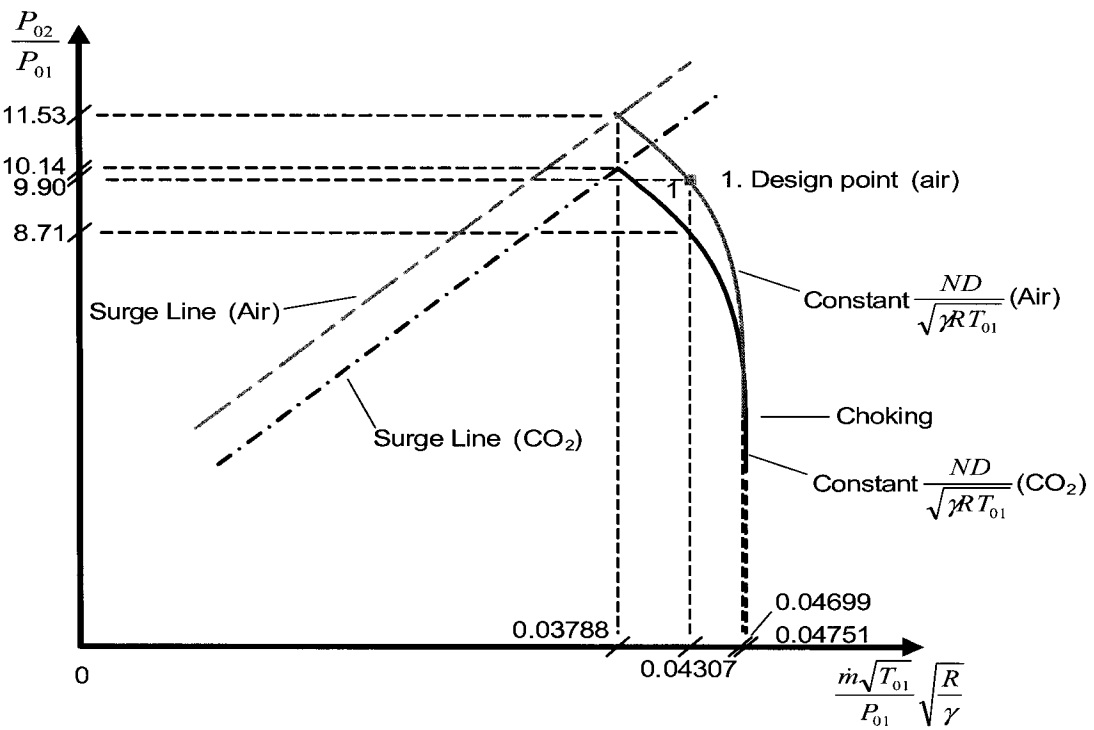

Figure 7-5: Estimated Mercury 50 compressor characteristic using CO_2

constant speed line. When this new partial compressor map is considered in context with the other components, it may contribute to a reduction in surge margin. This will be discussed in Section 7.4.6. No operating points are shown on the constant speed line for CO_2 because these have to be determined in Section 7.4.6.

7.4.4 Predicted Turbine Performance Characteristic for CO_2

As mentioned earlier, the corrections for efficiency and pressure ratio due to the changes in the ratio of specific heats are not available for turbines. The turbine characteristic is corrected for the effects of specific heat ratio on the choking mass flow only. This was done using Equation 7-8:

$$\frac{\Pi^*_{\dot{m}B}}{\Pi^*_{\dot{m}A}} = \frac{\left(\frac{\gamma_B+1}{2}\right)^{-(1/2)[(\gamma_B+1)/(\gamma_B-1)]}}{\left(\frac{\gamma_A+1}{2}\right)^{-(1/2)[(\gamma_A+1)/(\gamma_A-1)]}}$$

The values of specific heat ratios are taken from Table 7-3 as γ_A = 1.302 for the exhaust gases when using air and γ_B = 1.183 at the turbine inlet when using CO_2. The choking mass flow rate will increase as the correction factor is 1.0156. The choking mass flow parameter corrects to 0.010099 when using the machine in CO_2 from 0.009944 when using the machine in air.

The estimated turbine characteristic in CO_2 is shown as Figure 7-6. The constant speed line shifts upward to reflect the correction in choking mass flow due

to the change in the values of specific heat ratio. The constant speed line moves upward only a small amount. It is important to note that the constant speed parameters associated with the constant speed lines in Figure 7-6 are not equal; whereas, for the compressor in Figure 7-5, they are equal. In Figure 7-5, the two speed lines are the same because the speed parameters where equated using Equation 7-1. This is not the case in Figure 7-5 where the absolute speed selected for the compressor does not put the turbine in dynamically similar conditions to the design point when using air. The implication is that, consistent with the assumptions which

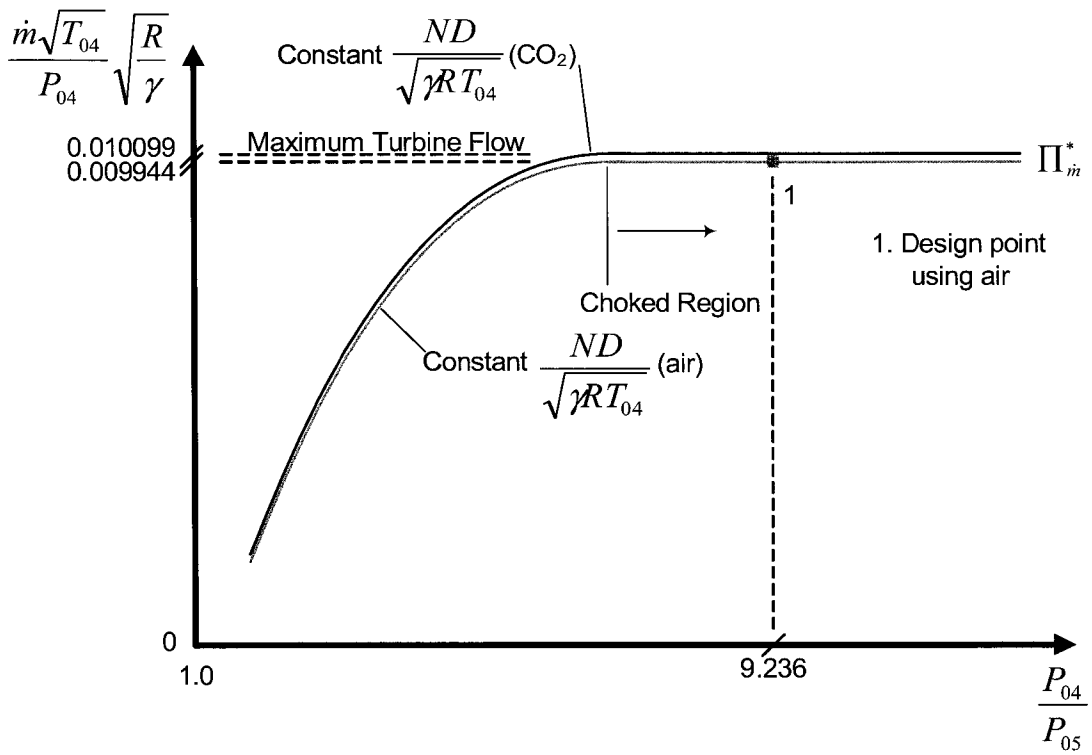

Figure 7-6: Estimated Mercury 50 turbine characteristic using CO_2

were used to generate Figure 7-3, in Figure 7-6, the location of the new constant speed line to the left of the choked flow region is guessed. As a result, the location of the constant speed lines to the left of the choked flow region relative to one another is also guessed. These guessed are not detrimental to this exercise because the design point will fall inside the choked region.

The location of the steady state operating point in CO_2 depends on the interaction between the compressor and turbine. The operating point will be determined by matching calculations. The matching calculation for the Mercury 50 in a zero-emission semi-closed combined cycle is the subject of the following section. Thus, the new operating point is not shown in Figure 7-6.

7.4.5 Compressor-Turbine Matching Concerns

Matching is the determination of the steady state operating points of a compressor and turbine that are connected to each other. For steady-state operation, they must have compatible flow rates and pressure ratios. In single-shaft fixed speed gas turbine engines used for power generation, the matched compressor and turbine should operate near their peak efficiency point during design point operation while providing adequate surge margin for the compressor.

In this study, a gas turbine which was designed for use with an air working fluid is being investigated for use with a primarily CO_2 working fluid. The matching

of the turbine to the compressor must be verified because the change in working fluid may have affected the steady-state operating points.

Checking the matching on a single-shaft fixed speed gas turbine engine is an iterative process. The following parameters are variable for the compressor:

$$\dot{m}, P_{02}, \eta_c$$

for the turbine:

$$\dot{m}, P_{04}, \eta_t, \gamma$$

In this case, no isentropic efficiency curves have been presented in either Figure 7-5 or 7-6. Both the compressor and turbine isentropic efficiencies have an effect on the overall efficiency and power output of the cycle; however, the efficiencies have little effect on the matching for a fixed speed engine. Thus, the effects of changes in isentropic efficiency were neglected in the present matching calculations. Remaining are two groups of two variables which are both related, and the ratio of specific heats at the turbine inlet. Since the turbine inlet temperature is fixed, the ratio of specific heats only varies with pressure. The ratio of specific heats is a small function of pressure and was neglected. Relations must be determined for the component inlet mass flows and compressor outlet to turbine inlet pressures. The mass flow at the turbine inlet is less than the mass flow at the compressor inlet due to the amount of cooling flow which bypasses the combustor. This is partially offset by the mass flows of fuel and oxygen added in the combustion chamber. The pressure

at the turbine inlet is less than the compressor outlet pressure by the amount of recuperator cold-side pressure losses, and combustor pressure losses. The following assumptions are used:

$$\dot{m}_t = 0.948\dot{m}_c \qquad (7\text{-}9)$$

$$P_{04} = 0.950PR \times P_{01} \qquad (7\text{-}10)$$

The matching can be determined by digitizing the CO_2 compressor constant speed curve from Figure 7-5, then calculating the corresponding values of mass flow parameter at the turbine inlet.

7.4.6 Determining Compressor-Turbine Matching

The first requirement is to digitize the data for the constant speed operating line from Figure 7-5. The range necessary spans the distance from the original design point in air to the surge line in CO_2. This digitized data is shown in Table 7-5. Using a spreadsheet, the mass flow for the turbine inlet was calculated for each data point from Table 7-5 using the Equations 7-1, 7-9, and 7-10. An interpolation function was then set up to find the pressure ratio corresponding to the mass flow. A

Table 7-5: Tabulated data for constant speed line from Figure 7-5

Horizontal Location	Compressor Mass flow kg/s	Compressor Pressure ratio
1	20.63	8.71
	20.01	9.11
	19.39	9.50
	18.77	9.82
Surge Line	18.14	10.14

solver was used to change the mass flow until the solution was found. The result is shown in Table 7-6. The steady state operation point has the compressor inlet flow at 19.62 kg/s, corresponding to a pressure ratio of 9.291. The corresponding compressor inlet mass flow parameter is 0.04074. This steady state operating point, labelled 3', is shown in Figure 7-7. The location of the point shows approximately a 15% surge margin. This is significantly less than the 25% surge margin when the Mercury 50 is operated in an open-cycle using air. There are options available which can address this potential problem. The best option may be to modify the turbine

Table 7-6: Tabulated data of showing steady state compressor operating point in bold type

Point	Mass flow kg/s	Pressure ratio
1'	20.63	8.708
	20.01	9.107
	19.62	**9.281**
	19.39	9.505
	18.77	9.823
Surge Line	18.14	10.140

section. The turbine components can be modified to accept increased mass flow. The mass flow is limited by choking, which typically occurs in the turbine nozzles. The throat area of the nozzles can often be increased somewhat without the need to redesign the subsequent turbine rotor. This increases the mass flow rate that can be passed by the turbine which in turn would increase the compressor's surge margin.

Growing the power output of gas turbine engines by increasing the mass flow rate has been done on many engines and is well understood.

More analysis could be done to verify that the steady-state operating point is as shown in Figure 7-7. More information would be required to increase the level of accuracy of the matching calculation. A strategy to accomplish improved accuracy of the prediction of the compressor operating point is presented in the section 7.5.

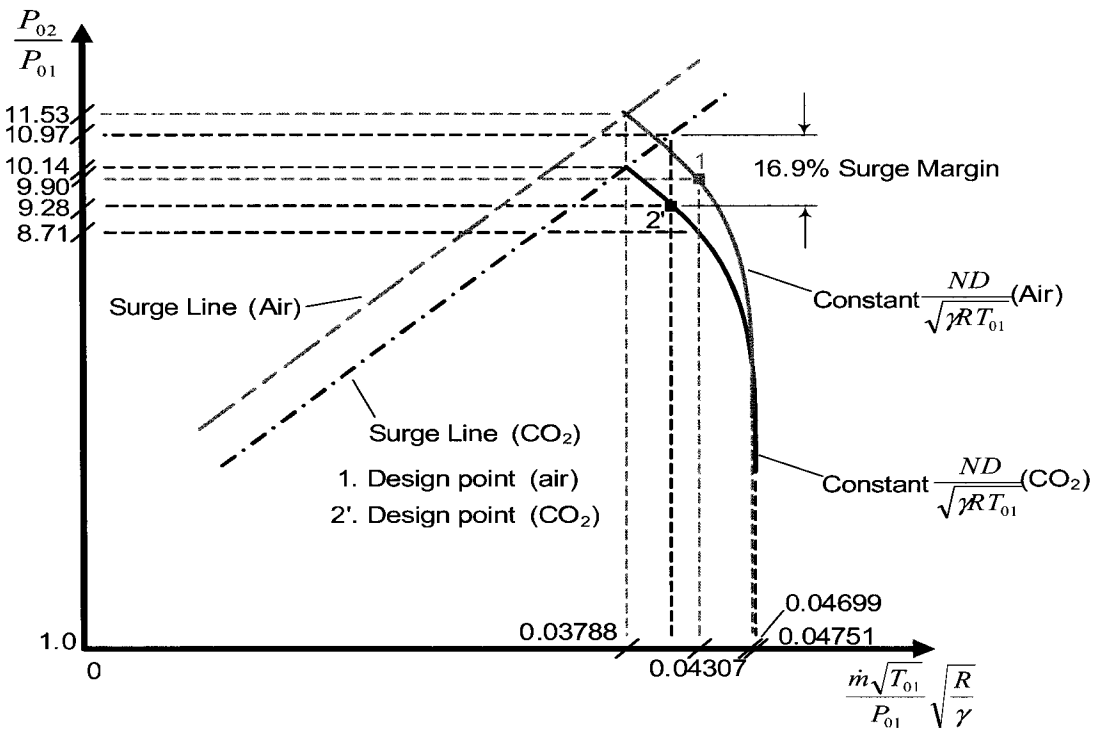

Figure 7-7: The steady-state operating point, 2', on CO_2 compressor characteristic

7.4.7 Summary of Results of Zero-Emission Mercury 50 with Dynamically Similar Compressor Operation

Table 7-7 summarizes the performance of the Mercury 50 when the compressor is operated at dynamically similar conditions for air and in a zero-emission cycle with CO_2. The semi-closed cycle produces 3.55 MW at an overall thermal efficiency of 31.7%.

Table 7-7: Mercury 50 performance potential in a zero-emission cycle

	Units:	Mercury 50 Air	Compressor in Dynamically Similar Operation at steady-state operating point
Rotational Speed	RPM	14186	11378
Overall Thermal Efficiency	%	38.5	31.7
Net Power Output	MW	4.6	3.55
Mass Flow	kg/s	17.78	19.62
Pressure Ratio		9.90	9.28

7.5 Future Work: Mercury 50 Performance Prediction

Section 7.4.6 indicates that there is reduced surge margin in the compressor when using a carbon dioxide working fluid with the existing compressor and turbine from the Mercury 50. To further quantify the extent of the reduction, more work can be done. The following approach could be used:

1. Obtain the compressor characteristic and turbine characteristic from Solar Turbines. If this is not possible, use gas turbine performance software, such as GASTURB (Kurzke, 2005), to estimate the maps for the Mercury 50 compressor and turbine in air. These maps will not be completely accurate, but should meet the needs of the study.
2. Correct the compressor characteristic for the Mercury 50.
3. Correct the turbine characteristic for the correct working fluid mixture. This step depends on the development of correction formulas for turbines for the effect of the ratio of specific heats. Such corrections, equivalent to the ones for compressors developed by Roberts and Sjolander (2005), remain to be determined.
4. Matching of the turbine and compressor can be done in GASTURB, ASPEN, or by hand as described by Savanamuttoo et al. (2001). Given the complexity of the overall zero-emission cycle, it may be best to perform this work in ASPEN. It will then be possible to achieve final performance figures for the cycle directly from ASPEN. As well, once the maps have been entered, it will be possible to look at a series of steady-state operating points to define the operating line on the compressor map for both design and off-design operating

points. This could be used to verify that there is sufficient compressor surge margin over a range of possible operating conditions.

If it is determined that the surge margin is not sufficient, another option can be investigated. The matching calculation of this chapter was performed with the assumption that the carbon dioxide was being bled for capture from just after the main compressor outlet. Increasing the surge margin can be accomplished by reducing the mass flow through the compressor. The mass flow through the compressor can be reduced by bleeding the carbon dioxide before the compressor inlet. From here the carbon dioxide could be processed for further purification or it can be compressed to the storage pressure using an auxiliary compressor. Thus, it remains as future work to perform the matching calculation as presented in this chapter for the case where the carbon dioxide working fluid is bled upstream of the compressor instead of downstream.

7.6 Conclusions

The Solar Turbines Mercury 50 shows potential for use in a zero-emission semi-closed cycle arrangement because of its mechanical arrangement which includes collectors or volutes at the inlet of both the compressor and turbine. The engine will require a novel combustor design for use as a basis for a zero-emission cycle. The combustor may be physically larger or smaller than the existing

combustor, but this can be accommodated because the configuration has the combustor located at one end.

A reduction in surge margin from 25% to 16.9% has been identified if both the existing compressor and turbine were used in the zero-emission configuration. Further work can be done to validate the current results and quantify the degree to which modifications are necessary. The surge margin can be increased by modifying the turbine. For example, it is possible to modify the turbine to pass more mass flow, potentially by redesigning the nozzles only if the required difference in mass flow is not too large.

Once the mechanical details have been addressed, the cycle performance should approach 31.7% in overall thermal efficiency with a power output of approximately 3.55 MW. This analysis was performed using numerous assumptions, some of which have the potential to significantly degrade the quality of the results. An important assumption is the slope of the constant speed line in the compressor characteristic above the design point. If the slope of that line is not accurate, then the steady state operating point from the matching calculation can be significantly affected. This directly affects the surge margin. A second important assumption could be the lack of correction of the turbine isentropic efficiency for the effects of Reynolds number and specific heat ratio. The turbine efficiency affects power output and overall thermal efficiency of the cycle.

Chapter 8 – Recommendations and Conclusions

8.1 Cycle Analysis

A review of previous literature found that the properties of carbon dioxide favour the use of recuperation in zero-emission gas turbine cycles. It was also noted that the performance prediction of recuperative cycles is rare. Thus, two separate cycle studies were conducted. The first compares the performance of two configurations of a 100 MW size zero-emission semi-closed O_2/CO_2 combined cycle. The two cycles are identical with the exception that the second cycle is recuperative. A recuperator is a heat exchanger which uses heat from the turbine outlet flow to pre-heat the flow entering the combustor. This reduces the fuel required in the combustor. The recuperative cycle, Cycle 2, achieved an overall thermal efficiency

of 51.5% when using low-purity oxygen. In comparison, Cycle 1, the simple combined cycle, achieves an overall thermal efficiency of 48.4% on low-purity oxygen. When the oxygen purity is increased to 99.5% purity by volume, the overall thermal efficiencies drop to 50.1% and 46.7% for Cycles 2 and 1, respectively.

Investigations were performed to better understand cycle behaviour. Some of the results are obvious, and others less so. It was found that increasing the purity of the oxygen and/or the fuel increases the carbon dioxide concentration in the working fluid. It was also found that forcing the semi-closed loop to operate with excess oxygen only marginally affects the overall thermal efficiency. The effect of working fluid properties on performance was reviewed by varying the oxygen purity. The oxygen purity has opposite effects on the performance of the gas turbine and steam system, but in terms of the overall plant performance, these effects largely balance one another. The decrease in overall thermal efficiency when operating with high-purity oxygen is caused by the increased load of the air separation unit. The air separation unit uses more power to produce high-purity oxygen. Steam injection power augmentation increases the efficiency of the gas turbine, but reduces the overall combined cycle thermal efficiency. Steam injection power augmentation does increase combined cycle net power output. Considering a combined cycle, it is best to minimize the pressure difference between the steam pressure and the pressure

in the gas turbine combustor shell, as the throttling of the steam to the combustor shell pressure reduces the steam temperature.

The second cycle study reviews the performance potential of the 4.6 MW Solar Turbines Mercury 50 gas turbine engine operating in a zero-emission semi-closed O_2/CO_2 power cycle. The Mercury 50 shows potential for use in a zero-emission semi-closed cycle arrangement because of its mechanical arrangement which includes collectors or volutes at the inlet of both the compressor and turbine. The engine will require a novel combustor design for use as a basis for a zero-emission cycle. The combustor may be physically larger or smaller than the existing combustor, but this can be accommodated because the configuration has the combustor located at one end.

A turbomachinery matching study has identified that the compressor surge margin is significantly reduced. Modification of the turbine may be the best way to address this issue. For example, it is possible to modify the turbine to pass more mass flow, potentially by redesigning the nozzles only if the required difference in mass flow is not too large.

Once the mechanical details with operating the Mercury 50 in a zero-emission cycle have been addressed, the performance should approach 31.7% in overall thermal efficiency with a power output of approximately 3.55 MW.

8.2 ASPEN Modeling and Optimization

ASPEN PLUS 12.1 is a possible tool for performing gas turbine combined cycle plant simulations. The ASPEN Optimizer tool shows good performance in multi-parameter optimization and the ASPEN equation oriented calculation mode is efficient. Use of ASPEN on a daily basis will result in efficient use of time. Inexperienced users can count on ASPEN to be challenging software to learn and use.

It is recommended that two additional blocks be added to the ASPEN software. These blocks could be a multi-stage axial compressor block and a multi-stage axial turbine block. Both blocks need cooling flow ports at locations which can be specified. Also, the turbine needs the option of specifying a polytropic efficiency.

It is recommended that the specification method of heat exchanger effectiveness be incorporated into the heat exchanger blocks in ASPEN.

8.3 Future Work

There is room for further optimization of the carbon dioxide storage compressor which is used in each of Cycle 1, Cycle 2, and the zero-emission Mercury 50.

As mentioned in Section 8.1, when the Mercury 50 gas turbine engine is used in a zero-emission cycle is appears that the compressor's surge margin is

significantly reduced. More work can be done to verify the current results and investigate potential solutions. Section 7.6 presented an approach which could be used to complete this work. More work can also be done to investigate the effect of the bleed location for the working fluid on the compressor surge margin.

References

Andan, S., Tangney, R., (2004) "Improving CHP Cycle with Once Through Steam Generators and Advanced Material Selection," Power Gen Europe. Website – October-2004: http://www.otsg.com/media/tech_downloads/OTSG_cold_end _improvement _paper.pdf

Anderson, R.E., Doyle, S.E., Pronske, K.L., (2004) "Demonstration and Commercialization of Zero-Emission Power Plants," 29th International Technical Conference on Coal Utilization & Fuel Systems, April 2004, Clearwater, Florida, USA

ASME, (1965) "ASME Power Test Code-10," American Society for Mechanical Engineers (ASME). Website – November-2005: www.asme.org

Aspen Online Support, (2004) "Aspen Plus 12.2 Equation Oriented Modeling Reference Manual," Website – May-2004: http://support.aspentech.com/CustomerSupport/Documents/Engineering/Aspen%20Plus/12.2/Equation%20Oriented%20Modeling%20Reference%20Manual%2012.2.pdf

Bolland, O., Mathieu, Ph. (1998) "Comparison of Two CO_2 Removal Options in Combined Cycle Power Plants," Energy Convers. Mgmt Vol. 39, No. 16-18, pp. 1653-1663.

Bolland, O., Sæther, S. (1992) "New Concepts for Natural Gas Fired Power Plants Which Simplify the Recovery of Carbon," Energy Conversion and Management, Vol 33, No. 5-8, pp. 476-475.

Bolland, O., Undrum, H. (1998). "Removal of CO_2 from Gas Turbine Power Plants - Evaluation of Pre- and Postcombustion Methods," 4th International Conference on Greenhouse Gas Control Technologies, Switzerland, September 1998.

Booras, G., Holt, N., (2004) "Pulverized Coal and IGCC Plant Cost and Performance Estimates," Gasification Technologies, Washington, DC, Oct 3-6, 2004.

Boston, J.F., Mathias, P.M., (1980) "Phase Equilibria in a Third-Generation Process Simulator," 2nd International Conference on Phase Equilibria and Fluid Properties in the Chemical Processing Industry, Berlin, March 17-21, 1980.

Bourgeois, A., Hutchinson, S., Lee, B., McDowell, S., Powers, M., Yaras, M.I. (2004) "Raven Zero-Emission GT Final Report – Part G, Advanced Design," Department of Mechanical and Aerospace Engineering, Carleton University, Ottawa, Ontario, Canada, April 2004.

Boza, J.J., Lear, W.E., Sherif, S.A. (2003) "Performance of a Novel Semi-Closed Gas Turbine Refrigeration Combined Cycle," ASME Turbo Expo Paper GT2003-38576.

Cau, G., Cocco, D. (2000) "Performance Assessment of a Semi-Closed Chemically Recuperated Gas Turbine System," ASME Turbo Expo Paper 2000-GT-161.

Carcasci, C., Zecchi, S., Oteri, G. (2002) "Comparison of Blade Cooling Performance Using Alternative Working Fluids," ASME Turbo Expo Paper GT-2002-30551

Corradetti, A., Desideri, U. (2004) "Analysis of Gas-Steam Combined Cycles With Natural Gas Reforming and CO_2 Capture," ASME Turbo Expo Paper GT2004-54091.

De Ruyck J., (1993) "Combined Cycle Project: CO_2 Mitigation Through CO_2/Steam/Argon Gas Turbine Cycles and CO_2/Steam/Argon Gasification," Contract Jou2-CT92-0128 – First Intermediate Report.

Dowell, S. (2004) "Effects of Turbine Cooling on the 100 MW Gas Turbine," DR497-03/161/003. Raven Zero-Emission Gas Turbine Project, Carleton University, Ottawa, Canada.

Eide, L.I., Bailey, D.W. (2005) "Precombustion Decarbonisation Processes" Oil and Gas Science and Technology, Vol. 60, No. 3, pp. 475-484

Friedli, H., Lotscher, H., Oeschger, H., Siegenthaler, U., Stauffer, B. (1996) "Ice Core Record of $^{13}C/^{12}C$ Ratio of Atmospheric CO_2 in the Past Two Centuries," Nature 324: 237-238

Fulkerson, W., Judkins, R.R., Sanghvi, M.K. (1990) "Energy From Fossil Fuels," Scientific American, September, 83-89.

Gabbrielli, R., Singh, R. (2002) "Thermodynamic Performance Analysis of New Gas Turbine Combined Cycles With No Emissions of Carbon Dioxide," ASME GT-2002-30117

Gas Turbine World, (2004) "Genset Plant Prices," Gas Turbine World Handbook 2004-05

Gasparovic, N. (1965) "The Advantage of Semi-Closed Cycle Gas Turbines for Naval Ship Propulsion," Naval Engineers Journal, April 1965, P.275-333.

Government of Canada, (2002) "Climate Change Plan for Canada," Website March-2005: www.climatechange.gc.ca; ISBN En56-183/2002E.

Haar, L., Gallagher, J.S., Kell, G.S. (1984) "NBS/NRC Steam Tables: Thermodynamic and Transport Properties and Computer Programs for Vapour and Liquid States of Water in SI Units," Hemisphere Publishing Corporation, Washington, DC.

Hustad C.W., Tronstad, I., Anderson, R.E., Pronske, K.L., Viteri, F,V. (2005) "Optimization of Thermodynamically Efficient Nominal 40 MW Zero Emission Pilot and Demonstration Power Plant in Norway," ASME Turbo Expo Paper GT2005-68640.

Imslad, L., Snarheim, D., Ulfsnes, R., Bolland, O., Foss, B.A. (2004) "Modeling and Control of a O_2/CO_2 Gas Turbine Cycle for CO_2 Capture," 7th International Symposium on Dynamics and Control of Process Systems. International Federation of Automatic Control, Cambridge, Massachusetts, USA, July 2004.

Jackson, A.J.B., Neto, A.C., Whellens, M.W. (2000) "Gas Turbine Performance Using Carbon Dioxide as Working Fluid in Closed Cycle Operation," ASME Turbo Expo Paper 2000-GT-153.

Jordal, K., Bolland, O., Klang, A. (2003) "Aspects of Cooled Gas Turbine Modeling for the Semi-Closed O_2/CO_2 Cycle With CO_2 Capture," ASME Turbo Expo Paper GT2003-38067.

Keeling, C.D., T.P. Whorf. (2004) "Atmospheric CO_2 records from sites in the SIO air sampling network. In Trends: A Compendium of Data on Global Change," Carbon Dioxide Information Analysis Center, Oak Ridge National Laboratory, U.S. Department of Energy, Oak Ridge, Tenn., U.S.A.

Kenny, S.C. (2003) "Genetic Optimization of Cycle Configurations with Steam Injection and Heat Recovery in Semi-Closed Cycle CO_2 Gas Turbines," A Carleton University Department of Mechanical and Aerospace Engineering Report prepared for the CANMET Energy Technology Centre

Kurzke, J., (2005) "GasTurb," Online sales site March-2006: www.gasturb.de

Kvamsdal, H.M., Ertesvåg, I.S., Bolland, O., Tolstad, T. (2002) "Exergy Analysis of Gas-Turbine Combined Cycle With CO_2 Capture Using Pre-Combustion Decarbonisation of Natural Gas," ASME Turbo Expo Paper GT-2002-30411.

Martinez-Frias, J., Aceves, S.M., Smith, J. R., Brandt, H. (2004) "Thermodynamic Analysis of Zero-Atmospheric Emissions Power Plant," ASME Journal for Gas Turbines and Power, Vol. 126 pp. 2-8, January 2004.

Mathieu, Ph., Dechamps, P., Distelmans, M. (1994) "Concepts and Applications of CO_2 Gas Turbines," Power-Gen Europe '94, Cologne, Germany, May 1994.

Mathieu, Ph., Dubuisson, R., Houyou, S., Nihart, R. (2000) "New Concept of CO_2 Removal Technologies in Power Generation, Combined With Fossil Fuel Recovery and Long Term CO_2 Sequestration," ASME Turbo Expo Paper 2000-GT-160.

Meier, N. (2005) "Civil Turbojet/Turbofan Specifications," Comprehensive jet engine database; Website Oct-2005: http://www.jet-engine.net/

Möller, B.F., Assadi, M., Linder, U. (2003) "CO_2-Free Power Generation – A Study of Three Conceptually Different Plant Layouts," ASME Turbo Expo Paper GT2003-38413.

Moran, M.J., Shapiro, H.N. (1996) "Fundamentals of Engineering Thermodynamics," 3rd Edition, John Wiley & Sons, Inc. Toronto. ISBN 0-471-07681-3

Moritsuka, H. (2004) "Proposal of Innovative Gas Turbine Combined Cycle Power Generation System," ASME Turbo Expo Paper GT2004-54177.

Navaratnam, M. (1994) "The Investigation of an Aero Derivative Gas Turbine Using Alternative Working Fluids in Closed/Semi Closed Cycles," MSc. Thesis, Cranfield University, School of Mechanical Engineering, 1994.

NRCan, (1999). "Canada's Emissions Outlook: An Update," National Climate Change Process Analysis and Modeling Group, NRCan. Website September-2004: http://www.nrcan.gc.ca/es/ceo/outlook.pdf

Peng, D.Y., Robinson, D.B. (1976) "A New Two-Constant Equation of State," Industrial Engineering Chemical Fundamentals, Vol. 15, pp. 58-64

Roberts, S.K., Sjolander, S.A. (2005) "Effect of the Specific Heat Ratio on the Aerodynamic Performance of Turbomachinery," ASME Journal of Engineering for Gas Turbines and Power, October 2005, Vol. 127, pp. 773-780

Sanz, W., Jericha, H., Luckel, F., Göttlich, E., Heitmeir, F. (2005) "A Further Step Towards a GRAZ Cycle Power Plant for CO_2 Capture," ASME Turbo Expo Paper ASME GT2005-68456

Sanz, W., Jericha, H., Moser, M., Heitmeir, F. (2004) "Thermodynamic and Economic Investigation of an Improved GRAZ Cycle Power Plant for CO_2 Capture," ASME Turbo Expo Paper ASME GT2004-53722.

Saravanamuttoo, H.I.H., Rogers, G.F.C., Cohen, H. (2001) "Gas Turbine Theory," 5th Edition, Prentice Hall, Upper Saddle River, New Jersey 07458, ISBN: 013015847X

Schultz, John M. (1962) "The Polytropic Analysis of Centrifugal Compressors," ASME Journal of Engineering for Power, January 1962

Shan, X. (2003) "Brankine Cycle Optimization Study – Effect of Water Injection/Re-injection on Semi-Closed Cycle CO_2 Gas Turbines," Department of Mechanical and Aerospace Engineering, Carleton University; Prepared for the CANMET Energy Technology Centre – Natural Resources Canada.

Sjolander, S.A., Shan, X., Roberts, S.K. (2003) "Aerodynamic Performance of Turbomachinery for Zero-Emission Gas Turbine Engines," CASI 9th Aerodynamics Symposium, Montreal, April 2003

Smith, A.R., Klosek, J. (2001) "A Review of Air Separation Technologies and Their Integration with Energy Conversion Processes," Fuel Processing Technology 70 pp 115-134.

Stambler, I. (2004) "Mercury 50 Rate at 4600 kW and 38.5 % Efficiency with 5 ppm NOx," Gas Turbine World, February-March 2004.

Taftan Data, (1998) "Applied Thermodynamics," Website May-2005: http://www.taftan.com/thermodynamics/

Tangney, R. Private communication, May 2005.

Teraji, D., Hettick, J., Robison, M. (2005) "*Mercury*™ 50 Product Durability, Operation and Maintenance Review," ASME Turbo Expo Paper ASME GT2005-69134

Toolbox, (2005) "Engineer's toolbox," Website January-2005: http://www.engineeringtoolbox.com/spesific-heat-capacity-gases-24_159.html

TransCanada Log, (2000) Personal Engineering Logbook, June 14-15 entry.

Turns, S.R. (2000) "An Introduction to Combustion: Concepts and Applications," The McGraw-Hill Companies, Inc. Boston.

Ulfsnes, R.E., Bolland, O., Jordal, K. (2003a) "Modeling and Simulation of Transient Performance of the Semi-Closed O_2/CO_2 Gas Turbine Cycle for CO_2-Capture," ASME Turbo Expo Paper GT2003-38068.

Ulfsnes, R.E., Karlsen, G., Jordal, K., Bolland, O., and Kvamsdal, H.M. (2003b) "Investigation of Physical Properties for CO_2/H_2O Mixtures for Use in Semi-Closed O_2/CO_2 Gas Turbine Cycle With CO_2 Capture," 16th Annual Conference on Efficiency, Costs, Simulation, and Environmental Impact of Energy Systems

Ulizar, I., Pilidis, P. (1997) "A Semiclosed-Cycle Gas Turbine With Carbon Dioxide-Argon as Working Fluid," ASME Journal of Engineering for Gas Turbines and Power, Vol. 119, pp 612-616, July 1997

Ulizar, I., Pilidis, P. (2000) "Handling of a Semiclosed Cycle Gas Turbine With a Carbon Dioxide-Argon Working Fluid," ASME Journal of Engineering for Gas Turbines and Power, Vol. 122, pp. 437-441, July 2000.

Union Gas Ltd. (2004) – Website; "Natural Gas Composition," – Union Gas is a subsidiary of Duke Energy Corporation of Charlotte, North Carolina. Website October-2004: http://www.uniongas.com/aboutus/aboutng/composition.asp

White, F.M., (1994) "Fluid Mechanics," 3rd Edition McGraw-Hill, Inc. New York

Wikipedia, (2006) "Greenhouse Effect," Website April-2006 http://en.wikipedia.org/wiki/Greenhouse_effect

World Nuclear Association, (2005) "Nuclear Power in the World Today," Website January-2005: http://www.world-nuclear.org/info/inf01.htm

Yadav, R., "Effect of Bottoming Cycle Alternatives on the Performance of Combined Cycle," ASME Turbo Expo Paper GT2003-38052.

Yan, J., Ji, X., Jonsson, M. (2003) "Thermodynamic Property Models for the Simulation of Advanced Wet Cycles," ASME Turbo Expo Paper GT2003-38298.

Yeh, J.T., Pennline, H.W., Resnik, K.P. (2000) "Study of CO_2 Absorption and Desorption in a Packed Column," U.S. Department of Energy, Website September-2004: http://www.netl.doe.gov/osta/techpapers/2000-204.pdf

Zanganeh, K.E., Shafeen, A., Thambimuthu, K. (2004) "A Comparative Study of Refinery Fuel Gas Oxy-Fuel Combustion Options for CO_2 Capture Using Simulated Process Data," CANMET Energy Technology Centre, Ottawa. 7th International Conference on Greenhouse Gas Control Technologies, Vancouver, British Colombia, Canada, September 2004.

Zhang, N., Cai, R., Wang, W. (2003) "Study on Near-Zero CO_2 Emission Thermal Cycles With LNG Cryogenic Exergy Utilization," ASME Turbo Expo Paper GT2003-38605

Zhou, M. Gauthier, J.E.D. (1998) "A Literature Survey on the Use of O_2/CO_2 Mixtures as the Primary Working Fluid in Combustion Engines," Mechanical Engineering Report #980503, Department of Mechanical Engineering, Royal Military College of Canada, May 1998.

Appendices

Appendix A - ASPEN User Interface

1. Process Flow-sheet

The process flow-sheet is the main window of the opened ASPEN file, and is where the system is modeled as a group of specified components and streams, as is shown as Figure 3-1. Available components are listed across the bottom of the process flow-sheet. To create a system, the desired component is selected from the

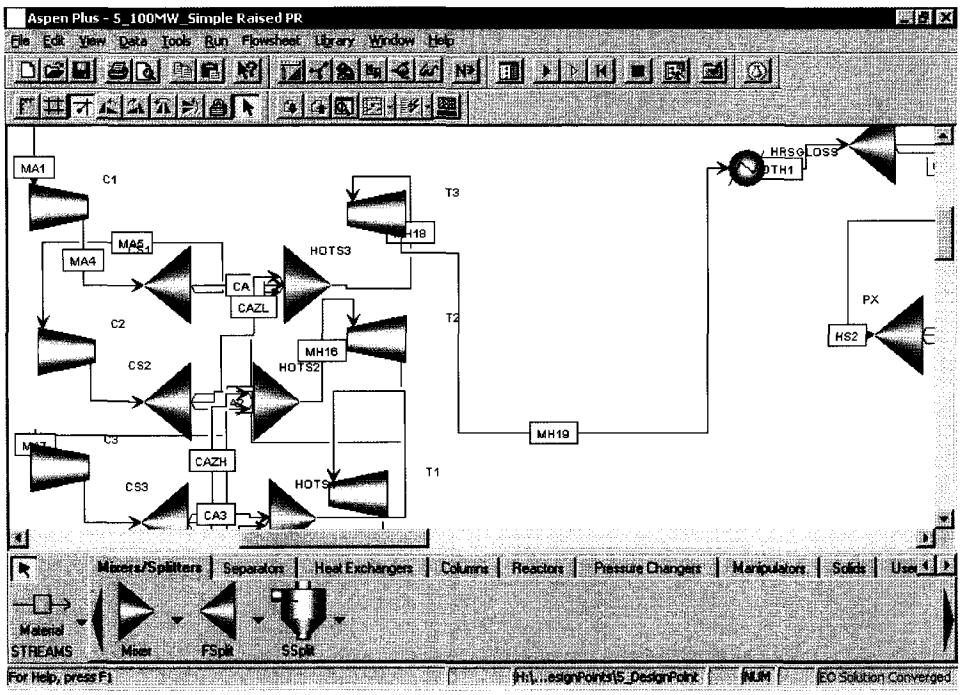

Figure A-8-1: ASPEN process flow-sheet

component list and placed at the desired location in the flow-sheet. The process flow-sheet is also useful in other stages of modeling, such as reviewing results and troubleshooting. All working fluid information into and out of a block can be reviewed by selecting *stream results* after right-clicking the block. The options available under right-click of a block are shown in Figure 3-2. The specifications of any block or stream can also be rapidly accessed in the *Data Browser* from the process flow-sheet.

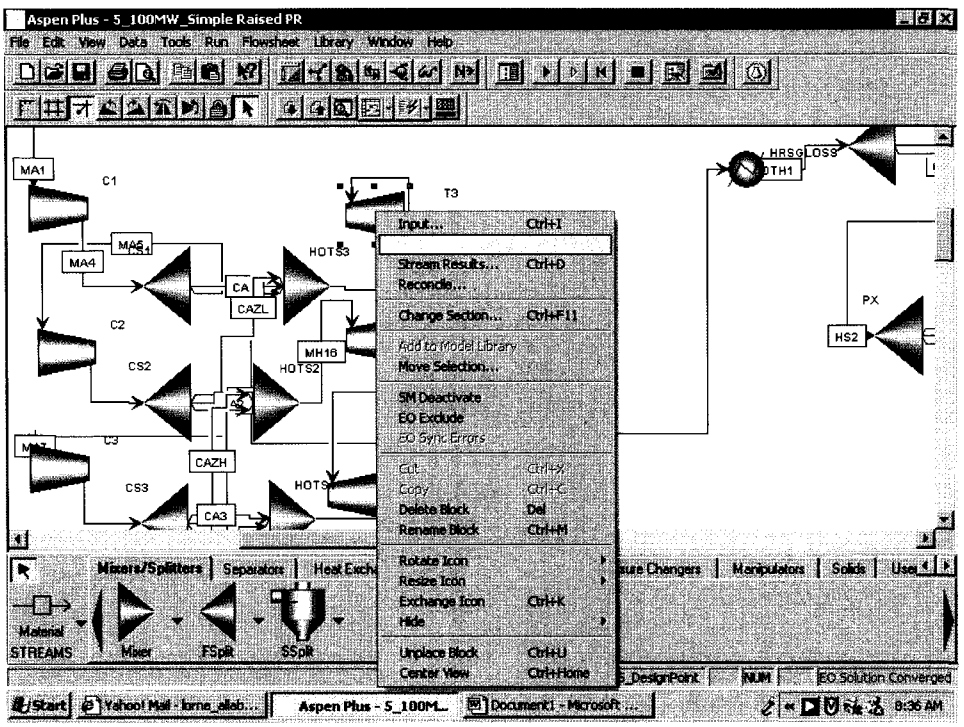

Figure A-8-2: Right-click of component in process flow sheet

2. Data Browser

The data browser operates in a similar manner as a Windows Explorer in the Microsoft Windows® operating system. Each stream, block, data specification, etc., has its own folder. In each folder there is access to inputs, options, and results. A view of the data browser is shown as Figure 3-3. The list of folders is on the left hand side of the figure.

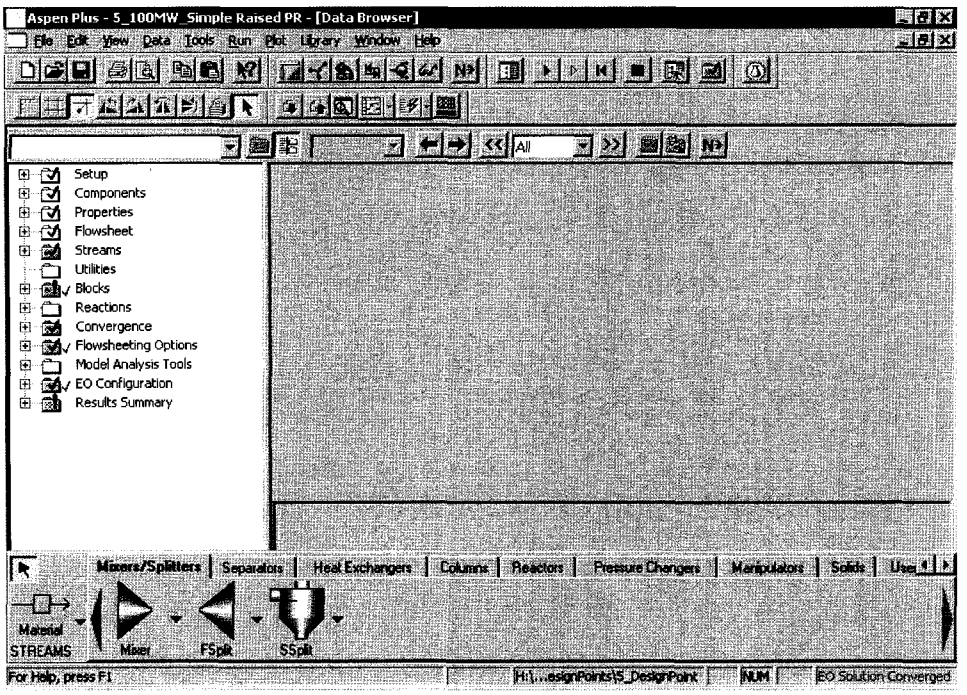

Figure A-8-3: ASPEN data browser

3. Control Panel

To run the simulation, open the *control panel.* In the control panel there are start and stop buttons and an output/progress screen. The output screen will show specified information as the simulation progresses, including errors, warnings, and iteration numbers. Depending on the calculation method, it may also show a measure of problem linearity and residuals. The calculation methods are outlined in the next section. The desired method can be selected from the control panel. Figure 3-4 shows the control panel.

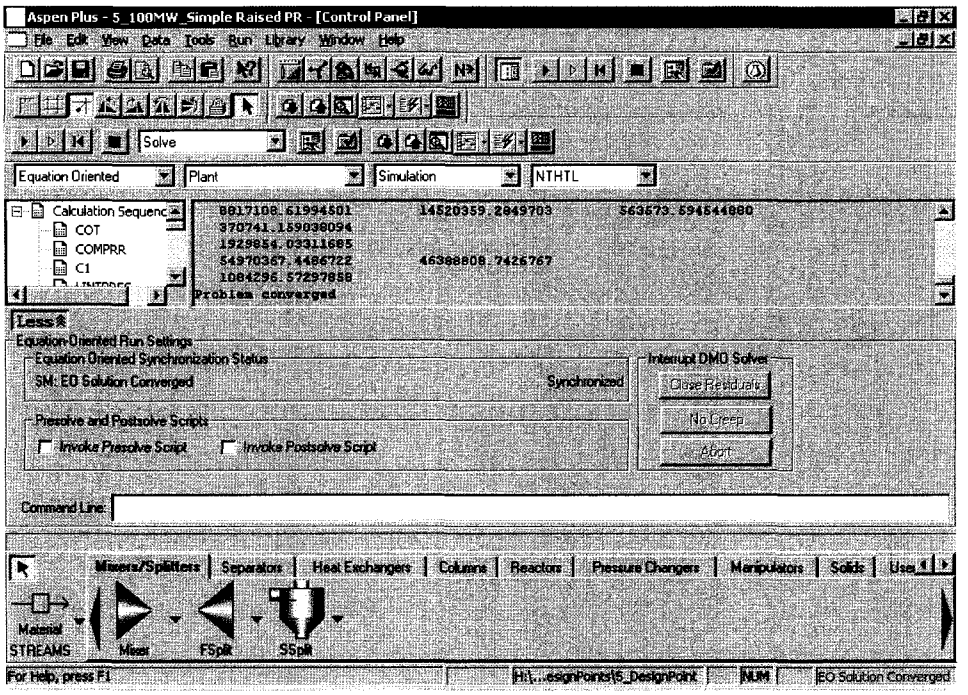

Figure A-8-4: ASPEN control panel

Appendix B – DMO Solver Algorithm

The general optimization problem that DMO solves can be expressed as follows:

Minimize $f(x)$

Subject to $c(x) = 0$

$x_{min} \leq x \leq x_{max}$

Where:

$x \in \boldsymbol{R}^n$	Vector of unknown variables
$\boldsymbol{R}^1$	Objective function
$\boldsymbol{R}^m$	Vector of constraint equations
$\boldsymbol{R}^n$	Vector of lower bounds on x
$x_{max} \in \boldsymbol{R}^n$	Vector of upper bounds on x

A simplified description of the DMO algorithm is outlined as follows:

1. Given an initial estimate of the solution vector, x_0

2. Set iteration counter, $k = 0$

3. Evaluate derivative of the objective function, gradient, and the derivative of the constraints, Jacobian.

4. Initialize or update an approximation of the second derivative matrix, or Hessian, of the Lagrange function. The Lagrange function, $f(x) + \Sigma(\lambda_i c_i)$,

accounts for constraints through weighting factors λ_i, often called Lagrange multipliers or shadow prices.

5. Solve a quadratic programming subproblem to determine a search direction, d_k In the quadratic programming subproblem, the objective function is replaced by a quadratic approximation, constraints are linearized, and bounds are included.

6. Check for convergence or failure. If the optimization convergence criteria are satisfied or if the maximum number of allowed iterations is reached, then end.

Convergence is achieved when:

– Objective function gradient $\leq$ objective function convergence tolerance

– Scaled or unscaled constraint residuals $\leq$ residual convergence tolerance

7. Perform a one-dimensional search to determine a search step α_k so that $x_k + \alpha_k d_k$ is a better approximation of the solution as measured by a line search or merit function. The reduction of merit function requirement is sometimes relaxed to achieve a full correction step.

8. Update iteration counter, $k = k + 1$, and loop back to step 3.

Reference: Aspen Plus 12.2 Equation Oriented Modeling Reference Manual.

Appendix C – LSSQP Solver Algorithm

The general optimization problem that LSSQP solves can be expressed as follows:

Minimize $f(x)$

Subject to $c(x) = 0$

$x_{min} \leq x \leq x_{max}$

Where:

$x \in \boldsymbol{R}^n$	Vector of unknown variables
$\boldsymbol{R}^1$	Objective function
$\boldsymbol{R}^m$	Vector of constraint equations
$\boldsymbol{R}^n$	Vector of lower bounds on x
$x_{max} \in \boldsymbol{R}^n$	Vector of upper bounds on x

A simplified description of the LSSQP algorithm is outlined as follows:

1. Given an initial estimate of the solution vector, x_0

2. Set iteration counter, $k = 0$

3. Evaluate derivative of the objective function, gradient, and the derivative of the constraints, Jacobian.

4. Initialize or update an approximation of the second derivative matrix, or Hessian, of the Lagrange function. The Lagrange function, $f(x) + \Sigma(\lambda_i c_i)$,

accounts for constraints through weighting factors λ_i, often called Lagrange multipliers or shadow prices.

5. Solve a quadratic programming subproblem to determine a search direction, d_k In the quadratic programming subproblem, the objective function is replaced by a quadratic approximation, constraints are linearized, and bounds are included.

6. Check for convergence or failure. If the optimization convergence criteria are satisfied or if the maximum number of allowed iterations is reached, then skip to step 10.

Convergence is achieved when:

- Kuhn- Tucker error (KTE) $\leq$ relative optimization convergence tolerance * max(0.01,$|f|$), and
- Relative change in $X \leq 0.001$, and
- Scaled or un-scaled constraint residual ≤ 0.001.

The KTE is the sum of predicted improvement to the objective function and the sum of constraint violations converted to objective function units through λ_i-like factors.

7. Perform a one-dimensional search to determine a search step α_k so that $x_k + \alpha_k d_k$ is a better approximation of the solution as measured by a line search or

merit function. The reduction of merit function requirement is sometimes relaxed to achieve a full correction step.

8. Perform up to the maximum feasibility correction steps allowed at each SQP iteration if constraint violation is greater than the specified tolerance on iteration constraint violations.

9. Update iteration counter, $k = k + 1$, and loop back to step 3.

10. Perform up to the maximum number of feasibility corrections allowed to try to reduce constraint violations below the tolerance on final constraint violations after the optimization calculation is terminated if the constraint violation is greater than the tolerance on final restraint violations.

Reference: Aspen Plus 12.2 Equation Oriented Modeling Reference Manual.

Appendix D – Working Fluid Composition

Alphabetical Order	High Purity O_2	Low Purity O_2	Low Purity O_2	Low Purity O_2
Oxygen Stream	**Mass Fraction**	**Mass Fraction**	**Mass Fraction**	**Mass Fraction**
Oxygen	0.994	0.944	0.944	0.944
Argon	0.006	0.056	0.056	0.056
	Fuel #1 (natural gas)	**Fuel#1 (natural gas)**	**Fuel#2 (ideal natural gas - HCs only)**	**Fuel#3 (methane)**
	Mass Fraction	**Mass Fraction**	**Mass Fraction**	**Mass Fraction**
Argon	0.008	0.077	0.078	0.079
Carbon Dioxide	**0.9689**	**0.9008**	**0.9089**	**0.9083**
Carbon Monoxide	3.68E-05	3.45E-05	3.32E-05	3.32E-05
Ethane	0	0	0	0
Hydrogen	1.39E-07	1.33E-07	1.27E-07	1.28E-07
Iso-Butane	0	0	0	0
Iso-Pentane	0	0	0	0
Methane	3.60E-23	3.01E-23	2.92E-23	3.07E-23
N-Butane	0	0	0	0
N-Hexane	0	0	0	0
Nitrogen	0.00968	0.00900	0.00000	0.00000
Nitrogen Dioxide	1.13E-06	1.08E-06	3.75E-17	5.36E-24
Nitrogen Oxide	1.10E-08	1.01E-08	1.35E-29	3.08E-35
Nitrous Oxide	8.23E-05	7.93E-05	1.18E-15	1.70E-22
N-Pentane	0	0	0	0
Oxygen	**0.01000**	**0.01000**	**0.01000**	**0.01000**
Propane	0	0	0	0
Water	0.0029	0.0029	0.0027	0.0027

Decreasing Concentration (by column 2)	High Purity O_2	Low Purity O_2	Low Purity O_2	Low Purity O_2
Oxygen Stream	**Mass Fraction**	**Mass Fraction**	**Mass Fraction**	**Mass Fraction**
Oxygen	0.994	0.944	0.944	0.944
Argon	0.006	0.056	0.056	0.056
	Fuel #1 (natural gas)	**Fuel#1 (natural gas)**	**Fuel#2 (ideal natural gas - HCs only)**	**Fuel#3 (methane)**
	Mass Fraction	**Mass Fraction**	**Mass Fraction**	**Mass Fraction**
Carbon Dioxide	**0.9689**	**0.9008**	**0.9089**	**0.9083**
Argon	0.0084	0.0772	0.0784	0.0790
Oxygen	**0.0100**	**0.0100**	**0.0100**	**0.0100**
Nitrogen	0.0097	0.0090	0.0000	0.0000
Water	0.0029	0.0029	0.0027	0.0027
Nitrous Oxide	8.23E-05	7.93E-05	1.18E-15	1.70E-22
Carbon Monoxide	3.68E-05	3.45E-05	3.32E-05	3.32E-05
Nitrogen Dioxide	1.13E-06	1.08E-06	3.75E-17	5.36E-24
Hydrogen	1.39E-07	1.33E-07	1.27E-07	1.28E-07
Nitrogen Oxide	1.10E-08	1.01E-08	1.35E-29	3.08E-35
Methane	3.60E-23	3.01E-23	2.92E-23	3.07E-23
Propane	0	0	0	0
N-Pentane	0	0	0	0
N-Hexane	0	0	0	0
N-Butane	0	0	0	0
Iso-Pentane	0	0	0	0
Iso-Butane	0	0	0	0
Ethane	0	0	0	0